Correlation functions in maximally supersymmetric Yang-Mills theory

Jakub Sikorowski
Jesus College
University of Oxford

A thesis submitted for the degree of
Doctor of Philosophy
Trinity 2015

Correlation functions in maximally supersymmetric Yang-Mills theory

Jakub Sikorowski, Jesus College

A thesis submitted for the degree of *Doctor of Philosophy*, Trinity 2015

Abstract

In this thesis we consider the planar maximally supersymmetric Yang-Mills theory. First, we look at the correlation function of a null Wilson loop with four edges and a local operator at weak coupling. We use the Lagrangian insertion technique to find the integral representation up to two loops. Performing the integrals with a method closely linked to the dual space formalism for the scattering amplitudes, we explicitly compute the two loop result. We demonstrate the connection between the calculated observable and the cusp anomalous dimension by recovering the three loop value of the cusp anomalous dimension. We also explore the advantages of expressing the loop integrand in twistor variables.

The second observable we look at is the four point correlation function of the BMN operators on a line at strong coupling. In order to access this regime we perform a semi-classical computation in the classical string theory. Considering area of an extended minimal surface stretched between the four operators, we find two different saddle points. We show that the extended minimal surface is sub-dominant to the saddle point composed of three geodesic strings joining the four operators in a sequence. The result is that, to the leading order at strong coupling, the considered correlation function is equal to its tree-level value when all operators are on a line.

Statement of Originality

The thesis is based on two published papers and a draft prepared for article submission. All of those were created in collaboration with other authors. Here, we list the relevant publications and contributions made by the author of the thesis.

Chapter 2 is based on article [1] co-authored with L. F. Alday and P. Heslop. I have contributed through the numerical checks and proofs to this work.

Chapter 3 originates in [2] published together with L. F. Alday and J. M. Henn. My contribution was to evaluate obtained Mellin-Barnes integrals by resummation and to check finiteness of the twistor diagram representation at two loops.

Chapter 4 is a result of work in collaboration with J. Toledo. Section 4.3 reviews the integrable model described in [3], together with the specific simplifications for the case we consider contributed mainly by J. Toledo. I was the main author of sections 4.2, 4.4, 4.5, 4.6, and 4.7.

Contents

1 Introduction **1**

1.1 Motivation for the study of N=4 SYM 1

1.2 Approaches to N=4 SYM 3

1.3 Approach taken in this thesis 7

1.3.1 Original work and thesis overview 8

2 Perturbative correlation functions of null Wilson loops and local operators **10**

2.1 Introduction 10

2.2 Explicit results 12

2.2.1 General expressions and one-loop result 12

2.2.2 Two-loop result 15

2.3 Conclusions 16

3 Mixed correlation function at two loops **18**

3.1 Introduction and main results 18

3.2 Analytic two-loop calculation from loop integrals 21

3.2.1 Expression in terms of loop integrals 22

3.2.2 Description of calculation 23

3.2.3 Evaluating Mellin-Barnes integrals. 25

3.3 Twistorial representation 27

3.3.1 One loop 28

3.3.2 Two loops 29

3.3.3 Checking finiteness 30

3.3.4 Observation on two loop result 32

3.4 Relation to the light-like cusp anomalous dimension 32

3.4.1 Massive regularization . . . 33
3.4.2 Integration of $F(x) = x^p$ over the insertion point . . . 34
3.4.3 Three-loop cusp anomalous dimension from integration over $F^{(2)}$. . . 35
3.4.4 Strong coupling . . . 36
3.5 Summary and outlook . . . 37

4 Correlation functions of heavy operators on a line 39
4.1 Introduction . . . 39
4.1.1 3-point functions and strong coupling . . . 40
4.1.2 3-point functions and classical integrability . . . 41
4.2 General properties and weak coupling . . . 42
4.2.1 Correlator and convenient parametrisation . . . 42
4.2.2 Weak coupling . . . 43
4.2.3 Crossing symmetry . . . 45
4.2.4 Dominant contribution for generic operators . . . 45
4.2.5 Euclidean OPE limit . . . 47
4.2.6 Dominant contribution for special cases . . . 48
4.2.7 Interesting questions . . . 49
4.3 Integrable System . . . 51
4.3.1 String in AdS . . . 51
4.3.2 Linear problem . . . 52
4.3.3 Solutions near the punctures . . . 53
4.3.4 WKB lines . . . 55
4.3.5 Stress-energy tensor and Virasoro . . . 56
4.3.6 Zeros of stress-energy tensor . . . 57
4.3.7 Triangulation . . . 58
4.3.8 Spike configuration, fold lines and Virasoro . . . 60
4.3.9 Chi coordinates . . . 62
4.3.10 Chi-system . . . 64
4.3.11 Inverting the chi-system . . . 66
4.3.12 Cross-ratios . . . 68

4.3.13 Area . . . 69
4.4 Imposing the Virasoro constraint . . . 72
4.4.1 Virasoro plateau for uudd spike configuration . . . 72
4.4.2 Virasoro kink . . . 73
4.4.3 udud spike configuration . . . 75
4.5 Crossing symmetry . . . 78
4.5.1 Inverted cross-ratio problem . . . 82
4.6 Particular limits . . . 83
4.6.1 Colliding zeros of the stress-energy tensor . . . 83
4.6.2 Self dual configuration . . . 85
4.6.3 OPE limit: special case . . . 87
4.6.4 Generic case . . . 93
4.6.5 Discussion of OPE . . . 95
4.7 Numerical results . . . 96
4.7.1 Implementation . . . 96
4.7.2 Symmetric configuration . . . 98
4.7.3 Special case . . . 100
4.8 Conclusions . . . 100

5 Summary and outlook **103**

A Correlation functions in N=4, permutation symmetry and procedure of Lagrangian insertions **105**

A.1 N=4 SYM stress-tensor supermultiplet . . . 105
A.2 Harmonic superspace . . . 106
A.3 Lagrangian insertion technique . . . 107
A.4 Integrand . . . 108

Bibliography **111**

List of Figures

2.1 All contributing double box integrals at 2 loops with the corresponding numerator. 16

2.2 Two mass pentabox which contributes at 2 loops with the corresponding numerator. 16

2.3 Three types of products of boxes which contribute at two loops with the corresponding numerator. 17

3.1 One-loop integrals contributing to $F^{(1)}$ with corresponding numerators. Below the diagrams, we write the corresponding factors that appear in the numerators of the form $x^2_{\dots}\, x^2_{\dots}$. The Fs label the diagrams. 22

3.2 Two-loop integrals contributing to $F^{(2)}$ with corresponding numerators. Below the diagrams, we write the corresponding factors that appear in the numerators. The Is label the diagrams. 23

3.3 One-loop chiral integral contributing to $F^{(1)}$. 29

3.4 Twistorial representation of two-loop integrals contributing to $F^{(2)}$. 30

4.1 Tree level Wick contractions contributing to four-point function. Diagrams, a) and b), have a linear topology; they correspond to the first two terms in eq. (4.9). Diagram c) with a disc topology corresponds to the last term in eq. (4.9). The grey and white circles represent $\mathrm{Tr}\, Z^{\mathbf{\Delta}}$ and $\mathrm{Tr}\, \bar{Z}^{\mathbf{\Delta}}$ respectively. 44

4.2 Log-log sketch of the magnitude of terms in the brackets in eq. (4.9) for large but finite $\mathbf{\Delta}$. For small q, the first term dominates. For large q, the second term dominates. For the intermediate values all three terms contribute. . . . 46

4.3 Plot of the magnitude of terms in the brackets in eq. (4.20) for $\mathbf{\Delta} \to \infty$. For small q, the first term dominates. For $q \sim 1$, the third term dominates. . . . 49

4.4 Opened-up string configuration in diagram a) and its degenerated versions in diagrams b) and c). We contrast the generic closed-up string configuration in diagram b) with a geodesic string configuration connecting the four operators in sequence in diagram c). Red dots denote the operator insertions, and the grey area represents the worldsheet surface. 49

4.5 Schematic plot of the separating WKB lines in complex w-plane, for $w_2^- < w_2 < w_2^+$ and $\phi = \pi/5$, see eq. (4.59) for definition of $w_2^\pm$. The real axis is along the blue dots, but it was not included for transparency. Blue/red dots represent poles/zeros of the stress-energy tensor. 58

4.6 Schematic plot of a single cell produced by the separating WKB lines represented by solid black curves. The dashed curves are the generic WKB lines. Blue/red dots represent poles/zeros of the stress-energy tensor. 59

4.7 WKB lines forming the triangulation of the worldsheet. Dashed lines represent the monodromy cuts for the solutions to the linear problem. Blue dots represent poles of the stress-energy tensor. 60

4.8 The process of a triangulation change. Schematic plot of separating WKB lines represented by solid black curves. The dashed curves are the generic WKB lines. Blue/red dots represent poles/zeros of the stress-energy tensor. Notice that, as a result of the triangulation change, the presented generic WKB lines join different operators before and after the transition. 84

4.9 Two zeros of the stress-energy tensor (marked as the red dots) colliding and leading to a triangulation change. Solid black curves represent WKB lines, and solid red curves represent separating WKB lines that pass through zeros. 85

4.10 Imposing the Virasoro constraint first and the OPE limit second we find that the χ-functions form two plateaux. The figure indices the relative order of limits. 88

4.11 Cycles corresponding to masses of each coordinate χ in the OPE limit when all roots collide on the real axis. Cycle corresponding to Z_{12} vanishes. The other cycles become a closed contour integrals. Zeros and double poles of the stress-energy tensor are marked red and blue respectively. 93

4.12 The negative of the area of two saddle points for different values of the cross-ratio x_2 for $\bar{\ell} = 0$. The curves in red to brown colour represent the area of the triple two-point function saddle point. The dark blue to purple curves are represent the extended minimal surface *i.e.* the *uudd* spike configuration. . . 98

4.13 The negative of the area of two saddle points for different values of ℓ for the symmetric configuration $x_2 = w_2 = 1/2$ and $\bar{\ell} = 0$. The red curve represents the area of the triple two-point function saddle point. The blue curve represents the extended minimal surface *i.e.* the *uudd* spike configuration. 99

4.14 The negative of the area of two saddle points for different values of the cross-ratio x_2 for $\ell = -\bar{\ell}$. The curves in red to brown colour represent the area of the triple two-point function saddle point. The dark blue to purple curves are represent the extended minimal surface *i.e.* the *uudd* spike configuration. . . 100

4.15 The negative of the area of two saddle points for different values of ℓ for the symmetric configuration $x_2 = 1/2$ and $\ell = -\bar{\ell}$. The red curve represents the area of the two disconnected two-point functions saddle point. The blue curve represents the extended minimal surface *i.e.* the *uudd* spike configuration. . 101

List of Tables

4.1 Numerical results obtained with relaxation method for $j = 1$, $\ell = \bar{\ell} = 0$. . . . 97

Chapter 1

Introduction

We take this chapter as an opportunity to advocate the choice of the subject of this thesis. We commence with an interpretation as to what drives the wider scientific community to study $\mathcal{N} = 4$ supersymmetric Yang-Mills theory. We place the topic of the thesis in the wider context of the Particle Physics as well as the history of the subject. We finish this chapter with an overview of the thesis, and a clear statement which parts of the thesis constitute original work.

1.1 Motivation for the study of N=4 SYM

We dedicate this thesis to the study of correlation functions in a very specific quantum field theory *i.e.* $\mathcal{N} = 4$ supersymmetric Yang-Mills theory often abbreviated as $\mathcal{N} = 4$ SYM. It is a four dimensional theory with maximal number of supersymmetric generators that does not involve gravity or gauging the supersymmetry transformations. This is quite the opposite to any physically viable model of a supersymmetric extensions of the Standard Model of Particle Physics currently tested at the Large Hadron Collider (LHC). These theories include minimal amount of supersymmetry supplemented with additional terms that explicitly break this supersymmetry, often referred to as the soft breaking terms. Only by including suitable adjusted soft terms can these theories be made consistent with current experimental observations, in particular, explain lack of any direct observation of supersymmetric partners of the Standard Model particles. For a recent review of experimental bound see for example [4]. Therefore, it is natural to ask what good can a study of $\mathcal{N} = 4$ SYM bring?

The importance of Yang-Mills theories to current understanding of Particle Physics cannot be overly emphasized. An extension of abelian gauge theory, that describes electro-

magnetism, to non-abelian gauge groups to provide an understanding of strong interactions was initially proposed in 1954 by Chen Ning Yang and Robert Mills [5]. It became part of mainstream Particle Physics once the electroweak symmetry breaking mechanism was proposed and enabled to give masses to the gauge bosons (a contribution recognised by the 2013 Nobel Prize in Physics). Another mile stone for Yang-Mills theories was working out its renormalization by Gerard 't Hooft [6, 7] (a contribution recognised by the 1999 Nobel Prize in Physics). When the Standard Model was formulated, Yang-Mills theory found its place describing both the electroweak as well as the strong interactions.

Our current understanding of the strong interactions proves challenging for the analysis of the LHC experiments. In particular, understanding the Standard Model background to new Physics demands cumbersome calculations to many loop precision, see for example [8]. Moreover, there are experimental evidence that analysis of the heavy-ion collisions at LHC cannot be described as perturbations around the weak coupling limit [9]. However, even after 60 years of intensive studies of the theory, its understanding outside the perturbative regime at weak coupling is very limited. A need for a better understanding of the Yang-Mills theory was recognised by the Clay Mathematics Institute by including the finite mass-gap and confinement problems in the list of "Millennium Prize Problems".

$\mathcal{N} = 4$ SYM is very special amongst supersymmetric Yang-Mills theories. Foremost, it is a conformally invariant theory. However, its special features are obscured by its Lagrangian formulation. This formulation is manifestly local and unitary but hides the extended list of symmetries that set $\mathcal{N} = 4$ SYM apart from other four dimensional theories. In the planar limit there is a plethora of evidence that the extended set of symmetries [10, 11] make the theory integrable; a recent review can be found in [12]. All those evidence rise the expectation of finding a set of methods for an efficient computation of the observables in this theory for any value of the coupling constant.

We might think of $\mathcal{N} = 4$ SYM as a toy model, the simplest quantum field theory with non-trivial dynamics resembling the Standard Model of Particle Physics. It is hoped that just like solving the hydrogen atom led to an in-depth understanding of methods for more complex system, solving $\mathcal{N} = 4$ SYM might give us a set of tools to extract physical observables from quantum field theories without use of Feynman diagrams in a much more efficient and straightforward way, and that these methods can be transferred or generalised to other

theories.

Possibly the most surprising property of $\mathcal{N} = 4$ SYM is its conjectured duality to type IIB string theory on specific background of $AdS_5 \times S^5$, usually referred to as the AdS-CFT duality [13–15]. Therefore, considering $\mathcal{N} = 4$ SYM we are in fact studying an example of a consistent theory of quantum gravity in a curved background. The conjectured duality is of a strong-weak type and allows access to both the strongly coupled regimes of the gauge theory as well as string theory in highly curved background. Before the discovery of the duality both regimes were far beyond reach of standard methods. It is hoped that understanding the two theories for both weak and strong coupling will significantly boost the process of solving them for any value of the coupling constant [12].

If one of the aims of Theoretical Physics is to understand natural phenomena from as many perspectives as possible and, in a particular situation, choose the most convenient description, then understanding $\mathcal{N} = 4$ SYM non-perturbatively gives an interesting angle on (strongly coupled) gauge theories. For a recent review see for example [9].

Last but not least, a reason to study this theory is a wealth of mathematical structures that arise studying its observables. This vast amount of mathematical structures inspires both Physicist and Mathematicians to form unprecedented collaborations.

1.2 Approaches to N=4 SYM

This section reviews some of the most important approaches and contributions over the years in the study of $\mathcal{N} = 4$ SYM. The aim is to provide a wider context for the approach we take in this thesis.

One of the earliest insights was the discovery of the large N limit [16]. When the rank of the gauge group, which we take to be $SU(N)$, becomes large, the theory simplifies. The terms in perturbation expansions in a gauge theory organise themselves according to the genus of the surface formed by the corresponding double-line Feynman diagram. The higher genus surfaces are suppressed by $1/N$ factors, and the expansion mirrors the genus expansion of an interacting string theory. In this thesis we deal with the planar $\mathcal{N} = 4$ SYM theory i.e. when $N \to \infty$, and only the planar diagrams survive.

Another important insight, the holographic principle [17, 18], came from considering

quantum information entering a black hole during its formation. Gerard 't Hooft argued that, in order to resolve an apparent paradox, the degrees of freedom of the gravitational theory should be described by a theory leaving on the boundary of the space.

Both of these insights got concrete realisation in the AdS-CFT duality conjectured by Juan Maldacena [13–15]. It states that $\mathcal{N} = 4$ SYM theory with an $SU(N)$ gauge group is equivalent to type IIB string theory on $AdS_5 \times S^5$. The duality was motivated by heuristic argument where we consider a stack of N parallel $D3$ branes in type IIB string theory. At low energies the open strings stretched between the branes are described by $\mathcal{N} = 4$ SYM theory with $U(N)$ gauge group. For example, the displacement in the six transverse directions between brane a and b form six scalars $(\Phi^i)^a{}_b$ in the four dimensional brane-world for $i = 1, ..., 6$. The indices a, b make the scalars transform in the adjoint representation of $U(N)$. Ignoring the overall position of the branes we are left with an $SU(N)$ gauge theory. Far from the stack of branes we find closed strings in flat space. Open and closed strings decouple at low energies and the closed strings are described by ten dimensional supergravity. An alternative view on the system at low energies is to treat the collection of branes as a space-time defect. In the supergravity description this defect warps the space around it. Solving the field equations near the branes we find the $AdS_5 \times S^5$ geometry. On the other hand, away from the branes we find ten dimensional supergravity in flat background. We notice that the two descriptions away from the branes are the same. Similarly, we are lead to identify the two theories describing the system close to the branes to be equivalent.

$\mathcal{N} = 4$ SYM theory is parameterised by the coupling constant g_{YM} as well as the number of colours N. In the large N limit the effective expansion parameter of the gauge theory is $\lambda = N g_{YM}^2$, the t' Hooft coupling constant. In the context of the AdS-CFT duality, these parameters can be expressed in terms of the string parameters. Considering the physics of open strings attached to D-branes one finds

$$4\pi g_s = g_{YM}^2 = \frac{\lambda}{N}, \tag{1.1}$$

where g_s is the string coupling constant. The relation between the curvature of space, expressed in terms of the common radius R of AdS_5 and S^5, and the number of branes in the stack N reads

$$\frac{R^4}{\alpha'^2} = \lambda, \tag{1.2}$$

where α' parameterises the string tension. We notice that the string coupling is proportional to $1/N$ as anticipated by Gerard 't Hooft. Therefore, the planar limit of $\mathcal{N} = 4$ SYM corresponds to the free string theory. Furthermore, we notice that a strong coupling computation in the planar limit on the gauge theory side is mapped onto a saddle point calculation in the weakly curved AdS space.

Although the AdS-CFT duality has passed many checks, it still remains a conjecture. Its strongest form asserts that both theories are equivalent for all values of the coupling constant g_{YM} and any number of colours N. One of the simplest checks was to compare the global symmetries of both theories and the spectrum of protected operators that does not depend on the coupling constant [19].

One of the first non-trivial checks was devised by Berenstein, Maldacena and Nastase [20]. Their approach was to study operators with a large R-charge that are close to BPS. For example, we can take two complex scalar fields X and Z, and form an operator of the form $\mathrm{Tr}(X^S Z^J)$. For $J \gg S$ we can treat the X fields as impurities, therefore, we introduce the following limit

$$N \to \infty \qquad \text{and} \qquad J \to \infty \qquad \text{with} \qquad \frac{J^2}{N} \qquad \text{and} \qquad g_{YM} \qquad \text{fixed.} \tag{1.3}$$

In this limit the expansion parameter is λ/J^2, and as long as it is small we can trust the perturbation theory. This is the case even for large λ in the limit when $J \to \infty$. Therefore, one should naively be able to compare gauge theory results directly with strong coupling computations. The dual strings were considered in [21–26], where the classical integrability of the equations of motion was used extensively. The agreement between the spectrum of BMN operators [27] and the dual string states was found up to second orders in perturbation theory. Then, at the third order the order of limits problem appeared. Four point correlation functions of BMN operators without any impurities at strong coupling are studied in chapter 4 of this thesis.

The BMN limit provided the first explicit example of how the "impurities" propagating inside a closed single trace operator can reproduce the world sheet picture of a string. Soon after Minahan and Zarembo showed how to map such operators into the states of integrable spin chains [28]. This and the subsequent contributions enabled to harness the methods used until now for two dimensional integrable systems to find the spectrum of $\mathcal{N} = 4$ SYM [29–

36]. This fascinating developments culminated with the discovery of the quantum spectral curve [37, 38], which formulated the spectrum problem in terms of a Riemann-Hilbert problem for eight Q functions. One of the advantages of this approach is its efficiency in producing explicit results [39–41]. Currently, the challenge is to extend those methods to calculate the structure constants for the three point functions.

Integrability has also found its use in computation of other observables. In parallel there was a tremendous progress in calculating the scattering amplitudes in $\mathcal{N} = 4$ SYM. One of the first surprising simplicities was the incredibly compact Park-Taylor formula for the tree-level maximally helicity violating (MHV) amplitudes [42]. The recent progress started with Edward Witten's publication [43] that showed that the Park-Taylor formula has a natural interpretation in a particular twistor string theory. This insight resulted in the discovery of CSW rules [44] that enabled "sewing" MHV amplitudes to construct more complicated amplitudes, also at the loop level [45]. Among the many tools developed subsequently, an especially important one was the BCFW on-shell recursion relation [46]. Its extension to loop level allowed Nima Arkani-Hamed and his collaborators to write all-loop integrands for the scattering amplitudes in the planar $\mathcal{N} = 4$ SYM and subsequently presented it in terms of a surprisingly elegant structure named amplituhedron [47, 48]. The challenge in this approach is to take the integrand for the scattering amplitudes and actually perform the divergent integrals.

One of reasons for such a tremendous progress with scattering amplitudes was the discovery of dual conformal symmetry at the tree-level [10]. However, it was first observed at strong coupling in a computation of gluon scattering amplitudes. It was shown through a T-duality transformation that the computation is equivalent to a light-like Wilson loop calculation, and it reduces to finding a minimal area in AdS space [49]; a review can be found in [50]. In this setting, the dual conformal symmetry is the conformal symmetry of the Wilson loop. At loop level the dual conformal symmetry is broken by infrared divergences. Solving the corresponding conformal Ward identity [51] we find an expression for the amplitudes in terms of known BDS part proposed in [52] supplemented by a finite function of conformal invariants, usually presented in terms of the remainder function. Recently, there has been quite some progress finding the remainder function, see for example [53].

Another interesting property of $\mathcal{N} = 4$ SYM is an extended list of dualities between

different observables. In a typical gauge theory scattering amplitudes, Wilson loops and correlation functions quantify different aspects of the theory; however, in $\mathcal{N} = 4$ SYM they are all related by a set of dualities. We have already mentioned a duality relating scattering amplitudes and Wilson loops defined on polygonal light-like contours. It was first observed at strong coupling, and later it was shown to be the property of $\mathcal{N} = 4$ SYM at weak coupling as well [54–58][1]. Moreover, it was shown that, for a very generic gauge theory, a correlation function in the limit when the distances between the operators become null reduces to a Wilson loop [60].

The duality between scattering amplitudes and Wilson loops inspired considerable effort to compute the latter. A particularly promising approach was introduced by Benjamin Basso, Amit Sever and Pedro Vieira [61]. It treats Wilson loop as an evolution of a flux tube and employs the concept of a Wilson loop OPE [62] to expand the contributions in terms of a number of excitations which evolve on the flux tube. One of the recent impressive results was the computation of hexagonal Wilson loops at finite coupling [63].

1.3 Approach taken in this thesis

Hopefully, the previous section convinced the reader that there was a huge leap in understanding techniques to compute the spectrum and the scattering amplitudes in $\mathcal{N} = 4$ SYM. Extending these developments to correlation functions is the overarching aim of this thesis.

The idea pursued in chapters 2 and 3 was to develop tools for calculating observables that interpolate between light-like Wilson loops and correlation functions. In particular, the correlation function of a null Wilson loop with four edges and a local operator proved to be an interesting candidate. It is a function of just one variable/cross-ratio. Moreover, it can easily be made finite by dividing by the expectation value of the same null Wilson loop. Hence it might be an ideal quantity to attempt interpolating between weak and strong coupling.

The progress in computing scattering amplitudes described in the previous section was strongly driven by the strong coupling results. The reason was that even the zeroth order computation had almost all of the features of the fully interacting theory. Therefore, if we

[1] It turn out that there are some difficulties with a naive interpretation of this duality related to the way we regularise the divergences of the observables [59].

find any simplifications, it is very likely they will remain valid for any value of the coupling constant. Inspired by this insight, in chapter 4 we study the four point correlation function at strong coupling, the simplest correlation function that is not fixed by the conformal symmetry.

1.3.1 Original work and thesis overview

Here we would like to give an overview of the thesis together with a list of the original results we present.

In chapters 2 and 3 we study the correlation function of a null Wilson loop with four edges and a local operator. In chapter 2 the new results are the formula for the integrand up to two loops and the explicit expression at one loop in the integrated form. In section 3.2, we carry out the integrals at two loops, then, in section 3.3 we simplify the two loop integrand by presenting it in twistor form. Finally, in section 3.4, we show how to check the finiteness of the twistor diagram representation at two loops, and check the two loop answer by integrating over the inserted local operator recovering the three loop cusp anomalous dimension.

In chapter 4 we compute the four point correlation function of BMN operators on a line at strong coupling. In section 4.2, we start with presenting a fresh perspective on the results already produced by [64]. Section 4.3 contains a review of the χ-system presented in [3], however, section 4.3.13 presents a new simplification for the case we consider. Original results are presented in sections 4.4-4.7 and they include the following:

- **Section 4.4** The outcomes of imposing the Virasoro limit on the χ-system.
- **Section 4.5** The realisation of the crossing symmetry for the χ-system.
- **Section 4.6.1** A study of triangulation changes.
- **Section 4.6.2** An analytic solution for the self-dual point.
- **Section 4.6.3** An analytic treatment of the OPE limit of the χ-system for a special case.
- **Section 4.7** Numerical studies of the χ-system.
- **Section 4.7** The observation that the extended minimal surface is sub-dominant to the geodesic saddle point consisting of three consecutive two point functions.

In appendix A we give a brief review of the procedure of Lagrangian insertions in the context of $\mathcal{N} = 4$ SYM theory. This review is based on [65–67]. The main purpose is to provide the reader with the necessarily background for chapter 2.

Chapter 2

Perturbative correlation functions of null Wilson loops and local operators

In this chapter we consider the correlation function of a null Wilson loop with four edges and a local operator in planar maximally supersymmetric Yang-Mills theory. By applying the insertion procedure, developed for correlation functions of local operators, we give an integral representation for the result at one and two loops. We compute explicitly the one loop result.

2.1 Introduction

Correlation functions of gauge invariant local operators are the natural observables of any conformal field theory. Over the last few years, there has been rapid progress in the understanding and computation of correlations functions of $\mathcal{N}=4$ SYM, see for instance [65, 68, 69], and now explicit results, that would be impossible to obtain by standard Feynman diagram techniques, are available.

Given an $n-$point correlation function $\langle \mathcal{O}(x_1)...\mathcal{O}(x_n)\rangle$ an interesting limit to consider is the one where consecutive (after choosing a specific ordering) distances became null $x_{i,i+1}^2 \to 0$, at equal rate. It was argued in [60] that in such a limit one obtains

$$\lim_{x_{i,i+1}^2\to 0} \frac{\langle \mathcal{O}(x_1)...\mathcal{O}(x_n)\rangle}{\langle \mathcal{O}(x_1)...\mathcal{O}(x_n)\rangle_{\text{tree}}} = \langle W_{\text{adj}}^n[\mathcal{C}]\rangle \tag{2.1}$$

where $W_{\text{adj}}^n[\mathcal{C}]$ is a Wilson loop in the adjoint representation, over the null polygonal path $\mathcal{C}$, with cusps at x_i. This relation is quite general and does not require the theory to be planar. If we focus on a planar theory, as we will do in this thesis, then $\langle W_{\text{adj}}^n[\mathcal{C}]\rangle = \langle W_{\text{fund}}^n[\mathcal{C}]\rangle^2$, the square of a Wilson loop in the standard fundamental representation.

One can also consider a generalization of the above limit, in which all distances but one become null. It was argued in [70], see also [71, 72], that in this limit one obtains

$$\lim_{x_{i,i+1}^2\to 0} \frac{\langle \mathcal{O}(x_1)...\mathcal{O}(x_n)\mathcal{O}(y)\rangle}{\langle \mathcal{O}(x_1)...\mathcal{O}(x_n)\rangle} = \frac{\langle W^n_{\rm adj}[\mathcal{C}]\mathcal{O}(y)\rangle}{\langle W^n_{\rm adj}[\mathcal{C}]\rangle} \ . \tag{2.2}$$

On the right hand side we obtain the correlation function of a null Wilson loop with a local operator. This is a very interesting class of objects, in particular, they interpolate between a Wilson loop and a correlation function, and they are finite, since UV divergences in the numerator and denominator cancel out. The planar limit of a Wilson loop with operator insertions was discussed in detail in [71], where it was shown that $\langle W^n_{\rm adj}[\mathcal{C}]\mathcal{O}(y)\rangle \to 2\langle W^n_{\rm fund}[\mathcal{C}]\rangle\langle W^n_{\rm fund}[\mathcal{C}]\mathcal{O}(y)\rangle$. Hence, in the planar limit

$$\lim_{x_{i,i+1}^2\to 0} \frac{\langle \mathcal{O}(x_1)...\mathcal{O}(x_n)\mathcal{O}(y)\rangle}{\langle \mathcal{O}(x_1)...\mathcal{O}(x_n)\rangle} = 2\frac{\langle W^n_{\rm fund}[\mathcal{C}]\mathcal{O}(y)\rangle}{\langle W^n_{\rm fund}[\mathcal{C}]]\rangle} \tag{2.3}$$

In this chapter we will focus on the simplest case, where the polygonal null Wilson loop has four edges, *i.e.* $n = 4$. For simplicity of notation we will call $y \equiv x_5$. In this case conformal symmetry implies:

$$\frac{\langle W^4(x_1,x_2,x_3,x_4)\mathcal{O}(x_5)\rangle}{\langle W^4(x_1,x_2,x_3,x_4)\rangle} = \frac{1}{\pi^2}\frac{x_{13}^2\,x_{24}^2}{x_{15}^2\,x_{25}^2\,x_{35}^2\,x_{45}^2}F(x) \ , \tag{2.4}$$

where x is the only cross-ratio that can be constructed out of the location of the local operator x_5 and the location of the cusps x_i

$$x = \frac{x_{25}^2\,x_{45}^2\,x_{13}^2}{x_{15}^2\,x_{35}^2\,x_{24}^2} \, . \tag{2.5}$$

Hence $F(x)$ is a function of a single variable x, in addition to the coupling constant

$$a = \frac{g^2 N}{4\pi^2}. \tag{2.6}$$

From the definition of the cross-ratio and cyclic symmetry of the location of the cusps, we expect $F(x)$ to have "crossing" symmetry

$$F(x) = F(1/x) \tag{2.7}$$

For the case of $\mathcal{O} = \mathcal{L}_{\mathcal{N}=4}$, this function was computed in [70] at leading order both in the weak and strong coupling expansions:

$$F(x) = -\frac{a}{4} + ... \qquad \text{for } a \ll 1, \tag{2.8}$$

$$F(x) = \frac{x}{(1-x)^3}\left(2(1-x) + (x+1)\log x\right)\frac{\sqrt{a}}{2} + ... \qquad \text{for } a \gg 1. \tag{2.9}$$

We can see that both expressions satisfy the crossing symmetry (2.7). The aim of the present chapter is to compute $F(x)$ to higher orders in perturbation theory.

A related quantity, namely the four-point correlation function of the stress-tensor multiplet, has been extensively studied in the past as well as more recently and has now been explicitly computed at the integrand level to 6 loops [65, 68, 73–76]. This multiplet, in particular, contains the chiral Lagrangian of $\mathcal{N}=4$ SYM. Computations of the correlator have made extensive use of the method of Lagrangian insertions, reviewed in appendix A. This method relies on the observation that derivatives with respect to the coupling constant of any correlation function can be expressed in terms of a correlation function involving an additional insertion of the $\mathcal{N}=4$ SYM action. For instance,

$$a\,\frac{\partial}{\partial a}\,\langle \mathcal{O}(x_1)...\mathcal{O}(x_4)\rangle = \int d^4x_5\,\langle \mathcal{O}(x_1)...\mathcal{O}(x_4)\mathcal{L}_{\mathcal{N}=4}(x_5)\rangle\,. \tag{2.10}$$

This method is very powerful. By successive differentiation with respect to the coupling, it allows one to express the $\ell-$loop correction for the four-point correlation in terms of the integrated tree-level correlation function with ℓ additional insertions of the $\mathcal{N}=4$ SYM Lagrangian.

From the discussion above it is clear that a particular limit of those integrands will produce the integrands for $\langle \mathcal{O}(x_1)...\mathcal{O}(x_4)\mathcal{L}_{\mathcal{N}=4}(x_5)\rangle$ in the particular null limit we are interested in. This will give integrand expressions for loop corrections to $\langle W^4\mathcal{L}_{\mathcal{N}=4}(x_5)\rangle$.

In the next section we start by writing down those integral expressions. Then we compute the one-loop correction to $F(x)$ (proportional to a^2) and show that the two-loop correction (proportional to a^3) is finite. This is to be expected, but it is far from obvious from the integral expressions, since each integral diverges as $\frac{1}{\epsilon^4}$ in dimensional-regularization.

2.2 Explicit results

2.2.1 General expressions and one-loop result

Following the results of [65–67], which we review in appendix A, we introduce

$$\langle \mathcal{O}(x_1)...\mathcal{O}(x_4)\rangle = G_4 = \sum_{\ell=0}^{\infty} a^\ell\, G_4^{(\ell)}(1,2,3,4)$$

$$\langle \mathcal{O}(x_1)...\mathcal{O}(x_4)\mathcal{L}(x_5)\rangle = \frac{1}{4}\int d^4\rho_5\, G_{5;1} = \frac{1}{4}\sum_{\ell=0}^{\infty} a^{\ell+1}\int d^4\rho_5\, G_{5;1}^{(\ell)}(1,2,3,4,5)$$

here ρ is a Grassmann variable, $\mathcal{O}$ is the lowest component of the stress-tensor multiplet and $\mathcal{L}$ is the component proportional to ρ^4. We define the 't Hooft coupling constant $a = g^2N/(4\pi^2)$. The object we want to compute is then simply given by

$$\frac{\langle \mathcal{O}(x_1)...\mathcal{O}(x_4)\mathcal{L}(x_5)\rangle}{\langle \mathcal{O}(x_1)...\mathcal{O}(x_4)\rangle} = \frac{1}{4\,G_4}\int d^4\rho_5\, G_{5;1} \tag{2.11}$$

Expressions for $G_4^{(\ell)}$ and $G_{5;1}^{(\ell)}$ (in terms of certain functions to be defined bellow), can be found in [65]. In general, those depend on the insertion points, together with certain auxiliary harmonic variables y_i. In the null limit considered in this chapter, however, the dependence on the harmonic variables factors out, and goes away when taking the ratio (2.11). In the null limit we obtain

$$G_4^{(\ell)}(1,2,3,4) = \frac{2\,x_{13}^2\,x_{24}^2}{(-4\,\pi^2)^\ell}\,\frac{G_4^{(0)}}{\ell!}\int d^4x_5\ldots d^4x_{4+\ell}\,f^{(\ell)}(x_1,\ldots,x_{4+\ell}) \tag{2.12}$$

$$\int d^4\rho_5\, G_{5;1}^{(\ell)} = \frac{8\,x_{13}^2\,x_{24}^2}{(-4\,\pi^2)^{\ell+1}}\,\frac{G_4^{(0)}}{\ell!}\int d^4x_6\ldots d^4x_{5+\ell}\,f^{(\ell+1)}(x_1,\ldots,x_{5+\ell}) \tag{2.13}$$

which is consistent with the insertion formula

$$a\,\frac{\partial}{\partial a}\,G_4 = \frac{1}{4}\int d^4x_5\int d^4\rho_5\,G_{5;1}\,. \tag{2.14}$$

Finally we also need expressions for the f functions. These have a remarkably simple form [65]. At $1,2,3$ loops these are given by[1]

$$\begin{aligned}
f^{(1)}(x_1,\ldots,x_5) &= \frac{1}{x_{15}^2x_{25}^2x_{35}^2x_{45}^2}\,,\\
f^{(2)}(x_1,\ldots,x_6) &= \frac{\frac{1}{48}\sum_{\sigma\in S_6}x_{\sigma_1\sigma_2}^2x_{\sigma_3\sigma_4}^2x_{\sigma_5\sigma_6}^2}{(x_{15}^2x_{25}^2x_{35}^2x_{45}^2)(x_{16}^2x_{26}^2x_{36}^2x_{46}^2)x_{56}^2}\\
f^{(3)}(x_1,\ldots,x_7) &= \frac{\frac{1}{20}\sum_{\sigma\in S_7}x_{\sigma_1\sigma_2}^4x_{\sigma_3\sigma_4}^2x_{\sigma_4\sigma_5}^2x_{\sigma_5\sigma_6}^2x_{\sigma_6\sigma_7}^2x_{\sigma_7\sigma_3}^2}{(x_{15}^2x_{25}^2x_{35}^2x_{45}^2)(x_{16}^2x_{26}^2x_{36}^2x_{46}^2)(x_{17}^2x_{27}^2x_{37}^2x_{47}^2)(x_{56}^2x_{57}^2x_{67}^2)}\,.
\end{aligned} \tag{2.15}$$

These functions satisfy certain symmetries. Upon multiplication by the product of all external kinematic invariants $(x_{12}^2x_{13}^2x_{14}^2x_{23}^2x_{24}^2x_{34}^2)$ and for generic (non-null-separated) points, these functions are completely symmetric under interchange of any two points and can be written as $\frac{P^{(\ell)}(x_1,\ldots,x_{4+\ell})}{\prod_{1\le i<j\le 4+\ell}x_{ij}^2}$, where $P^{(\ell)}$ is a homogeneous polynomial in x_{ij}^2 of uniform weight $-(\ell-1)$ at each point. These properties hold at all loops in perturbation theory [65]. When taking the null limit the functions $f^{(\ell)}$ will have fewer terms, but some symmetries will be

[1] Note that the functions $f^{(\ell)}$ are multiplied by the overall factor $(x_{12}^2x_{13}^2x_{14}^2x_{23}^2x_{24}^2x_{34}^2)$ compared to the definition in [65].

lost.

Let us now consider the ratio (2.11) order by order in perturbation theory

$$\frac{\int d^4\rho_5\, G_{5;1}}{G_4} = \int d^4\rho_5 \left\{ a \left[\frac{G^{(0)}_{5;1}}{G^{(0)}_4}\right] + a^2 \left[\frac{G^{(1)}_{5;1}}{G^{(0)}_4} - \frac{G^{(0)}_{5;1}}{G^{(0)}_4}\frac{G^{(1)}_4}{G^{(0)}_4}\right] \right.$$
$$\left. + a^3 \left[\frac{G^{(2)}_{5;1}}{G^{(0)}_4} - \frac{G^{(1)}_{5;1}}{G^{(0)}_4}\frac{G^{(1)}_4}{G^{(0)}_4} - \frac{G^{(0)}_{5;1}}{G^{(0)}_4}\frac{G^{(2)}_4}{G^{(0)}_4} + \frac{G^{(0)}_{5;1}}{G^{(0)}_4}\left(\frac{G^{(1)}_4}{G^{(0)}_4}\right)^2\right] + \dots \right\} \tag{2.16}$$

Hence, at leading order in perturbation theory (proportional to a) we find

$$\left(\frac{\langle W^4\mathcal{L}\rangle}{\langle W^4\rangle}\right)^{(0)} = \frac{a}{8}\frac{\int d^4\rho_5\, G^{(0)}_{5;1}}{G^{(0)}_4} = \frac{a\, x_{13}^2 x_{24}^2}{(-4\,\pi^2)} \times f^{(1)}(x_1,\dots,x_5)$$
$$= \frac{a}{(-4\,\pi^2)}\frac{x_{13}^2 x_{24}^2}{x_{15}^2 x_{25}^2 x_{35}^2 x_{45}^2}\ , \tag{2.17}$$

which precisely agrees with the leading order result found in [70]. At next order we find

$$\left(\frac{\langle W^4\mathcal{L}\rangle}{\langle W^4\rangle}\right)^{(1)} = \frac{a^2}{(-4\,\pi^2)^2} \times x_{13}^2 x_{24}^2 \times \left[\int d^4x_6\, f^{(2)}(x_1,\dots,x_5,x_6)\right.$$
$$\left. - 2x_{13}^2 x_{24}^2\, f^{(1)}(x_1,\dots,x_5)\int d^4x_6\, f^{(1)}(x_1,\dots,x_4,x_6)\right] \tag{2.18}$$

In the light-like limit the numerator of $f^{(2)}$ becomes simply

$$\frac{1}{48}\sum_{\sigma\in S_6} x^2_{\sigma(1)\sigma(2)} x^2_{\sigma(3)\sigma(4)} x^2_{\sigma(5)\sigma(6)}$$
$$= x_{13}^2 x_{24}^2 x_{56}^2 + x_{15}^2 x_{36}^2 x_{24}^2 + x_{25}^2 x_{46}^2 x_{13}^2 + x_{35}^2 x_{16}^2 x_{24}^2 + x_{45}^2 x_{26}^2 x_{13}^2 \tag{2.19}$$

When integrating over x_6 in (2.18) we recognize two kinds of contributions

$$F(1,2,3,4) = -\frac{1}{4\pi^2}\int d^4x_6\, \frac{x_{13}^2 x_{24}^2}{x_{16}^2 x_{26}^2 x_{36}^2 x_{46}^2} \tag{2.20}$$
$$F(1,2,3,5) = -\frac{1}{4\pi^2}\int d^4x_6\, \frac{x_{13}^2 x_{25}^2}{x_{16}^2 x_{26}^2 x_{36}^2 x_{56}^2} \tag{2.21}$$

The first is the conformal massless box function, while the second is the two mass hard box function (since x_{51} and x_{53} are not null).[2] To be more precise, we have

$$\left(\frac{\langle W^4\mathcal{L}\rangle}{\langle W^4\rangle}\right)^{(1)} = \frac{a^2}{(-4\,\pi^2)} \times \frac{x_{13}^2 x_{24}^2}{x_{15}^2 x_{25}^2 x_{35}^2 x_{45}^2} \times \tag{2.22}$$
$$\times \Big(F(1,2,3,5) + F(4,1,2,5) + F(3,4,1,5) + F(2,3,4,5) - F(1,2,3,4)\Big)\ .$$

[2] These integrals are of course infrared divergent and need regularisation. The combination of these integrals we consider below will be finite however and so we do not specify a regulator. In practise we will use dimensional regularisation (where the x's are interpreted as dual momenta).

The first ($f^{(2)}$) term in (2.18) contributes a similar expression with all coefficients +1 whereas the second term in (2.18) subtracts a term proportional to $2F(1,2,3,4)$ thus swapping the sign of the last term.

The explicit expression for the box functions can be found for instance in [77, 78], where dimensional regularization is used. Even though each box function is divergent, the above combination is finite. Furthermore this combination is dual conformally invariant (see for example (2.23, 2.22) of [79] for the divergences and conformal variation of the box functions in dimensional regularization). Plugging the analytic expressions for the box functions and expanding up to finite terms we obtain

$$\left(\frac{\langle W^4\mathcal{L}\rangle}{\langle W^4\rangle}\right)^{(1)} = \frac{a^2}{(-4\,\pi^2)} \times \frac{x_{13}^2 x_{24}^2}{x_{15}^2 x_{25}^2 x_{35}^2 x_{45}^2} \times \left(-\frac{1}{4}\right)\left(\log^2 x + \pi^2\right) \tag{2.23}$$

$$F(x) = \frac{a^2}{(-4)}\left(-\frac{1}{4}\right)\left(\log^2 x + \pi^2\right) \tag{2.24}$$

This result has homogeneous degree of transcendentality and the correct symmetry $F(x) = F(1/x)$.

2.2.2 Two-loop result

At $O(a^3)$ we have

$$\begin{aligned}\left(\frac{\langle W^4\mathcal{L}\rangle}{\langle W^4\rangle}\right)^{(2)} = \frac{1}{2}\frac{a^3 x_{13}^2 x_{24}^2}{(-4\,\pi^2)^3}\int d^4x_6\, d^4x_7 \Big(&f^{(3)}(x_1,\ldots,x_6,x_7) \\ &-4x_{13}^2x_{24}^2 f^{(2)}(x_1,\ldots,x_6)f^{(1)}(x_1,\ldots,x_4,x_7) - 2x_{13}^2x_{24}^2 f^{(1)}(x_1,\ldots,x_5)f^{(2)}(x_1,\ldots,x_4,x_6,x_7) \\ &+8(x_{13}^2x_{24}^2)^2 f^{(1)}(x_1,\ldots,x_5)f^{(1)}(x_1,\ldots,x_4,x_6)f^{(1)}(x_1,\ldots,x_4,x_7)\Big)\end{aligned} \tag{2.25}$$

The integrals which arise from this are a 2-mass pentabox, 2-mass (2 types) and massless double boxes, and products of massless and 2 mass boxes. All of these are illustrated in the figures. More specifically we have

$$\begin{aligned}\int d^4x_6\, d^4x_7\, \frac{f^{(3)}(x_1,\ldots,x_6,x_7)}{f^{(1)}(x_1,\ldots,x_5)} &= \sum_{16\text{ perms}}\Big(I_1 + I_2 + I_3 + I_4 + I_6 + I_7\Big) \\ \frac{x_{13}^2x_{24}^2x_{13}^2x_{24}^2}{f^{(1)}(x_1,\ldots,x_5)}\int d^4x_6 d^4x_7 f^{(2)}(x_1,\ldots,x_6)f^{(1)}(x_1,\ldots,x_4,x_7) &= \sum_{16\text{ perms}}\Big(I_5 + \frac{1}{2}I_6\Big) \\ x_{13}^2x_{24}^2\int d^4x_6\, d^4x_7\, f^{(2)}(x_1,\ldots,x_4,x_6,x_7) &= \sum_{16\text{ perms}}\Big(I_1 + I_5\Big) \\ (x_{13}^2x_{24}^2)^2\int d^4x_6\, d^4x_7\, f^{(1)}(x_1,\ldots,x_4,x_6)\, f^{(1)}(x_1,\ldots,x_4,x_7) &= \sum_{16\text{ perms}} I_5\end{aligned} \tag{2.26}$$

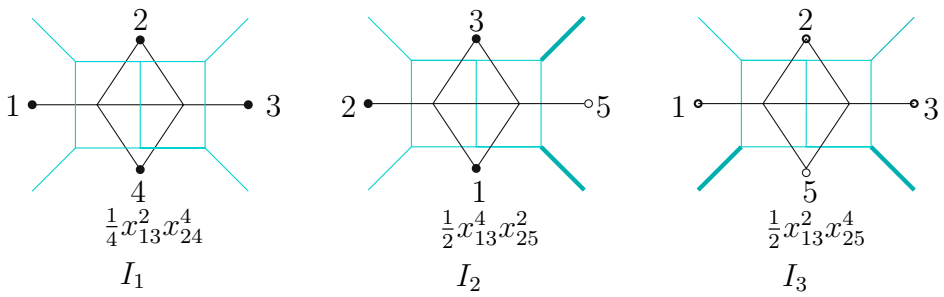

Figure 2.1: All contributing double box integrals at 2 loops with the corresponding numerator.

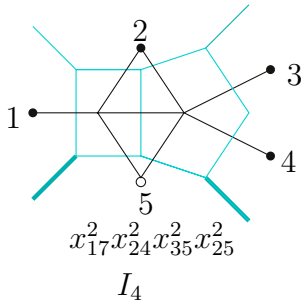

Figure 2.2: Two mass pentabox which contributes at 2 loops with the corresponding numerator.

where the sum over 16 permutations indicates that we must sum over 16 permutations generated by cycling the external points x_1, x_2, x_3, x_4, parity ($x_1 \leftrightarrow x_4,\ x_2 \leftrightarrow x_3$) together with swapping the internal coordinates x_6, x_7. These permutations will not always produce a different integrand (for example I_5 is completely symmetric under all such permutations). We have divided by the corresponding symmetry factor in the definition of the integral (see figures).

Putting this all together into (2.25) gives

$$\left(\frac{\langle W^4\mathcal{L}\rangle}{\langle W^4\rangle}\right)^{(2)} = \frac{1}{2}\frac{x_{13}^2x_{24}^2}{x_{15}^2x_{25}^2x_{35}^2x_{45}^2} \times \frac{a^3}{(-4\pi^2)^3} \times \\ \times \sum_{16\text{ perms}} \Big(- I_1 + I_2 + I_3 + I_4 + 2I_5 - I_6 + I_7 \Big)\,, \tag{2.27}$$

where $I_1, ..., I_7$ are obtained from eq. (2.26).

2.3 Conclusions

In this chapter we considered the correlation function of a local operator (the $\mathcal{N} = 4$ Lagrangian) with a four cusped null Wilson loop $\frac{\langle W^4\mathcal{O}(y)\rangle}{\langle W^4\rangle}$ in perturbation theory. This correlation function is expected to be finite, and conformal symmetry implies that the non-trivial

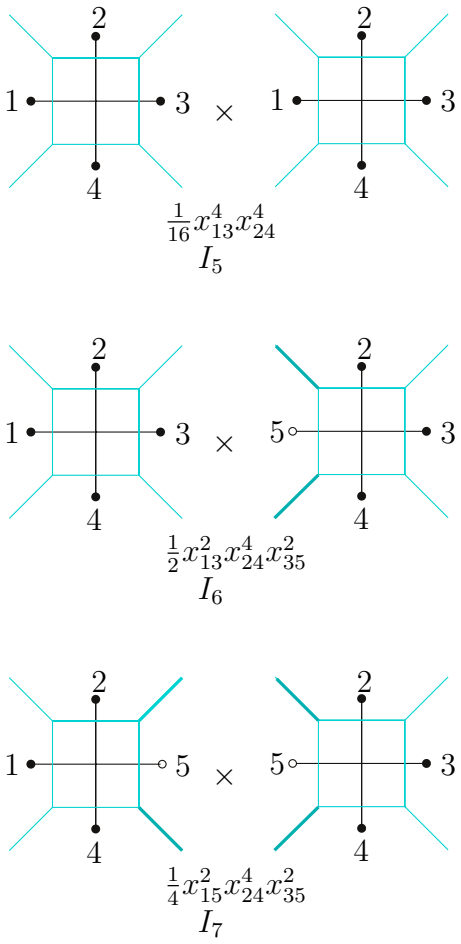

Figure 2.3: Three types of products of boxes which contribute at two loops with the corresponding numerator.

dependence is encoded in a function $F(x)$ of a single cross-ratio and the coupling constant. By using previous results on correlation functions, we computed $F(x)$ at one-loop in perturbation theory, obtaining

$$F(x) = -\frac{a}{4}\left(1 - \frac{1}{4}(\log^2 x + \pi^2)a + ...\right) \ . \tag{2.28}$$

Our result is consistent with crossing-symmetry $F(x) = F(1/x)$ and furthermore has the expected degree of transcendentality. Furthermore, we have given an integral representation for the two-loop contribution to $F(x)$. This is given in terms of seven integrals, including double boxes and pentaboxes, plus permutations. Even though each contribution diverges as $1/\epsilon^4$ in dimensional regularization, in the next chapter we argue that this particular combination is finite, and we calculate the two-loop contribution explicitly.

Chapter 3

Mixed correlation function at two loops

We compute analytically the two-loop contribution to the correlation function of the Lagrangian with a four-sided light-like Wilson loop in planar Maximally Super-symmetric Yang-Mills theory. As a non-trivial test of our result, we reproduce the three-loop value of the cusp anomalous dimension upon integration over the insertion point of the Lagrangian. The method we use involves calculating dual scattering amplitude. Moreover, we give a simple representation of the loop integrand of the latter in twistor variables.

3.1 Introduction and main results

Over the last few years there has been remarkable progress in the computation of observables in planar $\mathcal{N} = 4$ super Yang-Mills (SYM). These observables include the S-matrix, correlation functions of local operators, Wilson loops and combinations of these. An interesting class of observables is the correlation function of Wilson loops with local operators. In particular cases such correlators are fixed by the symmetries of the theory [80], but in general they contain useful dynamical information.

In this chapter we consider the simplest correlators not fixed by symmetries: the correlation function of a polygonal light-like (or null) Wilson loop with four edges and a local operator, which we take to be the Lagrangian $\mathcal{L}$ of the theory [70, 71]. Such a correlation function has ultraviolet (UV) divergences characteristic of light-like Wilson loops [51, 81]. In order to obtain a finite observable, we normalize this correlation function by the same correlator without the Lagrangian insertion. The finiteness of the ratio follows from the structure of UV divergences of light-like Wilson loops. Indeed our perturbative results agree

with this expectation.

Conformal symmetry implies that the overall scaling dimension of this observable is fixed. Moreover, it is a non-trivial function of one kinematic cross-ratio only,

$$\frac{\langle W_4(x_1,x_2,x_3,x_4)\mathcal{L}(x_5)\rangle}{\langle W_4(x_1,x_2,x_3,x_4)\rangle} = \frac{1}{\pi^2}\frac{x_{13}^2 x_{24}^2}{x_{15}^2 x_{25}^2 x_{35}^2 x_{45}^2} F(x)\,, \tag{3.1}$$

where $x_{ij}^2 = (x_i - x_j)^2$, and

$$x = \frac{x_{25}^2 x_{45}^2 x_{13}^2}{x_{15}^2 x_{35}^2 x_{24}^2} \tag{3.2}$$

is the only cross-ratio which can be formed by the locations of the cusps $x_1, ..., x_4$ (subject to the conditions $x_{12}^2 = x_{23}^2 = x_{34}^2 = x_{41}^2 = 0$), and the insertion point of the local operator x_5. Note that as a consequence of the symmetry under cyclic permutations of $x_{1,...,4}$, F satisfies the symmetry property $F(x) = F(1/x)$.

F also depends on the rank of the gauge group N and the 't Hooft coupling $\lambda = g^2 N$. We will consider F in the planar limit, where it has the perturbative expansion

$$F(x) = \sum_{L=1}^{\infty} \left(\frac{\lambda}{8\pi^2}\right)^L F^{(L-1)}(x)\,. \tag{3.3}$$

The first non-planar corrections can appear at four loops. The tree-level and one-loop contributions to F have been computed in [1, 70], with the result

$$F^{(0)}(x) = -\frac{1}{2}\,, \tag{3.4}$$

$$F^{(1)}(x) = \frac{1}{4}\left[\log^2 x + \pi^2\right]\,. \tag{3.5}$$

In this chapter, we compute analytically the two-loop contribution. We obtain

$$\begin{aligned} F^{(2)}(x) = -\frac{1}{8}\Bigg\{ &\frac{1}{2}\log^4 x + \log^2 x\Big[-\frac{2}{3}L_2(x) + 12\zeta_2\Big] + \log x\Big[-4L_3(x)\Big] \\ &+ \Big[-\frac{2}{3}(L_2(x))^2 - 8L_4(x) - 16\zeta_2 L_2(x) + 107\zeta_4\Big]\Bigg\}\,, \end{aligned} \tag{3.6}$$

where the functions

$$L_n(x) := \mathrm{Li}_n\left(\frac{1}{1+x}\right) + \mathrm{Li}_n\left(\frac{x}{1+x}\right) - \zeta_n\,, \quad n \text{ even}\,, \tag{3.7}$$

$$L_n(x) := \mathrm{Li}_n\left(\frac{1}{1+x}\right) - \mathrm{Li}_n\left(\frac{x}{1+x}\right)\,, \quad n \text{ odd}\,, \tag{3.8}$$

are manifestly symmetric (antisymmetric) under $x \to 1/x$ for n even (odd).

The correlation functions on the l.h.s. of eq. (3.1) can in principle be evaluated in configuration space. However, there is also a dual formulation of the same objects in terms of integrals resembling scattering amplitudes [60, 82]. In order to see this, one can think about loop corrections to the correlation functions being generated by Lagrangian insertions. Formally, i.e. neglecting regulator issues, one then has the integrand of an $(L+1)$-loop four-point scattering amplitude, with L integrations to be carried out. Since all divergences cancel in the ratio of eq. (3.1), one can argue that F can be also obtained from a dual calculation, where both numerator and denominator in eq. (3.1) are replaced by four-point on-shell scattering amplitudes, the numerator having an additional Lagrangian insertion. A representation of F in terms of scattering amplitude integrals was given in ref. [1]. Note that in this dual representation, UV divergences of the Wilson loop are transformed into infrared (IR) divergences of scattering amplitudes. Of course, the latter cancel in the final result for F.

The integrals one obtains are those for the scattering of four massless particles, but with the unusual feature of involving an operator insertion at the point x_5. If desired, one can use conformal symmetry of the Wilson loops (i.e. dual conformal symmetry in the scattering amplitude picture) to send this point to infinity.

We have performed the calculation both using dimensional regularization, as well as in a mass regularization set-up [83]. The quantity F is expected to be scheme independent, see [84], and indeed we verified (numerically) that both calculations gave the same finite result. We found that the calculation was simpler in the massive regularization, as expected based on previous experience with similar integrals [85, 86].

Over the last couple of years, twistor techniques have been tremendously successful in describing scattering amplitudes of $\mathcal{N} = 4$ SYM at weak coupling, both at the level of the integrand, see e.g. [87–90], and for obtaining analytic integrated expressions, [85, 86, 91, 92]. A natural question is whether such techniques will also be useful to understand correlation functions of local operators. As a step towards this, we give a simpler, twistorial representation of the integrand at two loops. This is closely related to similar simplifications observed when studying the exponentiation of scattering amplitudes [85]. This representation has several advantages, as we shall discuss. At the one-loop level, we see that the result can be

written in terms of a single finite integral. Being a one-loop integral, it is of course known. However, perhaps the simplest way of obtaining this result is to derive a differential equation [91] for this single-variable function, which can be readily solved. At two loops, we find a very compact representation in terms of five integrals, each of which has no subdivergences. We show that the remaining overall divergence cancels between the different terms. We find it likely that the differential equation technique of ref. [91] and related twistor-space methods will allow for a simpler evaluation of these integrals in the future.

Finally, another interesting feature of the above correlator is that by integrating over the point where the Lagrangian is inserted, we recover the expectation value of the four sided Wilson loop, and in particular, from its most divergent part, the light-like cusp anomalous dimension Γ_{cusp} [81]. Denoting the necessary infrared regulator by Λ, one obtains a formula (schematically)

$$\int_{\Lambda} \frac{d^4x_5}{i\pi^2} \frac{F(x)}{\prod_{j=1}^4 x_{j5}^2} \sim \lambda \frac{\partial}{\partial \lambda} \Gamma_{\text{cusp}} \, \log^2 \Lambda + \mathcal{O}(\log \Lambda) \,. \tag{3.9}$$

Regulator subtleties and the precise form of this identity for two different regularizations will be discussed in the body of the chapter. This allows to extract the cusp anomalous dimension from a finite quantity. Conversely, knowing the cusp anomalous dimension independently, we obtain an integral constraint on the result. We check that the perturbative results up to two loops as well as the strong coupling result, give rise to the correct value of the cusp anomalous dimension.

The outline of this chapter is as follows. In section 3.2 we describe how to obtain the analytic result at two loops from the integral representation previously found in [1]. In section 3.3 we give a twistorial representation for the loop integrals and in section 3.4 we show that by integrating over the insertion point of the local operator we reproduce the correct value of the cusp anomalous dimension. We end up with a summary of our results and outlook.

3.2 Analytic two-loop calculation from loop integrals

In this section we explain the procedure how we have obtained the explicit answer at two loops. We start by writing down the integrand up to two loops, already presented in section 2.2. In the second subsection we describe the steps we followed to obtain the explicit answer.

The hardest part of the calculation was resumming the asymptotic series to produce the answer. Therefore, in the third subsection give an explicit example how to resum the most complex part of the answer.

3.2.1 Expression in terms of loop integrals

The expression for F in terms of loop integrals has been written out in eq. 2.27. Converting to more standard conventions for Minkowski-space loop integrals, we have

$$\begin{aligned} F(x) = &-\frac{1}{2}\left(\frac{\lambda}{8\pi^2}\right) \\ &+\frac{1}{4}\left(\frac{\lambda}{8\pi^2}\right)^2 [F_{1235} + F_{4125} + F_{3415} + F_{2345} - F_{1234}] \\ &-\frac{1}{8}\left(\frac{\lambda}{8\pi^2}\right)^3 \sum_{8 \text{ perm}} \left[-\frac{1}{4}I_1 + \frac{1}{2}I_2 + \frac{1}{2}I_3 + I_4 + \frac{1}{8}I_5 - \frac{1}{2}I_6 + \frac{1}{4}I_7\right] . \end{aligned} \tag{3.10}$$

Here the 8 permutations refer to 4 cyclic permutations of the points x_1, x_2, x_3, x_4, and to the swap $x_1 \leftrightarrow x_4, x_2 \leftrightarrow x_3$.

The one- and two-loop integrals are shown in Fig. 3.1 and Fig. 3.2, respectively. In

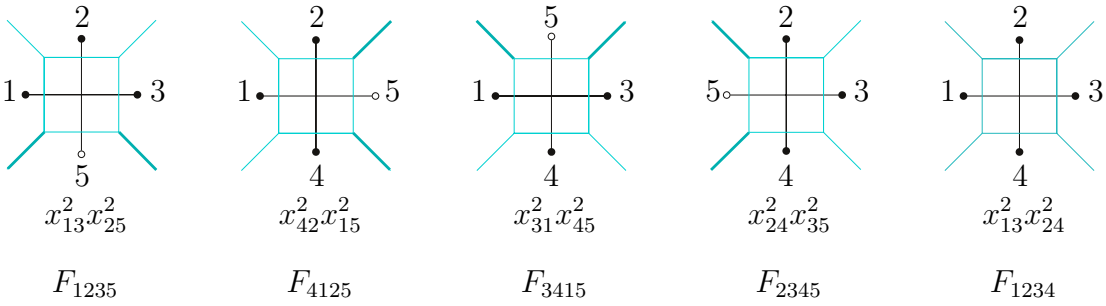

Figure 3.1: One-loop integrals contributing to $F^{(1)}$ with corresponding numerators. Below the diagrams, we write the corresponding factors that appear in the numerators of the form $x_{\dots}^2\, x_{\dots}^2$. The Fs label the diagrams.

dimensional regularization with $D = 4 - 2\epsilon$ and $\epsilon < 0$, they are defined by

$$F_{1235} = \int \frac{d^D x_6}{i\pi^{D/2}} \frac{x_{13}^2 x_{25}^2}{x_{16}^2 x_{26}^2 x_{36}^2 x_{56}^2} , \tag{3.11}$$

and

$$I_1 = \int \frac{d^D x_6 d^D x_7}{(i\pi^{D/2})^2} \frac{x_{13}^2 x_{24}^4}{x_{46}^2 x_{16}^2 x_{26}^2 x_{67}^2 x_{27}^2 x_{37}^2 x_{47}^2} , \tag{3.12}$$

and similarly for the remaining integrals.

Although the individual integrals are divergent, the final answer for F should be finite, as

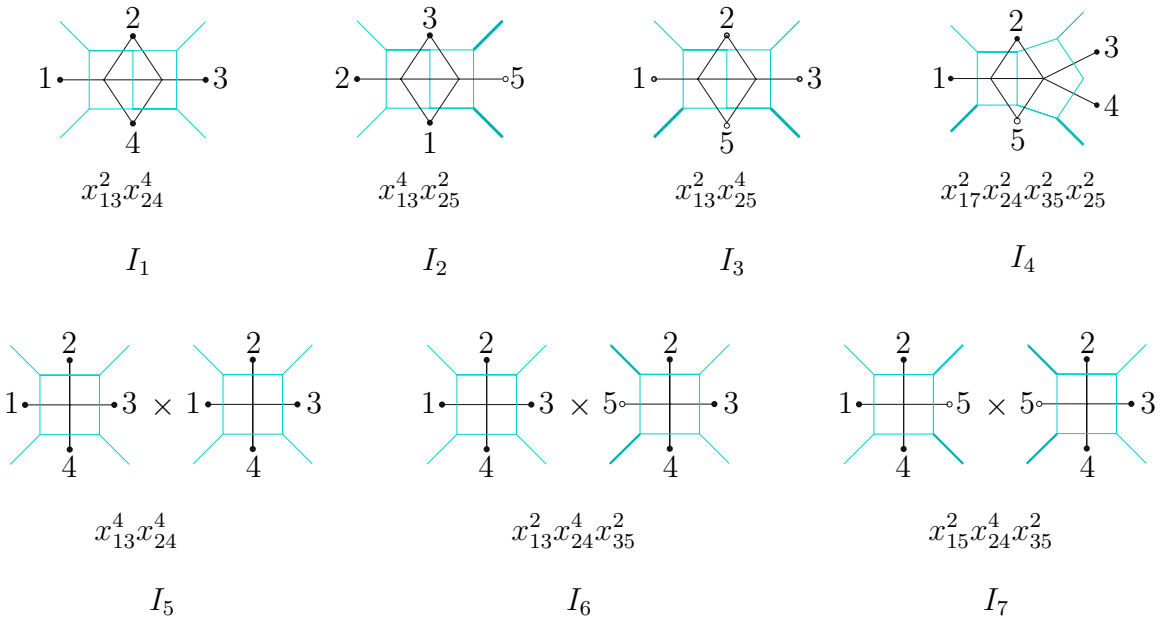

Figure 3.2: Two-loop integrals contributing to $F^{(2)}$ with corresponding numerators. Below the diagrams, we write the corresponding factors that appear in the numerators. The Is label the diagrams.

discussed in the introduction. We have performed the calculation in both dimensional regularization, as well as in a mass regularization set-up [83]. We found that the calculation was simpler in the massive regularization, as expected based on previous experience with similar integrals. Below we outline the steps that allow us to find an analytic answer in the massive regularization. We verify numerically that the calculation in dimensional regularization gives the same finite answer.

3.2.2 Description of calculation

In this subsection we would like to explain the steps we do to compute the explicit expression for the mixed correlator at two loops presented in eq. (3.6). Unfortunately, each intermediate step in the calculation is prohibitively long to be reproduced in detail; therefore, we confine ourselves to a summary of the steps taken.

The first step was to regularise the integrals in eq. (3.10) using both massive and dimensional regularisation. The next step was to transform those integrals into Mellin-Barnes (MB) representation as described in [93]. This was done by introducing Feynman parameters, which enabled us to perform the four dimensional loop integrations. Next, we introduce

the Mellin-Barnes parameters with

$$\frac{1}{(X+Y)^\lambda} = \frac{1}{\Gamma(\lambda)} \frac{1}{2\pi i} \int_{\gamma-i\infty}^{\gamma+i\infty} dz\, \Gamma(\lambda+z)\, \Gamma(-z) \frac{Y^z}{X^{\lambda+z}} \tag{3.13}$$

to get rid of the sums in the denominator. This, in turn, enabled us to carry out the integrals over Feynman parameters. At two loops we performed this operation twice introducing the MB parameters one loop at a time. This approach has the advantage that it is straightforward to automate and gives relatively compact answers.

Having obtained an expression in terms of (multiple) Mellin-Barnes integrals, we proceeded to extract the divergences as $\epsilon \to 0$ in dimensional regularization, or $m^2 \to 0$ in the massive regularization, respectively. In order to simplify the calculation, we used the fact that the answer is a conformally invariant. Therefore, it depends on x_i^μ only through the cross-ration x defined in eq. 3.2. Performing scaling limits such as e.g. $x_i \to \alpha\, x_i$, where we take $\alpha \to \infty$, leaves the cross-ratio and the function invariant, but it does simplify individual integrals. In taking several limits, we were able to simplify the expression to a point where one could verify the absence of divergences in $F^{(2)}(x)$ analytically.

We arrived at a representation for the finite part of $F^{(2)}(x)$ in terms of a number of one-fold Mellin-Barnes integrals, and one two-fold one. The only two-fold Mellin-Barnes integral we encountered is

$$\begin{aligned} I(x) = \int \frac{dz_1 dz_2}{(2\pi i)^2}\, x^{-1-z_1}\, \Gamma^2(-z_1)\, \Gamma^2(1+z_1)\, \Gamma(-z_2)\, \Gamma(1+z_2) \\ \times \Gamma(1+z_1-z_2)\, \Gamma(-1-z_1+z_2)\, (\Psi_0(z_2)+\gamma_E)\,, \end{aligned} \tag{3.14}$$

with $-1 < Re(z_1) < Re(z_2) < 0$, and Ψ_0 is the polygamma function $\Psi_n = \partial_z^{(n+1)} \log\Gamma(z)$.

One can also reduce this integral to a one-fold one, as we explain presently. First, one writes the polygamma functions as a derivative of a Γ function w.r.t. an auxiliary parameter,

$$\Gamma(1+z)\Psi_0(z) = \lim_{\delta_1\to 0} \frac{\partial}{\partial\delta_1} \Gamma(1+z+\delta_1) - \Gamma(z)\,. \tag{3.15}$$

Then one can see that the z_2 integration can be carried out using the first Barnes lemma. When doing this, it is useful to introduce another auxiliary parameter δ_2 in order to separate the left and right poles of

$$\Gamma(1+z_1-z_2)\,\Gamma(-1-z_1+z_2) \longrightarrow \lim_{\delta_2\to 0} \Gamma(1+z_1-z_2+\delta_2)\,\Gamma(-1-z_1+z_2+\delta_2) \tag{3.16}$$

and take $\delta_2 \to 0$ afterwards. Similarly, we resolved the poles for the term

$$\Gamma(-z_2)\,\Gamma(z_2) \longrightarrow \lim_{\delta_2 \to 0} \Gamma(-z_2+\delta_2)\,\Gamma(z_2+\delta_2). \tag{3.17}$$

In this way, we obtain a one-fold Mellin Barnes representation for $F^{(2)}$. At this stage, one can write the answer in terms of a series expansion that can be resummed. We give an explicit example in next subsection.

In this way, we arrived at our final result for $F^{(2)}$, which is given in eq. (3.6).

3.2.3 Evaluating Mellin-Barnes integrals.

In this section, we explain how to evaluate one of Mellin-Barnes integrals that arise in this chapter. In section 3.2.2, we introduced Mellin-Barnes representation of the two loop answer. Employing the conformal invariance of the answer, we were left with a number of one-fold and one two-fold Mellin-Barnes integrals. The two-fold integral is

$$\begin{aligned} I(x) = \int \frac{dz_1 dz_2}{(2\pi i)^2}\, x^{-1-z_1} \Gamma^2(-z_1)\Gamma^2(1+z_1)\Gamma(-z_2)\Gamma(1+z_2) \\ \times \Gamma(1+z_1-z_2)\Gamma(-1-z_1+z_2)(\Psi_0(z_2)+\gamma_E)\,, \end{aligned} \tag{3.18}$$

with $-1 < Re(z_1) < Re(z_2) < 0$, and Ψ_n is the polygamma function such that

$$\Psi_n = \partial_z^{(n+1)} \log\Gamma(z) \tag{3.19}$$

This integral can be reduced to one-fold integral with use of the first Barnes lemma with a little twist that we have just described in section 3.2.2. Taking particular care to separate right and left poles we obtain

$$\begin{aligned} I(x) = -\frac{1}{6}\int_{-\frac{1}{2}-i\infty}^{-\frac{1}{2}+i\infty} \frac{dz_1}{2\pi i} x^{-1-z_1}\Gamma(-1-z_1)\Gamma^2(-z_1)\Gamma^2(1+z_1) \\ \times \Big(6\Gamma(1+z_1)\big(2\gamma_E + \Psi_0(-1-z_1) + \Psi_0(1+z_1)\big) \\ + \Gamma(2+z_1)\big(\pi^2 - 6\gamma_E^2 - 12\gamma_E\Psi_0(2+z_1) - 6\Psi_0^2(2+z_1) - 6\Psi_1(2+z_1)\big)\Big) \end{aligned} \tag{3.20}$$

In the rest of this subsection, we will present how to evaluate this integral, as an example. We do it by expanding $I(x)$ in asymptotic series in the limit of $x \ll 1$ with a well-known procedure of closing the contour. Due to the factor of x^{-1-z_1} we close the contour on the left hand side of the complex plane. The first from the right pole of the integrand inside

the contour gives the leading contribution in the limit $x \ll 1$, the second gives the next-to-leading, etc. By summing residues corresponding to that series of poles we obtain the value of the integral for any value of x.

In order to extract those residues, we first simplify the integrand in eq. (3.20) with the use of the gamma function identities to

$$I(x) = \int_{-\frac{1}{2}-i\infty}^{-\frac{1}{2}+i\infty} \frac{dz_1}{2\pi i} \frac{\pi^3 x^{-1-z_1} \mathrm{Csc}^3(\pi z_1)}{6(1+z_1)} \Big(6\big(2\gamma_E(1+z1)-1\big)\Psi_0(1+z_1) - 6\Psi_0(-1-z_1) \\ (1+z1)\Big(6\gamma_E^2 - \pi^2 + 6\Psi_0^2(2+z_1) + 6\Psi_1(2+z_1)\Big)\Big). \tag{3.21}$$

The integrand in eq. (3.21) has poles at $z_1 \in \mathbb{Z}$ and involves polygamma functions with the following pole structure for $z \to n = 0, -1, -2, ...$

$$\begin{aligned} \lim_{z_1 \to n} \Psi_0(z_1) = &- \frac{1}{(z_1-n)} + \Big(S_1(-n) - \gamma_E\Big) + \Big(S_2(-n) + \zeta(2)\Big)(z_1-n) \\ &+ \Big(S_3(-n) - \zeta(3)\Big)(z_1-n)^2 + \Big(S_4(-n) + \zeta(4)\Big)(z_1-n)^3 + \mathcal{O}\big((z_1-n)^4\big) \\ \lim_{z_1 \to n} \Psi_1(z_1) = &\frac{1}{(z_1-n)^2} + \Big(S_2(-n) + \zeta(2)\Big) + 2\Big(S_3(-n) - \zeta(3)\Big)(z_1-n) \\ &+ 3\Big(S_4(-n) + \zeta(4)\Big)(z_1-n)^2 + \mathcal{O}\big((z_1-n)^3\big). \end{aligned} \tag{3.22}$$

From eq. (3.22) we see that the residues of the integrand at $z_1 = -1-i$ for $i \geq 1$ should involve the so-called S-series [94], which we define as

$$S_p(n) = \sum_{i=1}^{n} 1/i^p, \tag{3.23}$$

$$S_{p,r}(n) = \sum_{i=1}^{n} S(r)/i^p. \tag{3.24}$$

Using eq. (3.22) we find

$$\begin{aligned} &\mathrm{Residue}\big(z_1 = -1-k\big) = \\ &(-x)^k \Big(\frac{2}{k^4} - \frac{\log(x)}{k^3} + \frac{\pi^2}{3\,k^2} + \frac{\pi^2\log(x) + \log^3(x)}{6k} - \frac{\log^4(x)}{12} - \frac{\log^3(x) S_1(k)}{3} \\ &+ \log^2(x)\Big(S_2(k) - S_{1,1}(k) - \frac{\pi^2}{3}\Big) - 2\log(x)\Big(S_3(k) - S_{2,1}(k) - S_{1,2}(k) + \frac{\pi^2}{3}S_1(k)\Big) \\ &+ 2S_4(k) - 2S_{3,1}(k) - 2S_{2,2}(k) - 2S_{1,3}(k) - \pi^2 S_{1,1}(k) + \frac{2\pi^2 S_2(k)}{3} + 2S_1(k)\zeta(3) - \frac{7\pi^4}{45}\Big). \end{aligned} \tag{3.25}$$

All nested S-series, i.e. $S_{p,r}(n)$ in the above expression, originate from a product of two S-series, which we simplify with

$$S_j(n)\, S_k(n) = S_{j,k}(n) + S_{k,j}(n) - S_{k+j}(n). \tag{3.26}$$

Now, we would like to sum these residues. It turns out that those summations produce harmonic polylogarithms

$$\begin{aligned}
\sum_{i=1}^{\infty} \frac{(-1)^{i+1}x^i}{i^a} &= \begin{cases} H_{-a}(x) & \text{for } a > 0 \\ \frac{x}{1+x} & \text{for } a = 0 \end{cases} \\
\sum_{i=1}^{\infty} \frac{(-1)^{i+1}x^i}{i^a} S_b(i) &= \begin{cases} -H_{-a,-b}(x) + H_{-a-b}(x) & \text{for } a > 0 \\ \frac{1}{1+x} H_{-b}(x) & \text{for } a = 0 \end{cases} \\
\sum_{i=1}^{\infty} \frac{(-1)^{i+1}x^i}{i^a} S_{b,c}(i) &= \begin{cases} H_{-a,-b,-c}(x) - H_{-a,-b-c}(x) - H_{-a-b,-c}(x) + H_{-a-b-c}(x) & \text{for } a > 0 \\ -\frac{1}{1+x} H_{-b,-c}(x) + \frac{1}{1+x} H_{-b-c}(x) & \text{for } a = 0. \end{cases}
\end{aligned} \tag{3.27}$$

Summing the expression in eq. (3.25) from $i = 1$ to $i = \infty$ using eq. (3.27) and adding the residue at $z_1 = -1$, we found that the integral in eq. (3.18) in terms of harmonic polylogarithms is

$$\begin{aligned}
I(x) = {} & \frac{x \log^4(x)}{12\,(1+x)} - \frac{(x-1)\log^3(x)}{6\,(1+x)} H_{-1}(x) + \frac{\log^2(x)}{6\,(1+x)} \Big(2\pi^2 x - 6H_{-1,-1}(x)\Big) \\
& - \frac{\log(x)}{6\,(1+x)} \Big(6(1-x)H_{-3}(x) + (x-3)\pi^2 H_{-1}(x) - 12H_{-2,-1}(x) - 12H_{-1,-2}(x)\Big) \\
& + \frac{2(1-x)H_{-4}(x)}{1+x} - \frac{2H_{-3,-1}(x)}{1+x} - \frac{2H_{-2,-2}(x)}{1+x} - \frac{2H_{-1,-3}(x)}{1+x} \\
& - \frac{\pi^2 x H_{-2}(x)}{3(1+x)} - \frac{\pi^2 H_{-1,-1}(x)}{1+x} - \frac{2\zeta(3)H_{-1}(x)}{1+x} + \frac{\pi^4(-11+17x)}{180(1+x)}.
\end{aligned}$$

3.3 Twistorial representation

In the previous section we have presented the integrals that give us the observable under consideration up to second order and explained how to evaluate those using Mellin-Barnes methods. However, the set of Feynman integrals we used in eq. (3.10) has a drawback. Although the final answer is finite, each individual Feynman integral has divergences. Only when we sum all of the integrals together the dependence on the regulator drops out. On the other hand, we expect that a good choice of master integrals can significantly simplify calculations involving Feynman integrals. For example, introducing infrared finite master integrals into the set of basis of Feynman integrals, has both conceptual and practical advantages, see [85, 90, 91]. For example, one may hope that it will be easier in such representations to find powerful differential equations [91]. We give an example of this at the one-loop order. Recall that F is finite in four dimensions. We will therefore perform all manipulations in this section in four dimensions. When individual IR divergent parts of the answer are evaluated, it should go without saying that these should be regulated in a consistent way.

3.3.1 One loop

At one loop, one can use numerator identities described in [85] to express the one loop contribution to F in terms of a finite pentagon integral. This can be done directly in the dual space, but it is more convenient to switch to twistor space, which for the purpose of this section we can think of as a four-dimensional complex vector space. Here we will only present the necessary conventions and refer the reader to [87, 88, 90] for a more complete discussion. For any point x_i in the dual space we associate a line in twistor space e.g. to x_2 we associate a line denoted by (12) and spanned by two points Z_1 and Z_2 in twistor space (points in twistor space are described by 4 complex numbers $Z \in \mathbb{C}^4$). Similarly, to points x_5, x_6, x_7 we associate lines (AB), (CD), (EF). The points $x_1, ..., x_4$ define a null polygon, and so the corresponding lines in twistor space intersect. Therefore, it is natural to associate the point x_i for $i = 1, ..., 4$ with a line $(i-1\ \ i)$, where the number $i-1$ is defined modulo 4. In order to find the separations between the two points in the dual space, we use the antisymmetric four-bracket

$$x_{56}^2 \equiv (x_5 - x_6)^2 = \frac{\langle ABCD\rangle}{\langle AB\rangle\langle CD\rangle}, \tag{3.28}$$

where $\langle ABCD\rangle = \sum \epsilon_{ijkl} Z_A^i Z_B^j Z_C^k Z_D^l$ and $\langle AB\rangle = \langle AB I_\infty\rangle$, where I_∞ is the infinity twistor

$$I_\infty^{ij} = \begin{pmatrix} \epsilon^{\dot\alpha\dot\beta} & 0 \\ 0 & 0 \end{pmatrix} \tag{3.29}$$

Using eq. (3.28) we can rewrite our integrand in terms of twistor brackets. Moreover, as all integrals we deal with are conformally invariant, the dependence on I_∞ drops out and we are left only with the four-brackets. At one loop, the resulting expression for the integrand can be subsequently simplified by the following identity

$$\begin{aligned}\langle AB13\rangle\langle CD24\rangle + \langle AB24\rangle\langle CD13\rangle =& \langle 12AB\rangle\langle 34CD\rangle + \langle 34AB\rangle\langle 12CD\rangle \\ &- \langle 23AB\rangle\langle 41CD\rangle - \langle 41AB\rangle\langle 23CD\rangle - \langle 1234\rangle\langle ABCD\rangle\,. \end{aligned} \tag{3.30}$$

Eq. (3.30) is a special case of an identity described in [85]. Following the described steps, we end up with a very simple expression for the one loop integrand

$$\begin{aligned} F^{(1)} &= \frac{1}{4}\left(F_{1235} + F_{4125} + F_{3415} + F_{2345} - F_{1234}\right) \\ &= -\frac{1}{4}\int \frac{d^4 Z_{CD}}{i\pi^2} \frac{(\langle AB13\rangle\langle CD24\rangle + \langle AB24\rangle\langle CD13\rangle)\langle 1234\rangle}{\langle CD12\rangle\langle CD23\rangle\langle CD34\rangle\langle CD41\rangle\langle CDAB\rangle}. \end{aligned} \tag{3.31}$$

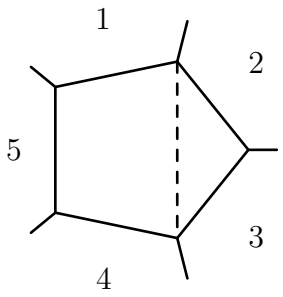

Figure 3.3: One-loop chiral integral contributing to $F^{(1)}$.

The chiral pentagon integral that we obtain in eq. (3.31) is presented in figure 3.3. For a generic value of x_{14}^2 it is given by

$$\Psi^{(1)}(u,v) = \log u \log v + \mathrm{Li}_2(1-u) + \mathrm{Li}_2(1-v) - \zeta_2 \tag{3.32}$$

with $u = x_{15}^2 x_{24}^2/(x_{25}^2 x_{14}^2)\,, v = x_{45}^2 x_{13}^2/(x_{35}^2 x_{14}^2)$. In the limit $x_{14}^2 \to 0$, both u and v diverge, with $v/u = x$ fixed. We find that

$$F^{(1)} = -\frac{1}{2}\lim_{x_{14}^2\to 0}\Psi^{(1)}(u,v) = \frac{1}{4}\left[\log^2 x + \pi^2\right]\,, \tag{3.33}$$

in perfect agreement with the one-loop result (3.5). Of course, this integral is so simple that it can be evaluated by many methods, e.g. using Feynman parameters, see e.g. [85, 92]. A much more elegant way of computing it is based on differential equations [91]. Here we wish to mention that the latter are compatible with the limit $x_{14}^2 = 0$. In other words, the differential equations of [91] directly apply to that case, and one obtains

$$x\partial_x x\partial_x F^{(1)}(x) = \frac{1}{2}\,. \tag{3.34}$$

This, together with the boundary condition $F^{(1)}(x \to -1) = 0$, which follows from inspection of the twistor numerator, leads to the result of eq. (3.33). It would be interesting to compute the integrals appearing at higher loop orders in a similar way.

3.3.2 Two loops

At two loops, we would like to find an identity, similar to eq. (3.30), that gives a chiral representation of the integrand, similar to eq. (3.31). In order to find such an identity, we proposed an ansatz for the integrand in terms of a set chiral integrals, that could potentially represent our integrand at two loops, with arbitrary coefficients. In order to fix the coefficients we performed quadruple cuts. Having determined all coefficients, we then checked the

equality of the two integrands analytically, by expanding out the twistor four-brackets. The representation we found is

$$F^{(2)} = \frac{1}{64} \sum_{8 \text{ perm}} \big(- I_a + 8I_b - 4I_c + 8I_d + I_e \big), \tag{3.35}$$

where the 8 permutations refer to 4 cyclic permutations of the points Z_1, Z_2, Z_3, Z_4, and swaps $Z_1 \leftrightarrow Z_4, Z_2 \leftrightarrow Z_3$. Here, I's are the chiral twistor integrals, presented in figure 3.4

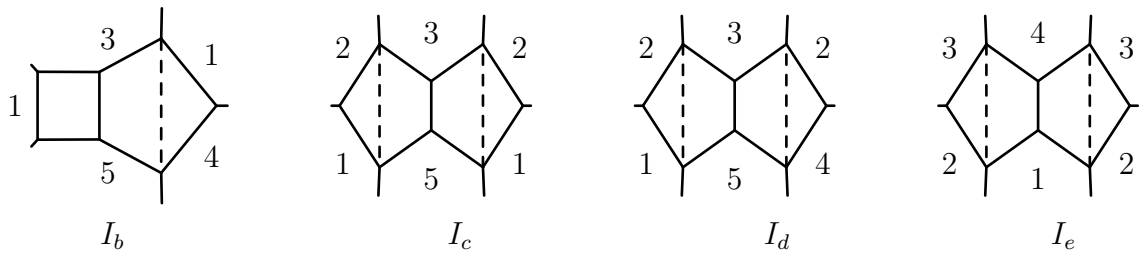

Figure 3.4: Twistorial representation of two-loop integrals contributing to $F^{(2)}$.

and are defined as follows

$$I_a = \int \frac{d^4Z_{CD}}{i\pi^2} \frac{d^4Z_{EF}}{i\pi^2} \frac{\langle AB13\rangle\langle CD24\rangle + \langle AB24\rangle\langle CD13\rangle}{\langle CD12\rangle\langle CD23\rangle\langle CD34\rangle\langle CD41\rangle\langle CDAB\rangle} \times \Big((CD) \leftrightarrow (EF)\Big)$$

$$I_b = \int \frac{d^4Z_{EF}}{i\pi^2} \frac{d^4Z_{CD}}{i\pi^2} \frac{\langle AB34\rangle\langle 1234\rangle\big(\langle EF13\rangle\langle AB24\rangle + \langle AB13\rangle\langle EF24\rangle\big)}{\langle CDAB\rangle\langle CD41\rangle\langle CD23\rangle\langle CDEF\rangle\langle EF23\rangle\langle EF34\rangle\langle EF41\rangle\langle EFAB\rangle}$$

$$I_c = \int \frac{d^4Z_{EF}}{i\pi^2} \frac{d^4Z_{CD}}{i\pi^2} \frac{\langle 1234\rangle\langle 12AB\rangle^2\big(\langle EF13\rangle\langle CD24\rangle + \langle EF24\rangle\langle CD13\rangle\big)}{\langle CDAB\rangle\langle CD41\rangle\langle CD12\rangle\langle CD23\rangle\langle CDEF\rangle\langle EF41\rangle\langle EF12\rangle\langle EF23\rangle\langle EFAB\rangle}$$

$$I_d = \int \frac{d^4Z_{EF}}{i\pi^2} \frac{d^4Z_{CD}}{i\pi^2} \frac{\langle 1234\rangle\langle 12AB\rangle\langle 23AB\rangle\big(\langle EF13\rangle\langle CD24\rangle + \langle EF24\rangle\langle CD13\rangle\big)}{\langle CDAB\rangle\langle CD41\rangle\langle CD12\rangle\langle CD23\rangle\langle CDEF\rangle\langle EF34\rangle\langle EF12\rangle\langle EF23\rangle\langle EFAB\rangle}$$

$$I_e = \int \frac{d^4Z_{CD}}{i\pi^2} \frac{d^4Z_{EF}}{i\pi^2} \frac{\langle 1234\rangle^3\big(\langle CD13\rangle\langle EF24\rangle + \langle CD24\rangle\langle EF13\rangle\big)}{\langle CD12\rangle\langle CD23\rangle\langle CD34\rangle\langle CD41\rangle\langle CDEF\rangle\langle EF12\rangle\langle EF23\rangle\langle EF34\rangle\langle EF41\rangle}.$$

I_a is just the chiral twistor integral, that we found at one loop in figure 3.3, squared.

3.3.3 Checking finiteness

Let us now discuss the finiteness properties of the new representation presented in eq. (3.35). I_a is the square of the one loop pentagon integral in figure 3.3, which is finite, and it is easy to see that I_b is also finite. Moreover, one can see that none of the integrals I_c, I_d, I_e has one-loop subdivergences. However, they do separately have overall double logarithmic infrared singularities. This is very similar to the behaviour of the logarithm of the four-particle amplitude discussed in [85]. Here, the remaining divergence cancels for the particular combination $\sum_{8 \text{ perm}}(-4I_c + 8I_d + I_e)$, making the final answer finite. Twistor space also makes it

easy to demonstrate the above statements about IR properties, and we devote the remainder of this subsection to show this.

In order to investigate the divergences of the integrals in figure 3.4 we adopt the parametrization used in [95]. The dual conformal integrals discussed in this chapter have only infrared divergences. These arise when the loop momentum becomes collinear with the momentum of an external massless particle. These limits can be conveniently parametrized in twistor space. For example, consider the integration variable x_6, which corresponds to Z_c and Z_d. One of the collinear limits is described by Z_c tending to Z_2, while Z_d tends to a generic point on the hyperplane spanned by Z_1, Z_2, Z_3,

$$Z_c \to Z_2 + \mathcal{O}(\epsilon) \tag{3.36}$$

$$Z_d \to \alpha_1 Z_1 + \alpha_2 Z_2 + \alpha_3 Z_3 + \mathcal{O}(\epsilon)\,. \tag{3.37}$$

For the present purpose, we also need to parametrize the $\mathcal{O}(\epsilon)$ terms. In doing so, we must make sure that the parametrization is generic enough. That is, we do not impose any additional constrains, which can make some factors vanish faster than in the generic case. On the other hand, we need to restrict the integration variable x_6 to be real. This corresponds to considering an integration bitwistor $Y^{IJ} = Z_c^{[I} Z_d^{J]}$ of the form

$$Y = \alpha_1\,(12) + \alpha_3\,(23) + \epsilon\left(\alpha_4\,(12) + \alpha_5\,(23) + \alpha_6\,(34) + \alpha_7\,(41)\right) + \mathcal{O}(\epsilon^2)\,. \tag{3.38}$$

Here the bracket (ij) denotes a line in twistor space spanned by Z_i and Z_j. Note that Y does not contain "non-local" terms like (13) or (24). Moreover, due to the fact that we are dealing with an integrand that is explicitly symmetric under cyclic permutations of $Z_1, ..., Z_4$ we only have to consider the collinear limit presented in eq. (3.38). Imposing that limit we confirmed that I_b vanishes while I_c, I_d, I_e diverge for generic α's as I_c, I_d, $I_e \sim \epsilon^{-1}$. However, the considered combination of integrals behaves as $\sum_{8\text{ perm}}(-4I_c + 8I_d + I_e) \sim \epsilon^0$. Therefore, it is finite in all collinear limits, even though I_c, I_d, I_e separately suffer from logarithmic divergences[1].

[1]It is very interesting to note that the combination $-4I_c + 8I_d + I_e$ is finite if and only if we sum over the four cyclic permutations.

3.3.4 Observation on two loop result

We would like to finish this section on chiral representation of integrands by making an interesting observation that relates the two loop result found in section 3.2 to finite integrals recently computed in the literature. Recall that sending x_5 to infinity via a conformal transformation our integrals become (in general non-planar) integrals for the scattering of four massless particles. The planar master integrals for such a process are all known, see [96] and references therein. Recently [97] computed two finite two-loop master integrals, called I_{++} and I_{+-} with double-box topology using twistor methods. It is interesting to note that these two functions together with their transforms $x \to 1/x$ are related to our two-loop result in the following way,

$$F^{(2)}(x) + 2\zeta(2)F^{(1)}(x) + \left(F^{(1)}(x)\right)^2 = \left[-\frac{1}{4}I_{++}(x) + \frac{1}{4}I_{+-}(x)\right] + \left[x \leftrightarrow \frac{1}{x}\right] + 3\zeta_3\,. \quad (3.39)$$

As is well-known, $3\zeta_3$ could also be written as a finite two-loop integral, see for example section 3.5. of [93]. It would be natural to absorb this into the definition of I_{++} and I_{+-}. We suspect that one can find a connection between the integrals for our observable from section 3.2 and the 4-point integrals computed in [97], by sending x_5 to infinity via a conformal transformation. However, further work needs to be done to clarify this point.

3.4 Relation to the light-like cusp anomalous dimension

The Lagrangian insertion procedure would naively imply

$$\int \frac{d^4x_5}{i\pi^2}\,\frac{F(x)}{x_{15}^2x_{25}^2x_{35}^2x_{45}^2} \overset{naively}{=} \lambda\frac{\partial}{\partial\lambda}\log\langle W_4\rangle\,. \quad (3.40)$$

We wrote "naively" because both sides of eq. (3.40) diverge double logarithmically, due to soft-collinear divergences. A valid equation can be written down within a given regularization. However, F is defined in the limit where the regulator tends to zero. Therefore, we can at most hope that re-instating a regulator in eq. (3.40) will allow us to compare the leading divergence of its l.h.s. and r.h.s..

As we will see, this can be successfully done using for example a massive regulator.

3.4.1 Massive regularization

Consider the four-particle scattering amplitude dual to the four-cusp Wilson loop, defined with a massive regulator, M_4 [83]. Based on the structure of infrared divergences of the latter, we expect the following equation to hold,

$$I_{m^2}[F] := \int \frac{d^4x_5}{i\pi^2} \frac{F(x)}{\prod_{i=1}^4 (x_{i5}^2 + m^2)} = \lambda \frac{\partial}{\partial \lambda} \log\langle M_4 \rangle + \mathcal{O}(\log m^2)\,. \tag{3.41}$$

Here we only need the leading infrared divergences of $\log\langle M_4 \rangle$, which are given by (see e.g. [84, 98])

$$\log\langle M_4 \rangle = -\frac{1}{2} \log^2 m^2\, \Gamma_{\text{cusp}} + \mathcal{O}(\log m^2)\,, \tag{3.42}$$

with the cusp anomalous dimension

$$\Gamma_{\text{cusp}} = \sum_{L=1}^{\infty} \left(\frac{\lambda}{8\pi^2}\right)^L \Gamma_{\text{cusp}}^{(L)}\,, \tag{3.43}$$

$$= 2\left(\frac{\lambda}{8\pi^2}\right) - 2\zeta_2 \left(\frac{\lambda}{8\pi^2}\right)^2 + 11\zeta_4 \left(\frac{\lambda}{8\pi^2}\right)^3 + \mathcal{O}(\lambda^4)\,. \tag{3.44}$$

One might worry that eq. (3.41) does not make sense, since we did not keep the dependence on m^2 in F. However, one can argue that this additional dependence will not affect the leading divergence.

We wish to verify the above relation (3.41) using our result for $F^{(2)}$. In order to do this, it is convenient to compute the auxiliary integral

$$\int \frac{d^4x_5}{i\pi^2} \frac{x^p}{\prod_{i=1}^4 (x_{i5}^2 + m^2)} = 2\log^2 m^2\, \frac{\sin(\pi p)}{\pi p} + \mathcal{O}(\log m^2)\,. \tag{3.45}$$

This formula is derived for $|p| < 1$, but can be extended to other values of p by analytic continuation. Due to the $x \to 1/x$ symmetry of F we can assume $0 < x < 1$ without loss of generality. Then, we write $F(x)$ as a series in x around 0 and use eq. (3.45) to perform the integration.

In doing so, one sees that only constants and logarithmically enhanced terms in F contribute to the cusp anomalous dimension. Note however that we do need to keep terms like $\log^k(x)x^n$, to all orders in n.[2] The one- and two-loop calculations are elementary. Technical

[2] An instructive example of this is the function $\log(x/(1+x))\log(1+x)$, which could have appeared at two loops. Although it vanishes as $x \to 0$ (and as $x \to \infty$, due to the inversion symmetry), it would give a contribution of ζ_2 to the cusp anomalous dimension.

details of the three-loop calculation are given in the following two subsections. To three loops, we find

$$I_{m^2}[F] = \log^2 m^2 \left[-\left(\frac{\lambda}{8\pi^2}\right) + \frac{1}{3}\pi^2 \left(\frac{\lambda}{8\pi^2}\right)^2 + \frac{33}{2}\zeta_4 \left(\frac{\lambda}{8\pi^2}\right)^3 + \mathcal{O}(\lambda^4) \right] + \mathcal{O}(\log m^2)\,. \tag{3.46}$$

Taking into account eqs. (3.42) and (3.43), we see that this is in perfect agreement with eq. (3.41).

3.4.2 Integration of $F(x) = x^p$ over the insertion point

We would like to compute the leading divergent term of the following integral

$$I_D(p) = st \int \frac{d^D y}{i\pi^2} \frac{x^p}{\prod_{i=1}^4 |y - x_i|^2}$$

where $D = 4 - 2\epsilon$ and recall that $x = (x_{25}^2 x_{45}^2 x_{13}^2)/(x_{15}^2 x_{35}^2 x_{24}^2)$. This integral is finite in the range $-1 < p < 1$. Using Feynman parameters we obtain

$$\frac{x^p}{\prod_{i=1}^4 |y - x_i|^2} = \frac{6}{\Gamma^2(1+p)\Gamma^2(1-p)} \left(\frac{s}{t}\right)^p \int_0^\infty d\alpha_1 ... d\alpha_4\, \delta(\sum \alpha_i - 1)\, \frac{(\alpha_1\alpha_3)^p (\alpha_2\alpha_4)^{-p}}{(\sum_i \alpha_i (y - x_i)^2)^4}.$$

where we have introduced $s = x_{13}^2, t = x_{24}^2$. After performing the Wick rotation, the integral over the insertion point y can be readily done, and we obtain

$$I_D(p) = \frac{\pi^{(D-4)/2}\,\Gamma(4 - D/2)}{\Gamma^2(1+p)\Gamma^2(1-p)} s^{1+p} t^{1-p} \int d\alpha\; \delta(\sum \alpha_i - 1)\, \frac{(\alpha_1\alpha_3)^p (\alpha_2\alpha_4)^{-p}}{(\alpha_1\alpha_3 t + \alpha_2\alpha_4 s)^{4-D/2}}. \tag{3.47}$$

Now we introduce new variables (see e.g. [93]) $\alpha_1 = \eta_1\zeta_1, \alpha_2 = \eta_1(1-\zeta_1), \alpha_3 = \eta_2\zeta_2$ and $\alpha_4 = \eta_2(1-\zeta_2)$. The Jacobian is simply $\eta_1\eta_2$ and the delta-function constraint implies $\eta_1 + \eta_2 = 1$. The integration over η_1, η_2 can be easily done and we are left with

$$I_{D=4-2\epsilon} = \frac{\pi^{-\epsilon}\Gamma^2(-\epsilon)\Gamma(2+\epsilon)}{\Gamma(-2\epsilon)\Gamma^2(1+p)\Gamma^2(1-p)} s^{1+p} t^{1-p} \int_0^1 d\zeta_1 d\zeta_2 \frac{(\zeta_1\zeta_2)^p ((1-\zeta_1)(1-\zeta_2))^{-p}}{(s\zeta_1\zeta_2 + t(1-\zeta_1)(1-\zeta_2))^{2+\epsilon}}\,.$$

We can separate the s, t dependence by using the Mellin-Barnes representation

$$\frac{1}{(X+Y)^\lambda} = \frac{1}{\Gamma(\lambda)} \frac{1}{2\pi i} \int_{\gamma - i\infty}^{\gamma + i\infty} dz \frac{Y^z}{X^{\lambda+z}} \Gamma(\lambda + z)\Gamma(-z) \tag{3.48}$$

and performing the integration over ζ_1 and ζ_2. We are left with

$$I_{D=4-2\epsilon} = \frac{\sin^2(p\pi)}{(\pi p)^2 \pi^\epsilon s^{2+\epsilon}} \frac{s^{1+p} t^{1-p}}{\Gamma(-2\epsilon)} \frac{1}{2\pi i} \int_{\gamma - i\infty}^{\gamma + i\infty} dz \left(\frac{t}{s}\right)^z \Gamma^2(1-p+z)\Gamma(2+z+\epsilon)\Gamma(-z)\Gamma^2(-1+p-z-\epsilon)$$

The contour of integration has to be chosen such that all the poles of $\Gamma(... + z)$ are to the left and the poles of $\Gamma(... - z)$ are to the right. We see that the contour is 'trapped' between the poles of $\Gamma^2(1 - p + z)$ and $\Gamma^2(-1 + p - z - \epsilon)$. After analytically continuing the contour (and thereby picking up a residue), we can take the limit $\epsilon \to 0$. We obtain

$$I_{D=4-2\epsilon}(p) = \frac{\sin \pi p}{\pi p} \frac{4}{\epsilon^2} + \mathcal{O}(\epsilon^{-1}) \tag{3.49}$$

The limit $p \to 0$ exactly reproduces the divergence of the massless scalar box function, as expected.

3.4.3 Three-loop cusp anomalous dimension from integration over $F^{(2)}$.

Here we give details of the evaluation of the integral over the insertion point in eq. (3.41). We found it technically useful to rewrite eq. (3.6) in terms of the more general class of harmonic polylogarithms [99],

$$\begin{aligned} F^{(2)}(x) = -\frac{1}{8}\Big[&24\zeta_2 H_{-1,-1}(x) - 12\zeta_2 H_{-1,0}(x) + 24\zeta_2 H_{0,0}(x) - 4H_{-2,0,0}(x) \\ &+ 8H_{-1,-1,0,0}(x) - 4H_{-1,0,0,0}(x) + 12H_{0,0,0,0}(x) - 12\zeta_2 H_{-2}(x) \\ &+ 8\zeta_3 H_{-1}(x) - 4\zeta_3 H_0(x) + 107\zeta_4\Big]. \end{aligned} \tag{3.50}$$

This has the advantage that it is straightforward to make the logarithmic dependence of $F^{(2)}$ manifest. We have (e.g. using the algorithm implemented in ref. [100])

$$\begin{aligned} F^{(2)}(x) = -\frac{1}{8}\Big\{&\frac{1}{2}\log^4 x + 12\zeta_2 \log^2 x - 4\zeta_3 \log x + 107\zeta_4 \\ &+ \log^3 x \left[-\frac{2}{3} H_{-1}(x)\right] \\ &+ \log^2 x \left[4H_{-1,-1}(x)\right] \\ &+ \log x \left[-8H_{-2,-1}(x) - 8H_{-1,-2}(x) - 12\zeta_2 H_{-1}(x) + 4H_{-3}(x)\right] \\ &+ \left[24\zeta_2 H_{-1,-1}(x) + 8H_{-3,-1}(x) + 8H_{-2,-2}(x) + 8H_{-1,-3}(x) + 8\zeta_3 H_{-1}(x) - 8H_{-4}(x)\right]\Big\}. \end{aligned} \tag{3.51}$$

In order to perform the integration over the insertion point, we proceed as follows. First, we can generate any logarithm from powers of x by differentiating formula (3.45) w.r.t. p. Second, we use the expansions of the harmonic polylogarithms encountered above in power

series around $x = 0$. We have (see [99])

$$H_{-n}(x) = -\sum_{i=1}^{\infty} \frac{(-1)^i x^i}{i^n}\,, \tag{3.52}$$

$$H_{-1,0,-1}(x) = \sum_{i=1}^{\infty} \frac{(-1)^i x^i}{i} S_2(i) - \sum_{i=1}^{\infty} \frac{(-1)^i x^i}{i^3}\,, \tag{3.53}$$

$$H_{-1,-1}(x) = \sum_{i=1}^{\infty} \frac{(-1)^i x^i}{i} S_1(i) - \sum_{i=1}^{\infty} \frac{(-1)^i x^i}{i^2}\,, \tag{3.54}$$

$$H_{0,-1,-1}(x) = \sum_{i=1}^{\infty} \frac{(-1)^i x^i}{i^2} S_1(i) - \sum_{i=1}^{\infty} \frac{(-1)^i x^i}{i^3}\,. \tag{3.55}$$

Here $S_p(n) = \sum_{i=1}^{n} 1/i^p$.

Following these steps, we see that the first line of eq. (3.51) gives a contribution of $56\zeta_4$ to $\Gamma^{(3)}_{\rm cusp}$. Moreover, the second, third, and forth lines contribute $-6\zeta_4, -2\zeta_4$ and $18\zeta_4$, respectively, while the last line does not contribute. Combining these formulas we straightforwardly obtain the result quoted in eq. (3.46).

3.4.4 Strong coupling

In ref. [70] the following answer for $F(x)$ was found at strong coupling,

$$F(x) = \frac{x}{(1-x)^3}\,[2(1-x) + (1+x)\log x]\,\frac{\sqrt{\lambda}}{4\pi} + \dots\,, \quad \lambda \gg 1\,, \tag{3.56}$$

We also note the value of the cusp anomalous dimension at strong coupling, see ref. [101, 102],

$$\Gamma_{\rm cusp} = \frac{\sqrt{\lambda}}{2\pi} + \dots\,, \quad \lambda \gg 1\,. \tag{3.57}$$

Let us now verify the relation between $F(x)$ and $\Gamma_{\rm cusp}$, using eq. (3.41).

We could employ the Mellin transform of $F(x)$, but we find it easier just to use a series expansion near $x = 0$. Recall that in this approach the non-logarithmically enhanced terms in $F(x)$ do not play a role. (They are needed however in order for $F(x)$ to be well-defined at $x \to 1$.)

There is a subtle point in this calculation, which concerns interchanging the expansion of $F(x)$ for small x and the space-time integration in eq. (3.45). If one does this naively, one obtains a sum of the type $\sum_{n\geq 0}(-1)^n$. A slightly more careful treatment, to be given presently, shows that this can be interpreted as $1/2 = 1/(1+1) = 1 - 1 + 1 - 1 + \dots$.

Let us first compute the integral over the insertion for some generating functions, for

which the convergence of the series is clear, and then differentiate w.r.t. certain parameters. In fact we will see that letting $x \to ax$ and using a as such a parameter will be sufficient. This will give a result valid for $a < 1$, which we can extend to $a \to 1$. Indeed, we find that with

$$g_1(x) = -x\,, \qquad g_2(x) = -\frac{x\log x}{1-x}\,, \qquad g_2(x) = -\frac{x^2\log x}{1-x}\,, \tag{3.58}$$

we can write

$$\frac{x}{(1-x)^3}\,[-2(1-x)-(1+x)\log x] = \lim_{a\to 1}\left[g_1(x) + \frac{\partial}{\partial a}g_2(ax) + \frac{\partial^2}{\partial^2 a}g_3(ax)\right]\,. \tag{3.59}$$

Moreover, we have, for $a < 1$,

$$I_{m^2}[g_1(ax)] = 0 + \mathcal{O}(\log m^2)\,, \tag{3.60}$$

$$I_{m^2}[g_2(ax)] = 2\log^2 m^2\,\log(1+a) + \mathcal{O}(\log m^2)\,, \tag{3.61}$$

$$I_{m^2}[g_3(ax)] = 2\log^2 m^2\,\left[-a + \log(1+a)\right] + \mathcal{O}(\log m^2)\,, \tag{3.62}$$

so that we arrive at

$$I_{m^2}\left[\frac{x}{(1-x)^3}\,[-2(1-x)-(1+x)\log x]\right] = \frac{1}{2}\,\log^2 m^2\, + \mathcal{O}(\log m^2)\,. \tag{3.63}$$

Comparing to eq. (3.41) and (3.42), we find perfect agreement with the strong coupling value of the cusp anomalous dimension given in eq. (3.57).

3.5 Summary and outlook

In this chapter we considered the correlation function of a local operator (the Lagrangian) with a four-sided null Wilson loop, in planar $\mathcal{N} = 4$ SYM. This is an interesting quantity due to several reasons: it is finite; it interpolates between a scattering amplitude/Wilson loop and a correlation function and it is a non-trivial function, not fixed by symmetries, of a single cross-ratio. Hence it is an ideal quantity to try to interpolate from weak to strong coupling.

We computed analytically the two loop contribution to the above observable. The result has the expected degree of transcendentality and reproduces the correct value of the cusp anomalous dimension. Furthermore, we have given a twistorial representation for the result,

which possesses several advantages.

There are several open problems. It would be interesting to understand better the limit $x_{i5}^2 \to 0$ at loop level. At tree-level, or, what is the same, the level of the loop integrands, this is related to a forward limit of a NMHV amplitude. It would be interesting if, despite regulator issues, the corresponding limit at loop level was related to results for loop-level NMHV amplitudes. The relevant six-point NMHV amplitudes are known analytically to the two-loop order [86]. More generally, one would like to understand different OPE limits of our mixed correlator and understand which quantities/anomalous dimensions can be obtained from the answer presented in this chapter. Finally, it would be extremely nice to guess a recursion relation/expression for this correlator, for instance by using twistor techniques along the lines of [72].

Chapter 4

Correlation functions of heavy operators on a line

In the final chapter we consider semi-classical computations of four point correlation functions of heavy operators on a line in planar $\mathcal{N} = 4$ supersymmetric Yang-Mills theory at strong coupling. We compute a contribution coming from an extended minimal surface saddle point using a TBA-like integrable model described by Caetano, Toledo in [3]. We show that the minimal surface saddle point is sub-dominant to another saddle point composed of three geodesic strings joining the four operators in sequence. We conclude that the considered four point function on a line to leading order at strong coupling is equal to its tree-level value.

4.1 Introduction

Among four dimensional quantum field theories the planar limit of $\mathcal{N} = 4$ super Yang-Mills theory (SYM) is a very special theory. It possesses an extended set of symmetries [10, 11], and it has been conjectured to be integrable and solvable. The possibility of the solving a non-trivial four dimensional interacting quantum field theory made the scientific community invest a lot of efforts in finding a set of methods for an efficient computation of the observables in this theory. In particular it is a four dimensional conformal field theory. As a result, the spacial dependence of its two and three point functions is fixed, and they are determined by a discrete set of numbers: the weights of the operators and the structure constants. It turns out this discrete set of numbers left unspecified in the two and three point functions is enough to define the fully interacting conformal field theory and reconstruct all higher point functions by summing appropriate OPE expansions. For this reason a considerable amount

of effort was put into calculating those numbers. The main efforts were concentrated on calculating the weights of the operators that determine the two point functions. They have culminated in the development of an efficient numerical algorithm to compute the spectrum of $\mathcal{N} = 4$ SYM at finite coupling in the planar limit [37, 38, 103], referred to as the quantum spectral curve.

The problem of finding the three point functions is in general much harder. It was initially considered in [104–107]. Later the procedure of "tailoring" was devised and enabled to calculate the three point function of single trace operators to first few orders in perturbation theory at weak coupling [108–113]. These results were further extended to operators in the semi-classical limit [114–116].

4.1.1 3-point functions and strong coupling

Another special feature of $\mathcal{N} = 4$ super Yang-Mills theory is its duality to type IIB string theory on $\mathrm{AdS}_5 \times S^5$ background [13–15]. This duality maps strong coupling computations in the planar limit on the gauge theory side onto a saddle point calculation in the free classical string theory. An example of such a computation was finding the explicit classical string solutions corresponding to two point function carried out by [117–119], which enabled the authors to find the two point functions to leading order at strong coupling.

Unfortunately, the saddle point solutions corresponding to three point functions correspond to quite complicated surfaces and have not yet been constructed for generic operators. The exceptions are special limits, for example, when the operators are heavy-heavy-light, the three point function can be evaluated as a two point function of two heavy operators "perturbed" by a light operator. These kind of 3-point functions were studied in quite detail by [120–133].

Another important exception is when the string configuration in the AdS space collapses into three geodesic strings glued together. For example the authors of [134–136] considered 3-point correlation functions of heavy (BMN) operators. They have shown that the string collapses, and they have constructed an explicit solution to the equation of motion with use of the Schwarz-Christoffel map. The explicit solution enabled the authors to find the three point functions to leading order at strong coupling. The calculation reveals that the corresponding 3-point function is given by its tree level value, and the structure constant

equal to one when we impose the R-charge conservation. We would also like to mention other important contributions in studying the three point functions [137–143].

4.1.2 3-point functions and classical integrability

A different approach to three point functions at strong coupling was proposed in [144] for the study correlation function of three heavy operators. The authors of [144] start by assuming that the string forms an extended string surface. Considering such an extended surface, the classical integrability of the string sigma model in $\mathrm{AdS}_5 \times S^5$ background enables one to express the area of the string in term of cycles on the string worldsheet. As a result, one does not need to find the shape of the string in order to find its area. Moreover, the authors have noticed that the computation factorises into the operator dependent sphere part, and a universal AdS part, coupled together by the stress-energy tensor. In [144] the authors calculate the universal AdS contribution to the area for generic semi-classical operators. For the case of BMN operators dual to the strings rotating in S^5 this can be combined with known expression for the sphere contribution [101] to produce the full expression for three point function. Once again, the calculation reveals that the string collapses and the corresponding 3-point function is given by its tree level value. A summery of this calculation in the notation, we present in this thesis, is presented in Appendix E of [3].

A similar study was performed for operators dual to the large spin limit of the GKP strings in [145, 146] and was later extended to the full SU(2) sector [147].

Even though two and three point functions are in principle all that is needed in order to reconstruct all higher point functions, in order to find higher point functions it is much more efficient to consider them directly. Inspired by the success in the null surface calculation for polygonal Wilson loop at strong coupling [148–151], which has been expressed as a finite set of integral equations that can be used to compute the area, the authors of [3] considered the four point function *i.e.* the first N-point function with a non-trivial space-time dependence, concentrating on the case of all operators on a line. Analogously to authors of [144], the exact shape of the string was not found. Instead they have presented a system of integral equations, which enables to compute the area of the string. The corresponding four point functions at weak coupling were considered in [64, 152].

In this work we take the construction presented in [3] and apply it to the case of BMN

operators. Our main aim is get a reliable numerical results for the four point function considered. To do this we need to compare the different saddle points, which arise for the four point function. We also need to check if the system can reproduce some simple properties like the OPE expansion and the crossing symmetry, and check if it is actually useful as a numerical tool for calculating the four point functions. Furthermore, we expect that investigating the four point function directly we might be able to uncover some interesting features of N-point functions that might be obscured in the language of two and three point functions.

4.2 General properties and weak coupling

The purpose of this section is to introduce the studied correlation function. We start with the symmetries and a set of convenient parameters to describe these correlators. Subsequently, we take a closer look at weak coupling limit. It was first calculated in [64], however, we present it in a different perspective relevant for the later comparison with the strong coupling computation.

4.2.1 Correlator and convenient parametrisation

In what follows we study the four-point correlation function in planar $\mathcal{N} = 4$ SYM of heavy operators *i.e.* operators with conformal weight $\mathbf{\Delta}$ of order $\sqrt{\lambda}$, where λ is the 't Hooft coupling constant, $\lambda = g_{\rm YM}^2 N$. We also define a scaled conformal weight Δ for future convenience

$$\mathbf{\Delta} \sim \mathcal{O}(\sqrt{\lambda}), \qquad\qquad \mathbf{\Delta} = \sqrt{\lambda}\,\Delta. \tag{4.1}$$

In particular, we consider

$$G_4(x_1, x_2, x_3, x_4) = \langle \mathcal{O}^{\mathbf{\Delta}_1}(x_1)\, \overline{\mathcal{O}}^{\mathbf{\Delta}_2}(x_2)\, \mathcal{O}^{\mathbf{\Delta}_3}(x_3)\, \overline{\mathcal{O}}^{\mathbf{\Delta}_4}(x_4) \rangle, \tag{4.2}$$

where the operators $\mathcal{O}^{\mathbf{\Delta}}(x) \sim \mathrm{Tr}\, Z^{\mathbf{\Delta}}(x)$ are often referred to as the BMN operators, and their conformal weights $\mathbf{\Delta}$ are protected from receiving any quantum corrections. The space-time conformal symmetry of $\mathcal{N} = 4$ SYM fixes the space-time dependence of the correlator as

$$G_4(x_1, x_2, x_3, x_4) = \mathcal{F}(u, v) \prod_{A>B}^{4} (x_{AB}^2)^{\mathbf{\Delta}_{AB}}, \tag{4.3}$$

where $x_{AB} = x_A - x_B$ and

$$\boldsymbol{\Delta}_{AB} = \Big(\sum_{C=1}^{4} \frac{\boldsymbol{\Delta}_C}{3}\Big) - \boldsymbol{\Delta}_A - \boldsymbol{\Delta}_B, \qquad u = \frac{x_{14}^2 x_{23}^2}{x_{13}^2 x_{24}^2}, \qquad v = \frac{x_{12}^2 x_{34}^2}{x_{13}^2 x_{24}^2}, \qquad q = \frac{u}{v}. \tag{4.4}$$

In this chapter we use Latin capital letters for the indices labelling the operators ($A, B, ... = 1, 2, 3, 4$). $\mathcal{F}(u, v)$ is a non-trivial function of the cross-ratios u and v, the coupling constant and the operator dimensions. In order for the tree-level correlator to be non-zero, we further specialise to the case with a net zero R-charge $\boldsymbol{\Delta}_1 + \boldsymbol{\Delta}_3 = 2\boldsymbol{\Delta} = \boldsymbol{\Delta}_2 + \boldsymbol{\Delta}_4$. We make this explicit by introducing ℓ and $\bar{\ell}$ parameters via

$$\boldsymbol{\Delta}_1 = \boldsymbol{\Delta}\,(1+\ell), \qquad \boldsymbol{\Delta}_2 = \boldsymbol{\Delta}\,(1+\bar{\ell}) \qquad \boldsymbol{\Delta}_3 = \boldsymbol{\Delta}\,(1-\ell), \qquad \boldsymbol{\Delta}_4 = \boldsymbol{\Delta}\,(1-\bar{\ell}). \tag{4.5}$$

In what follows we restrict ourselves to operators on a line

$$\sqrt{v} - \sqrt{u} = 1. \tag{4.6}$$

In this case, we can use a conformal transformation to choose

$$\vec{x}_1 = (0,0,0,0), \qquad \vec{x}_2 = (x_2,0,0,0), \qquad \vec{x}_3 = (1,0,0,0), \qquad \vec{x}_4 = (\infty,0,0,0), \tag{4.7}$$

and parametrise the cross-ratios in eq. (4.4) by x_2

$$u = (1-x_2)^2, \qquad v = x_2^2, \qquad q = \left(\frac{1-x_2}{x_2}\right)^2. \tag{4.8}$$

4.2.2 Weak coupling

At weak coupling, these correlators were studied in [64]. Here we cite the tree-level connected contribution up to a normalisation factor for $\ell \geq |\bar{\ell}| \geq 0$

$$\mathcal{F}^{\text{Tree}}(u,v) = u^{-\frac{2\boldsymbol{\Delta}}{3}+\boldsymbol{\Delta}\,(\ell+\bar{\ell})/2}\; v^{\frac{\boldsymbol{\Delta}}{3}-\boldsymbol{\Delta}\,(\ell+\bar{\ell})/2} \left((\ell+\bar{\ell}) + (\ell-\bar{\ell})\,q^{\boldsymbol{\Delta}_3} + \frac{q^{\boldsymbol{\Delta}_3}-q}{\boldsymbol{\Delta}\,(q-1)}\right). \tag{4.9}$$

We would like to point out that the first two terms in eq. (4.9) arise from diagrams with different topology than the last term, see fig. 4.1. These are the diagrams with two operators, $\text{Tr}\, Z^{\boldsymbol{\Delta}}$ and $\text{Tr}\, \bar{Z}^{\boldsymbol{\Delta}}$, with no Wick contractions directly from one to the other, see diagrams a) and b) in fig. 4.1. We call them the linear topology diagrams. On the other hand, the last term originates from the diagram with contractions between all pairs of $\text{Tr}\, Z^{\boldsymbol{\Delta}}$ and $\text{Tr}\, \bar{Z}^{\boldsymbol{\Delta}}$.

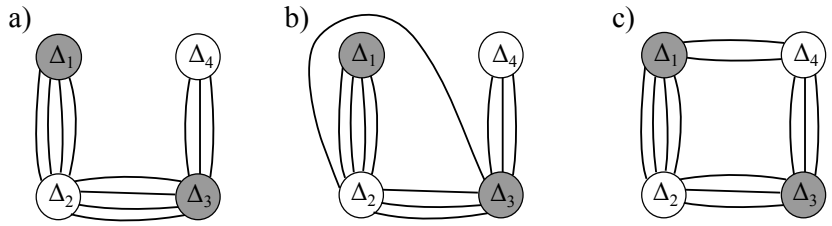

Figure 4.1: Tree level Wick contractions contributing to four-point function. Diagrams, a) and b), have a linear topology; they correspond to the first two terms in eq. (4.9). Diagram c) with a disc topology corresponds to the last term in eq. (4.9). The grey and white circles represent $\mathrm{Tr}\, Z^{\mathbf{\Delta}}$ and $\mathrm{Tr}\, \bar{Z}^{\mathbf{\Delta}}$ respectively.

We call it the disc topology contribution.

Furthermore, the authors of [64] observe that the one loop result is proportional to $\frac{q^{\mathbf{\Delta}_3}-q}{q-1}$,

$$\delta\mathcal{F}^{\text{1-loop}}(u,v) = -\frac{\lambda}{8\pi^2}\, u^{-\frac{2\mathbf{\Delta}}{3}+\mathbf{\Delta}\,(\ell+\bar{\ell})/2}\, v^{\frac{\mathbf{\Delta}}{3}-\mathbf{\Delta}\,(\ell+\bar{\ell})/2}\, \frac{q^{\mathbf{\Delta}_3}-q}{\mathbf{\Delta}\,(q-1)}\, \Phi(u,v), \tag{4.10}$$

$$\Phi(u,v) = \frac{|\log u|}{\sqrt{v}} + \frac{|\log v|}{\sqrt{u}} \qquad \text{when } \sqrt{v}-\sqrt{u}=1.$$

Hence it only corrects the disc topology contribution. It does not correct the contribution coming from diagrams with linear topology, which look like three independent two-point functions joined together. In other words, in the expansion around $q=0$, the q^0 term does not get corrected at one loop. Therefore, we can unambiguously differentiate between the linear topology contribution and the disk topology at one loop. We go even further and assume that we can differentiate the two even at any value of the coupling. Let us give an argument of why we think it is a reasonable assumption. In section 4.2.5 we argue that in the OPE expansion around $q=0$ the leading term is coming from exchange of operators of the form $\mathrm{Tr}\, Z^{\mathbf{\Delta}}(x)$ or $\mathrm{Tr}\, \overline{Z}^{\mathbf{\Delta}}(x)$. Therefore, the coefficient in front of the q^0 term is just the structure constant of the corresponding three point function squared. At strong coupling these structure constants were calculated to be equal to one in [144]. Because this coefficient is equal to one at weak and strong coupling we conjecture it stays one for all values of the coupling constant. Another point of view is to define the linear topology contribution as the one composed of three independent two-point functions joined together, where we stress the word independent. On the ground that two-point functions of protected operators in conformal field theory do not receive quantum corrections, we assert that also the linear topology contribution does not receive quantum corrections. As a result, we can

unambiguously differentiate the linear topology contribution from the disc topology one.

In the following subsections, we take a closer look at the properties of weak coupling results we have just presented.

4.2.3 Crossing symmetry

In the special case, when $\bar{\ell} = 0$, the result in eq. (4.9, 4.10) has an extra crossing symmetry. The operators at x_2 and x_4 are identical, and the correlator must be invariant under interchanging them. When we exchange the points $x_2 \leftrightarrow x_4$, the cross-ratios defined in eq. (4.4) interchange $u \leftrightarrow v$. Consequently, the non-trivial function of the cross-ratios defined in eq. (4.3) must satisfy

$$\mathcal{F}(u, v) = \mathcal{F}(v, u) \qquad \text{for } \bar{\ell} = 0. \tag{4.11}$$

It is easy to check that the correlator in eq. (4.9, 4.10) is invariant under the crossing symmetry. The disc topology terms are invariant just by themselves, and the two linear topology terms get swapped under the crossing transformation.

Furthermore, we would expect that for $\ell = 0$, the correlator must be invariant under interchanging operators at x_1 and x_3. That is indeed the case with the caveat that the result in eq. (4.9, 4.10) was written for $\ell \geq |\bar{\ell}| \geq 0$. Therefore, setting $\ell = 0$ automatically sets $\bar{\ell} = 0$ as well.

In eq. (4.8) we introduced a parametrisation of cross-ratios in terms of x_2 by conformally transforming to $x_1 = 0,\ x_2 \in \mathbb{R},\ x_3 = 1,\ x_4 = \infty$. In this parametrisation, the transformation that switches the cross-ratios must interchange x_2 and $1 - x_2$, see eq. (4.8). Hence, in our parametrisation the substitution $x_2 \to 1 - x_2$ is the crossing transformation. In section 4.5, we show that the correlator is invariant under such a transformation at strong coupling when $\ell = 0$ or $\bar{\ell} = 0$.

4.2.4 Dominant contribution for generic operators

In this section we would like to discuss the relative magnitude of the linear and the disc topology terms in eq. (4.9). We concentrate on the case when $\boldsymbol{\Delta}$ is large. This is because at strong coupling the heavy operators defined in section 4.2.1 have large conformal weights $\boldsymbol{\Delta}$. Therefore, it is particularly relevant to compare them to large $\boldsymbol{\Delta}$ results at weak coupling.

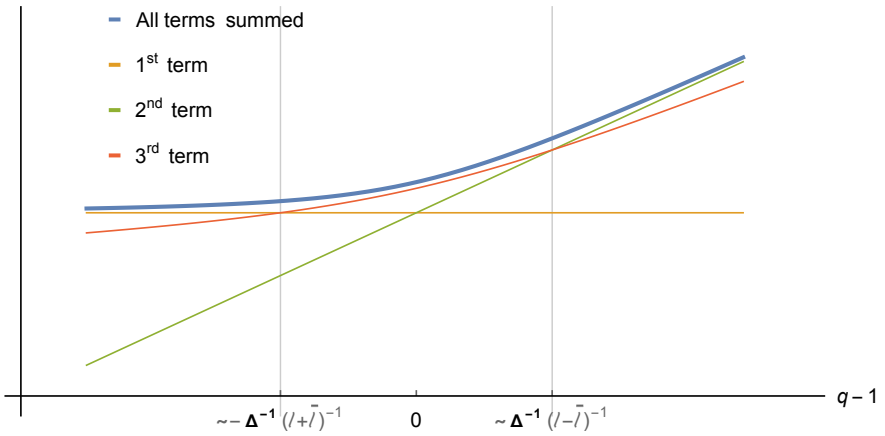

Figure 4.2: Log-log sketch of the magnitude of terms in the brackets in eq. (4.9) for large but finite $\boldsymbol{\Delta}$. For small q, the first term dominates. For large q, the second term dominates. For the intermediate values all three terms contribute.

For the sake of argument, let us consider large, but finite, $\boldsymbol{\Delta}$. For such $\boldsymbol{\Delta}$ we have sketched in fig. 4.2 the typical behaviour of the three different terms in bracket in eq. (4.9). For small q the first term in eq. (4.9) dominates the four-point function, whilst for large q it is the second term. Both regimes are dominated by a linear topology diagrams (*i.e.* diagrams a) and b) in fig. 4.1). In the intermediate regime, for $q \sim 1$, all three terms are of the same order in $\boldsymbol{\Delta}$, in particular the disc topology diagrams give a contribution of the same order.

Increasing $\boldsymbol{\Delta}$ shrinks the intermediate regime, which in the limit as $\boldsymbol{\Delta} \to \infty$ produces a cusp at $q = 1$, see fig. 4.2. It arises when the four-point function jumps from being dominated by the first term for $q < 1$ to being dominated by the second term for $q > 1$. To the leading order we have

$$\log \mathcal{F}^{\text{weak}}(u,v) = \left(-\frac{2}{3} + \frac{\ell+\bar{\ell}}{2}\right)\boldsymbol{\Delta}\log u + \left(\frac{1}{3} - \frac{\ell+\bar{\ell}}{2}\right)\boldsymbol{\Delta}\log v \qquad q<1, \tag{4.12}$$

$$\log \mathcal{F}^{\text{weak}}(u,v) = \left(\frac{1}{3} - \frac{\ell-\bar{\ell}}{2}\right)\boldsymbol{\Delta}\log u + \left(-\frac{2}{3} + \frac{\ell-\bar{\ell}}{2}\right)\boldsymbol{\Delta}\log v \qquad q>1.$$

At one loop the linear topology contribution becomes even more dominant. First, notice that the function $\Phi(u,v)$ in eq. (4.10) is always positive. Comparing eq. (4.9, 4.10) we see that the disc topology contribution gets modified by a factor of $1 - \frac{\lambda}{8\pi^2}\Phi(u,v)$, which is always smaller or equal to 1. This factor for small enough coupling constant makes the disc topology even more sub-dominant with respect to the linear topology contribution. At the same time, the linear topology terms are not corrected by any quantum corrections. As a

result, the expressions in eq. (4.12), which come only from the linear topology terms, are not corrected at the one loop. In fact eq. (4.12) is not corrected at any loop order as long as the disc topology terms are sub-dominant with respect to the linear topology terms in $\mathbf{\Delta}$. For that reason, we add the superscript "weak" in eq. (4.12).

4.2.5 Euclidean OPE limit

Another interesting property of the four-point function is the OPE limit. First, let us take two operators with the opposite sign of the R-charge close together. Due to the conformal symmetry, there are only two independent ways to do it. One can take the first and the second operator close $x_2 \to 0$, which means that $v \to 0,\ u \to 1$. The alternative is to take the second and the third operator close $x_2 \to 1$, which gives $v \to 1,\ u \to 0$. In these limits, using eq. (4.12), we obtain the leading order expressions

$$\log \mathcal{F}^{\text{weak}}(u,v) = \left(-\frac{4}{3} + \ell - \bar{\ell}\right) \mathbf{\Delta}\, \log x_2 \qquad x_2 \to 0, \tag{4.13}$$

$$\log \mathcal{F}^{\text{weak}}(u,v) = \left(-\frac{4}{3} + \ell + \bar{\ell}\right) \mathbf{\Delta}\, \log(1-x_2) \qquad x_2 \to 1.$$

We can also take two operators with the same sign of the R-charge close together. When $x_2 \to \infty$, we take second and fourth operator close. In these limits, eq. (4.12) gives

$$\log \mathcal{F}^{\text{weak}}(u,v) = -\frac{2\,\mathbf{\Delta}}{3}\, \log x_2 \qquad x_2 \to \infty. \tag{4.14}$$

Deriving the eq. (4.12-4.14), we have assumed that neither of the terms in brackets of eq. (4.9) vanish. However, when $\ell \neq \pm\bar{\ell}$, one of the linear topology terms vanishes. The corresponding diagram becomes two disconnected two-point functions and produces only a disconnected contribution, which is not included in eq. (4.9). As a result one would expect eq. (4.12-4.14) to change. However, the expressions in eq. (4.12-4.14) are true even when $\ell = \pm\bar{\ell}$. This is because the leading order behaviour of the disc topology contribution at tree-level and one loop in eq. (4.48, 4.10) is still captured by eq. (4.12-4.14). Only the subleading pieces in $\mathbf{\Delta}$ carry the information about which of the diagrams contribute to the correlator in the OPE limit.

We find another perspective on eq. (4.13, 4.14) by looking at the operator exchanged between the two pairs of operators. If we OPE expand the operators at x_1 and x_2 we get

$$\mathcal{O}^{\mathbf{\Delta}_1}(x_1)\, \overline{\mathcal{O}}^{\mathbf{\Delta}_2}(x_2) = \sum_{\mathcal{O}'} \frac{c_{\mathcal{O}^{\mathbf{\Delta}_1}\overline{\mathcal{O}}^{\mathbf{\Delta}_2}\mathcal{O}'}\, \mathcal{O}'(x_2)}{x_{12}^{\mathbf{\Delta}_1+\mathbf{\Delta}_2-\mathbf{\Delta}_{\mathcal{O}'}}}. \tag{4.15}$$

In the OPE limit, when $x_{12} \to 0$, the R-charge conservation implies that the leading term is

$$\mathcal{O}^{\mathbf{\Delta}_1}(x_1)\,\overline{\mathcal{O}}^{\mathbf{\Delta}_2}(x_2) \sim \frac{\mathcal{O}^{\mathbf{\Delta}_1-\mathbf{\Delta}_2}(x_2)}{x_{12}^{2\mathbf{\Delta}_2}} + \ldots \qquad \text{for } \mathbf{\Delta}_1 > \mathbf{\Delta}_2, \tag{4.16}$$

where $\mathcal{O}^{\mathbf{\Delta}_1-\mathbf{\Delta}_2} \sim \mathrm{Tr}\, Z^{\mathbf{\Delta_1}-\mathbf{\Delta_2}}$. All the other allowed terms are subleading in the OPE limit. Due to the conformal symmetry when $x_{12} \to 0$ we can also take $x_{34} \to 0$ and find

$$\mathcal{O}^{\mathbf{\Delta}_3}(x_3)\,\overline{\mathcal{O}}^{\mathbf{\Delta}_4}(x_4) \sim \frac{\overline{\mathcal{O}}^{\mathbf{\Delta}_4-\mathbf{\Delta}_3}(x_4)}{x_{34}^{2\mathbf{\Delta}_3}} + \ldots \qquad \text{for } \mathbf{\Delta}_3 < \mathbf{\Delta}_4, \tag{4.17}$$

Combining eq. (4.16-4.17), we find that in the OPE limit

$$\langle \mathcal{O}^{\mathbf{\Delta}_1}(x_1)\,\overline{\mathcal{O}}^{\mathbf{\Delta}_2}(x_2)\,\mathcal{O}^{\mathbf{\Delta}_3}(x_3)\,\overline{\mathcal{O}}^{\mathbf{\Delta}_4}(x_4)\rangle \sim \frac{1}{x_{12}^{2\mathbf{\Delta}_2} x_{24}^{2\mathbf{\Delta}_1-2\mathbf{\Delta}_2} x_{34}^{2\mathbf{\Delta}_3}}. \tag{4.18}$$

Using the conventions defined in sec 4.2.1, we find that eq. (4.18) reproduces eq. (4.13). Similarly, in the special case when $\mathbf{\Delta}_1 = \mathbf{\Delta}_2$, or equivalently $\mathbf{\Delta}_3 = \mathbf{\Delta}_4$, the leading term is the identity operator

$$\mathcal{O}(x_1)\,\overline{\mathcal{O}}(x_2) \sim \frac{\mathbb{1}}{x_{12}^{2\mathbf{\Delta}}} + \ldots \tag{4.19}$$

Again using the conventions defined in sec 4.2.1, we find that eq. (4.19) reproduces eq. (4.13) for the case when $\ell = \bar{\ell}$. Analogously, we can also reproduce eq. (4.14).

We notice that there is a jump between the general case of OPE in eq. (4.16, 4.17) when the exchanged operator is heavy and the special case in eq. (4.19) when the exchanged operator is light. Further, we note that we were able to reproduce eq. (4.13-4.14) assuming only that the leading operator exchanged in the Euclidean OPE limit must conserve R-charge. Therefore, the leading term in the OPE limit is fixed by the R-charge conservation.

4.2.6 Dominant contribution for special cases

When $\ell \neq \pm\bar{\ell}$, one of the linear topology terms vanishes, and the corresponding diagram becomes two disconnected two-point functions. Eq. (4.9) does not include that disconnected contribution to our correlator. However, we will see in section 4.6.5 that at strong coupling we need to consider also the disconnected contribution. Therefore, let us have a closer look at the relative magnitude of the connected and disconnected components. For example, when $\ell = \bar{\ell} = 0$, both of the linear terms in eq. (4.9) vanish. Including the disconnected two two-point functions, we find that up to a normalisation factor

$$\mathcal{F}^{\text{Tree}}_{\text{+disconnected}}(u,v) = u^{-\frac{2\mathbf{\Delta}}{3}}\, v^{\frac{\mathbf{\Delta}}{3}} \left(1 + q^{\mathbf{\Delta}} + \frac{q^{\mathbf{\Delta}} - q}{(q-1)}\right). \tag{4.20}$$

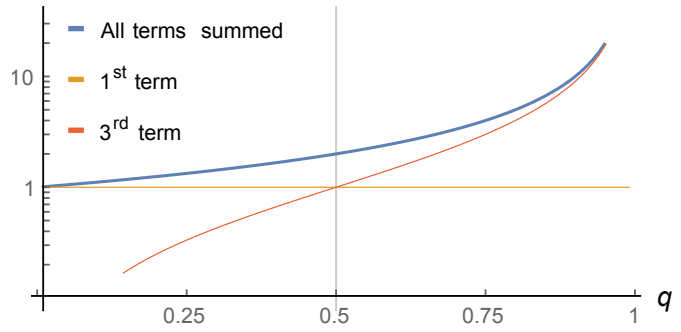

Figure 4.3: Plot of the magnitude of terms in the brackets in eq. (4.20) for $\boldsymbol{\Delta} \to \infty$. For small q, the first term dominates. For $q \sim 1$, the third term dominates.

We have plotted the different terms in the bracket of the above equation in fig. 4.3. We see for $q = 1$ the disc topology contribution dominates, whilst for $q \to 0$, and for $q \to \infty$ by crossing symmetry, the two two-point functions dominate. We find a transition between the two regimes around $q = 1/2$ and $q = 2$, but unlike the transition involving the two linear topology terms in section 4.2.4, it is a smooth transition.

4.2.7 Interesting questions

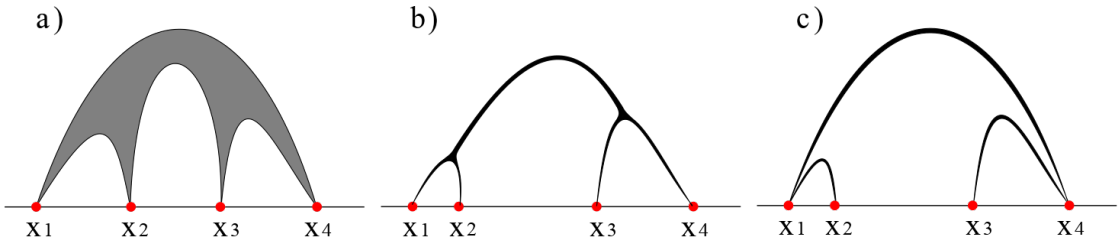

Figure 4.4: Opened-up string configuration in diagram a) and its degenerated versions in diagrams b) and c). We contrast the generic closed-up string configuration in diagram b) with a geodesic string configuration connecting the four operators in sequence in diagram c). Red dots denote the operator insertions, and the grey area represents the worldsheet surface.

In the above subsections, we have explored some curious properties of our correlator at weak coupling. In the following sections we compare them with the string theory predictions at strong coupling. Therefore, let us look at the correlator and its properties from the string theory perspective.

At strong coupling, through the AdS-CFT correspondence, the four-point correlator can

be expressed as a sum over the saddle points of the string action

$$G_n = e^{-S_1} + e^{-S_2} + ... \tag{4.21}$$

where S_i is the value of the action at the i-th saddle point. For example, the saddle point for two-point functions of the heavy operators, $\mathrm{Tr}Z^{\mathbf{\Delta}}$ and $\mathrm{Tr}\bar{Z}^{\mathbf{\Delta}}$, correspond to geodesic strings stretched between two insertion points at the boundary of AdS space [118]. However, in general there is more than one competing saddle point.

We argue that for the considered four-point function there are competing saddle points. One of them is the direct analogue to the linear topology diagram we have already encountered in fig. 4.1. It is composed of three geodesic strings connecting the four insertion points on the boundary in sequence[1], see diagram c) in fig. 4.4. There are two possibilities for such a geodesic configuration. In our setting the operator at x_3 has the smallest weight. Therefore, it either connects to the second or to the fourth operator, but not both. These cases correspond to first and second term in eq. (4.9) respectively and constitute two distinct saddle points. Another saddle point potentially contributing is an opened up string worldsheet, which is stretched between the insertion points forming a opened up minimal surface. Under certain circumstances such a surface can collapse to form infinitesimally thin tubes joined together to form a capital letter H. We often refer to an opened up string as the opposite to a collapsed or a geodesic string, see fig. 4.4.

Most of the time one of the saddle points is dominating all the other saddle points. When another saddle points wins over and becomes the dominant, we have a phase transition. The string jumps from one dominant configuration in one parameter region to a new dominant configuration in the other region.

In the light of this discussion, we can ask a few interesting questions. Which saddle point produces the dominant contribution at strong coupling? Are there any transitions between the geodesic dominated and the opened up worldsheet dominated phase? Does the opened up worldsheet saddle point give a good description of the correlator? Does the cusp at $q = 1$, we found at weak coupling, persist at strong coupling?

We plan to answer these questions in the following order. First, in section 4.3 we present an integrable system that enables us to calculate the contribution from an opened up string.

[1]The equations of motion are satisfied by each geodesic string individually. In order to satisfy the R-charge conservation, we divide the R-charge of each operator between the strings sourced by this operator.

Second, in section 4.6.1 we find that the structure of the stress-energy tensor for the string can reveal many interesting features. Next, in section 4.6 we describe the analytically accessible limits. Section 4.7 is left for the numerical results.

4.3 Integrable System

In this section, we review the integrable system presented in [3] as a tool to calculate the four-point function described in section 4.2 at strong coupling. We start by considering an extended string with a spherical topology and four punctures that is confined to move in $AdS_2 \times S^1$ space[2]. The equations of motion for the AdS coordinates is reduced to the sinh-Gordon equation and presented as a linear system. By considering transporting solutions of the linear problem we recast the problem as a set of difference equations. Given a solution to these equations, we present how to find the area of the string worldsheet and its contribution to the four-point function.

4.3.1 String in AdS

In this section, we consider motion of a Euclidean string in $AdS_2 \times S^1$, which factorises into the AdS part and the sphere part with only the energy-momentum tensor coupling the two. For now, we concentrate our attention on the AdS part described by the Polyakov action

$$S = \frac{1}{2} \int d^2\sigma \ \left[\partial_\alpha Y \cdot \partial^\alpha Y + \lambda \left(Y \cdot Y + 1\right)\right], \tag{4.22}$$

with Lagrangian multiplier λ that constrains the string to AdS space

$$Y \cdot Y = (Y_1)^2 - (Y_2)^2 + (Y_3)^2 = -1. \tag{4.23}$$

Introducing complex coordinates on the worldsheet, $w = e^{\tau + i\sigma}$ and $\overline{w} = e^{\tau - i\sigma}$, we find the equations of motion

$$Y^2 = -1, \qquad\qquad \partial\bar{\partial} Y = \left(\partial Y \cdot \bar{\partial} Y\right) Y. \tag{4.24}$$

The Virasoro constraint require that the total energy-momentum tensor must vanish $T_{AdS} + T_S \stackrel{!}{=} 0$. Therefore, solving the equation of motion of the string in AdS_2 space, we look for

[2] It corresponds to considering only correlators of operators of the type $\mathrm{Tr}\, Z^{\Delta}$ and $\mathrm{Tr}\, \overline{Z}^{\Delta}$ on a line [3].

solutions with a prescribed non-zero energy tensor

$$T_{AdS}(w) \equiv T(w) \equiv \partial Y \cdot \partial Y \stackrel{!}{=} -T_S, \tag{4.25}$$

where T_S is the sphere stress-energy tensor. Notice that, eq. (4.24) is covariant under $SO(2,1)$ isometry of the embedding AdS_2 space. We now proceed to rewrite the equations of motion as a non-linear but scalar equation. For this purpose, we define three independent unit vectors that span the embedding space

$$\begin{aligned} &Y^m, && Y^m_+ \equiv \partial_+ Y^m, && Y^m_- \equiv \partial_- Y^m, \\ & && \partial_+ \equiv T^{-1/2}\,\partial_w, && \partial_- \equiv \overline{T}^{-1/2}\,\partial_{\bar{w}}. \end{aligned} \tag{4.26}$$

The only non-trivial scalar we can form with these vectors, we call

$$Y_+ \cdot Y_- \equiv \cosh(\gamma). \tag{4.27}$$

As a consequence of the equations of motion, γ satisfies the sinh-Gordon equation

$$\partial_w \partial_{\bar{w}} \gamma - \sqrt{T\,\overline{T}}\,\sinh(\gamma) = 0. \tag{4.28}$$

4.3.2 Linear problem

We have just shown that the equations of motion for the string in AdS_2 space lead to the sinh-Gordon equation for the reduced field γ. On the other hand, given a solution to the sinh-Gordon equation we can construct a linear system (notice that the definition of the connection $B(\theta)$ involves γ)

$$\Big(\partial_w + B(\theta)\Big)\,\psi_a(\theta) = 0, \qquad \Big(\partial_{\bar{w}} + \bar{B}(\theta)\Big)\,\psi_a(\theta) = 0. \tag{4.29}$$

We use index a to distinguish the two independent solutions to the linear problem. The connection is defined as

$$B(\theta) \equiv -\begin{pmatrix} \frac{1}{4}\partial_w\gamma & \frac{\sqrt{T}\,e^{-\gamma/2}}{2}e^{-\theta} \\ \frac{\sqrt{T}\,e^{\gamma/2}}{2}e^{-\theta} & -\frac{1}{4}\partial_w\gamma \end{pmatrix}, \quad \bar{B}(\theta) \equiv -\begin{pmatrix} -\frac{1}{4}\partial_{\bar{w}}\gamma & \frac{\sqrt{\overline{T}}\,e^{\gamma/2}}{2}e^{\theta} \\ \frac{\sqrt{\overline{T}}\,e^{-\gamma/2}}{2}e^{\theta} & \frac{1}{4}\partial_{\bar{w}}\gamma \end{pmatrix}. \tag{4.30}$$

For the linear system to be compatible, it must satisfy

$$\big[\partial_w + B, \partial_{\bar{w}} + \bar{B}\big] = \partial_w \bar{B} - \partial_{\bar{w}} B + \big[B, \bar{B}\big] = 0, \tag{4.31}$$

which for the connection in eq. (4.30) is equivalent to the sinh-Gordon equation in eq. (4.28).

For each solution to the sinh-Gordon equation we can find two independent solutions to the linear system. Given these two solutions, we are about to recover the solution to the original equations of motion for a string in AdS_2. First, we notice a natural anti-symmetric measure on the space of solutions

$$\psi_a \wedge \psi'_b \equiv \det(\psi_a, \psi'_b), \tag{4.32}$$

Notice that, $\psi_a \wedge \psi'_b$ is independent of w and invariant under rotations $\psi_a \to R\,\psi_a$. We normalise our solutions such that

$$\psi_a \wedge \psi_b \stackrel{!}{=} \epsilon_{ab}. \tag{4.33}$$

Finally, using eq. (4.29), we find that the solution to the equations of motion can be recovered with

$$Y^\mu = q_1^\mu = -\frac{1}{2}\mathrm{Tr}\left(\psi_a(\theta=0)\,\bar{\sigma}^\mu_{ab}\,\sigma_2\,\psi_b(\theta=0)^T\,\sigma_1\right), \tag{4.34}$$

where $\bar{\sigma}^\mu = (\sigma_1, -i\sigma_2, \sigma_3)$.

4.3.3 Solutions near the punctures

In order for our classical string solution to correspond to the four-point correlation function of the heavy operators, we must impose appropriate boundary conditions. The worldsheet goes to the boundary of AdS space at the four insertion points x_A. The corresponding points on the worldsheet are called w_A. Sufficiently close to those points, the shape of the worldsheet is solely determined by the operator being inserted. We can extract this shape from a two-point function of the same operators considered in [120]. We find that the right boundary conditions for the worldsheet to have punctures at four worldsheet points w_A

$$\begin{aligned} T &\to \frac{\Delta_A^2}{4\,(w-w_A)^2} & w &\to w_A, \\ \gamma &\to 0 & w &\to w_A. \end{aligned} \tag{4.35}$$

These, together with eq. (4.29, 4.30), enable us to find two solutions to the linear problem near the insertion points

$$\psi^\pm(\theta) = \frac{i}{\sqrt{2}}(w-w_A)^{\pm\frac{e^{-\theta}}{4}\Delta_A}(\bar{w}-\bar{w}_A)^{\pm\frac{e^{\theta}}{4}\Delta_A}\begin{pmatrix}\mp 1\\ +1\end{pmatrix}. \tag{4.36}$$

We normalise such that $\psi^+ \wedge \psi^- = 1$. Notice that, as one approaches the puncture w_A for a particular value of spectral parameter θ, one solutions becomes exponentially small, and the other becomes exponentially large. As a result, demanding a function is a solution to the linear problem and is small close the puncture A, uniquely defines a solution for all w. This is how we define s_A. For example, for $-i\pi/2 < \theta < i\pi/2$ we have

$$s_A(\theta) \sim \psi_A^+(\theta) \qquad\qquad w \to w_A. \tag{4.37}$$

However, demanding a function is large close to the puncture does not uniquely specify it. We can always add a small solution component that does not change the boundary conditions. In spite of that we notice a $\mathbb{Z}_2$ symmetry of the connection

$$\sigma_1 \, B(\theta - i\pi) \, \sigma_1 = B(\theta), \tag{4.38}$$

which enables us to uniquely define a large solution. Given a solution to the linear problem $s_A(\theta)$ that is small near w_A, we can define the large solution to be

$$\tilde{s}_A(\theta) \equiv \sigma_1 \, s_A(\theta - i\pi). \tag{4.39}$$

Moreover, from eq. (4.36) we observe that the solutions have non-trivial monodromies around the punctures. Transporting a solution by homotopically different paths will give different results. Therefore, we introduce cuts emanating from each puncture, see fig. 4.7. When we cross it counter-clockwise, we pick a monodromy matrix associated with the puncture A, denoted by M_A. A direct inspection of the solution in eq. (4.36) reveals that the solutions s_A and $\tilde{s}_A$ are eigenvectors of the monodromy matrix

$$M_A \, s_A = \mu_A \, s_A, \qquad\qquad M_A \, \tilde{s}_A = \mu_A^{-1} \, \tilde{s}_A. \tag{4.40}$$

For example, for $-i\pi/2 < \theta < i\pi/2$, we can read of

$$M_A \, \psi_A^{\pm} = (\mu_A)^{\pm 1} \, \psi_A^{\pm}, \qquad\qquad \mu_A = e^{-i\,\pi\,\Delta_A \, \sinh(\theta)}. \tag{4.41}$$

Finally, the four monodromy cuts all come together at infinity and cancel out. They need to cancel as a path encirculating all punctures is contractible on a sphere.

4.3.4 WKB lines

In this section, we explain how to take a small solution from one puncture, transport it to the other puncture and compare it to the small solution at the second puncture. We will find the answer perturbatively in an expansion around large positive and negative θ.

The first step is to go to the diagonal gauge where the connection is diagonal to leading order. For example, for $\theta \to -\infty$, we perform a gauge transformation

$$B \to \hat{B} = h^{-1} B h + h^{-1} \partial h, \tag{4.42}$$

$$h = \left(T\overline{T}\right)^{1/8} \begin{pmatrix} 1 & 1 \\ -e^{\gamma/2} & e^{\gamma/2} \end{pmatrix}, \tag{4.43}$$

$$\hat{B} = \sqrt{T}\, e^{-\theta} \begin{pmatrix} -1 & 0 \\ 0 & 1 \end{pmatrix} + \mathcal{O}(e^{\theta})^0. \tag{4.44}$$

We remark that small and large solution are proportional to $|\pm\rangle$ in this gauge, where $|\pm\rangle$ are the eigenvectors of σ_3. For the moment we assume that we do not need to cross any monodromy cuts; therefore, transporting $|+\rangle$ along a path $\mathcal{C}$ to leading order in WKB approximation we get

$$\exp\left(-\int_{\mathcal{C}} \Phi\, e^{-\theta}\right) |+\rangle = \exp\left(\int_{\mathcal{C}} \omega\, e^{-\theta}\right) |+\rangle\,, \tag{4.45}$$

where we have used the following one forms

$$\Phi \equiv \frac{1}{2} \begin{pmatrix} -\omega & 0 \\ 0 & \omega \end{pmatrix}, \qquad\qquad \omega \equiv \sqrt{T(w)}\, dw, \tag{4.46}$$

which are single valued on the double cover of the worldsheet. The WKB approximation is accurate provided that the solution in eq. (4.45) is the growing solution along the $\mathcal{C}$ path. This is the case when $\mathrm{Re}(\omega\, e^{-\theta}) > 0$, and it is satisfied the strongest along WKB lines defined as the integral curves

$$\mathrm{Im}\left(\sqrt{T(w)}\, e^{-\theta}\, dw\right) = \mathrm{Im}\left(\omega\, e^{-\theta}\right) = 0. \tag{4.47}$$

We define the direction of WKB line as the direction in which $\mathrm{Re}(\omega\, e^{-\theta}) > 0$. Notice that in the limit when $\theta \to -\infty$ eq. (4.45) is singular. In the diagonal gauge we extract the singular contribution eq. (4.45), and we treat the sub-leading terms as perturbations, see [3] for details. Expanding the sub-leading terms up to second order, we find

$$s_A \wedge s_B = \exp\left(\frac{1}{2} e^{-\theta}\, \varpi_{AB} + \alpha_{AB} + \frac{1}{2} e^{\theta}\, \overline{\varpi}_{AB} + e^{\theta}\, \eta_{AB} + \mathcal{O}(e^{\theta})^2\right), \tag{4.48}$$

where ϖ_{AB}, η_{AB} are one forms integrated along the WKB lines

$$\eta_{AB} = \int_{w_A}^{w_B} \frac{1}{2}\sqrt{\overline{T}}\,(\cosh\gamma - 1)\,d\bar{w} + \frac{1}{4}\frac{1}{\sqrt{T}}(\partial_w\gamma)^2 dw, \tag{4.49}$$

$$\alpha_{AB} = -\frac{1}{4}\int_{w_A}^{w_B} \partial_w\left(\gamma - \log\sqrt{T\overline{T}}\right)dw + \partial_{\bar{w}}\left(\gamma + \log\sqrt{T\overline{T}}\right)d\bar{w}, \tag{4.50}$$

$$\omega_{AB} = \lim_{\substack{w'_A\to w_A \\ w'_B\to w_B}}\left(\int_{w'_A}^{w'_B}\sqrt{T}\,dw + \frac{\Delta_A}{2}\log(w_A - w'_A) + \frac{\Delta_B}{2}\log(w_B - w'_B)\right). \tag{4.51}$$

4.3.5 Stress-energy tensor and Virasoro

In this subsection, we discuss the stress-energy tensor of the string worldsheet and present it in a nice parametrisation.

We have argued in section 4.3.3 that the worldsheet stress-energy tensor must have a double pole corresponding to each operator insertion. Assuming there are no other poles, the most general stress-energy tensor is

$$T_{AdS} = \frac{c_0 + c_1\,w + c_2\,w^2 + c_3\,w^3 + c_4\,w^4}{(w-w_1)^2\,(w-w_2)^2\,(w-w_3)^2\,(w-w_4)^2}. \tag{4.52}$$

Notice that, this stress-energy tensor has in general four distinct zeros. Subsequently, we would like to impose the Virasoro constraint

$$T = T_{AdS} + T_{S^5} \stackrel{!}{=} 0. \tag{4.53}$$

In this chapter we confine the discussion to BMN operators whose sphere contribution to the stress-energy tensor is known [135]

$$T_{AdS} = -T_{S^5} = \frac{1}{4}\left(\sum_{A=1}^{4}\frac{\sigma_A\,\Delta_A}{w - w_A}\right)^2, \tag{4.54}$$

where $\sigma_A = \pm 1$ for Z and $\overline{Z}$ respectively. Δ_A are the scaled weights of the operators, see eq. (4.1), which as a consequence of R-charge conservation satisfy

$$\sum_A \sigma_A\,\Delta_A = \Delta_1 - \Delta_2 + \Delta_3 - \Delta_4 = 0. \tag{4.55}$$

It is natural to use the conformal invariance of the string world-sheet to set $w_1 = 0$, $w_3 = 1$, $w_4 = \infty$. For all operators on a line we can take $w_2 \in \mathbb{R}$. w_2 is the worldsheet cross-ratio

which is related to the space-time cross-ratio x_2 that describes the correlator[3]. Furthermore, adopting the conventions from section 4.2, $\Delta_{1,3} = \Delta\,(1 \pm \ell)$, $\Delta_{2,4} = \Delta\,(1 \pm \bar{\ell})$, $\sigma_i = \{1, -1, 1, -1\}$, we find

$$T_{AdS} = \frac{\Delta^2}{4}\left(\frac{(w^2 - 2w_2\,w + w_2) + \ell\,(w_2 - w) + \bar{\ell}\,(1-w)w}{w\,(w-w_2)\,(w-1)}\right)^2. \tag{4.56}$$

We can see that the resulting stress-energy tensor has only two distinct zeros. The initial four zeros form two pairs, and the two zeros in each pair collide with each other when we impose the Virasoro constraint in eq. (4.53). In what follows, we will put infinitesimal excitations on S^5 which take T_{AdS} away from a perfect square such that

$$T_{AdS} = \frac{\Delta^2}{4}\,\frac{\left((w^2 - 2w_2\,w + w_2) + \ell\,(w_2 - w) + \bar{\ell}\,(1-w)w\right)^2 - w\,(w-w_2)\,(w-1)\,\delta U^2}{w^2\,(w-w_2)^2\,(w-1)^2}. \tag{4.57}$$

When we take δU small, we approach the Virasoro limit[4]. In this section and in section 4.6.1, we will keep δU finite and use the stress-energy tensor in eq. (4.57). Therefore, it is essential to always take δU small enough such that the properties of the stress-energy tensor do not significantly change because of the finite value of δU used[5]. In section 4.4, we will strictly impose the Virasoro limit and set $\delta U = 0$.

4.3.6 Zeros of stress-energy tensor

In this subsection, we present the properties of the zeros of the stress-energy tensor. We start by taking the stress-energy tensor in eq. (4.57) with 4 zeros. We expand these zeros around $\delta U = 0$

$$w_{\pm\pm} = \frac{l - \bar{\ell} + 2w_2 \pm \sqrt{(\ell-\bar{\ell})^2 + 4w_2\,(\ell\,\bar{\ell} - 1) + 4w_2^2}}{2(1-\bar{\ell})} \pm f(w_2, \ell, \bar{\ell})\,\delta U^2 + \mathcal{O}(\delta U)^3. \tag{4.58}$$

The red and blue colours of $\pm$ signs indicate that the choice of the first $\pm$ is independent from the second choice. The argument of the square root is negative for $w_2^- < w_2 < w_2^+$, where

$$w_2^{\pm} \equiv \frac{1 - \ell\,\bar{\ell} \pm \sqrt{(1-\ell^2)\left(1-\bar{\ell}^2\right)}}{2}. \tag{4.59}$$

[3]Performing numerical tests we observed that x_2 was a monotonic function of w_2.

[4]The precise prefactor in front of δU^2 is determined such that the eq. (4.35) is satisfied for all δU.

[5]When we introduce δU, the two double zeros of the stress energy tensor split into four different zeros. However, as we increase δU, two of these roots can collide at finite δU only due to the change in δU. We always make sure we use δU smaller than this value.

In this interval function $f(w_2, \ell, \bar{\ell})$ is nonzero; we do not quote the exact form of $f(w_2, \ell, \bar{\ell})$ as it is lengthy. Therefore, as long as we consider all operators on the line and take w_2 in that range, all four roots are distinct and complex. Moreover, as the stress-energy tensor in eq. (4.57) does not contain any imaginary factors, two zeros are above real axis and the two others are complex conjugates of the first two, see fig. 4.5. When w_2 approaches $w_2^{\pm}$, two zeros of the stress-energy tensor, that are complex conjugates of one another, approach the real axis and eventually collide. We describe this limit in more details in section 4.6, but for the purpose of this section we will take zeros to be distinct and in complex conjugate pairs.

4.3.7 Triangulation

In section 4.3.5 we have constructed the stress-energy tensor in eq. (4.57). It depends on the operator weights, an infinitesimal parameter δU, and w_2 that encodes the cross-ratio. In this subsection, we use the stress-energy tensor to determine the structure of WKB lines defined in eq. (4.47).

An efficient way to present the structure of WKB lines is to plot the separating WKB

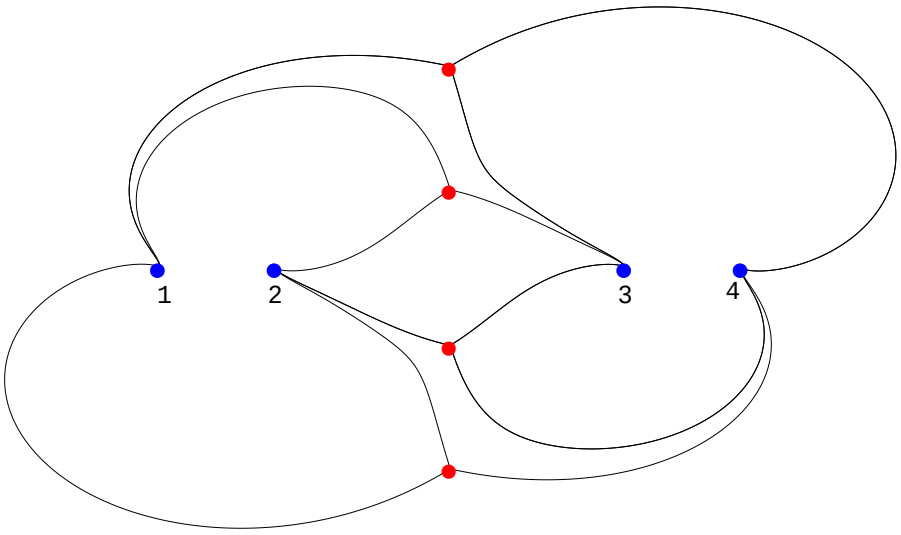

Figure 4.5: Schematic plot of the separating WKB lines in complex w-plane, for $w_2^- < w_2 < w_2^+$ and $\phi = \pi/5$, see eq. (4.59) for definition of $w_2^{\pm}$. The real axis is along the blue dots, but it was not included for transparency. Blue/red dots represent poles/zeros of the stress-energy tensor.

lines [153] *i.e.* WKB lines that join a zero and a pole of the stress-energy tensor. Plotting those lines we have observed that for a small enough δU and for several values of $w_2^- < w_2 < w_2^+$, where $w_2^{\pm}$ are defined in eq. (4.59), the graph formed by the separating WKB lines does

not change. We present it in fig. 4.5.

One has to keep in mind that in fig. 4.5 we only included the separating WKB lines. However, there are many other WKB lines in between them. All the other WKB lines join two poles of the stress-energy tensor. In fact, there is one WKB lines that passes through every single point in the w-plane. The exceptions are the punctures which are the sources and the sinks for the WKB lines, and the zeros of the stress-energy tensor that yield a fixed number of separating WKB lines that depend on the order of the zero.

We notice that the separating WKB lines divide the w-plane into six regions. Each

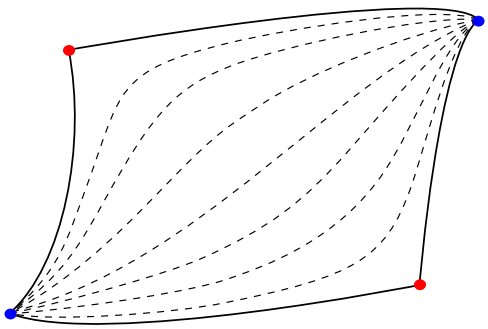

Figure 4.6: Schematic plot of a single cell produced by the separating WKB lines represented by solid black curves. The dashed curves are the generic WKB lines. Blue/red dots represent poles/zeros of the stress-energy tensor.

region has two zeros and two punctures on its boundary. All the WKB lines inside the region connect these two punctures, see fig. 4.6. For each region we pick one of these WKB line. These representatives for each region form a triangulation of the worldsheet. The triangulation is tetrahedron, and we present it in the fig. 4.7. The set of edges of the triangulation we will call

$$\mathbb{E} = \{E_{12}, E_{34}, E_{13}, E_{24}, E_{14}, E_{23}\}, \tag{4.60}$$

where for example E_{12} joins punctures 1 and 2. We will also equip the edges with a skew-symmetric inner product $I(E, E')$. It is non-zero only when the two edges meet. If at the meeting point E' is in counter-clockwise direction from E we assign 1, if it is in clockwise direction we assign -1. This inner product, written in the $\mathbb{E}$ basis, can be represented by

an intersection matrix which for our triangulation reads

$$I = \begin{pmatrix} 0 & 0 & 1 & 1 & -1 & -1 \\ 0 & 0 & 1 & 1 & -1 & -1 \\ -1 & -1 & 0 & 0 & 1 & 1 \\ -1 & -1 & 0 & 0 & 1 & 1 \\ 1 & 1 & -1 & -1 & 0 & 0 \\ 1 & 1 & -1 & -1 & 0 & 0 \end{pmatrix} . \tag{4.61}$$

In the following subsections we concentrate on the triangulation presented in fig. 4.5. Later,

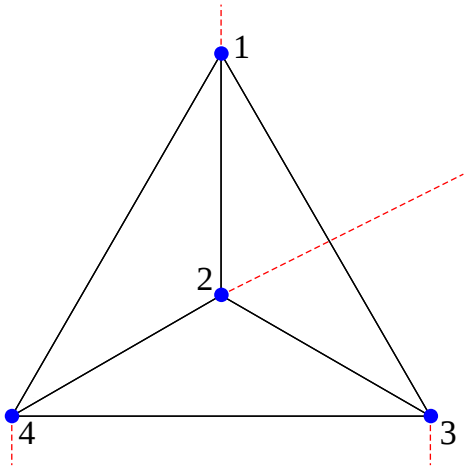

Figure 4.7: WKB lines forming the triangulation of the worldsheet. Dashed lines represent the monodromy cuts for the solutions to the linear problem. Blue dots represent poles of the stress-energy tensor.

in section 4.6.1 we argue that the triangulation stays the same even outside the $w_2^- < w_2 < w_2^+$ range. Nevertheless, using the tetrahedral triangulation for all w_2 is an assumption on which our results depend.

4.3.8 Spike configuration, fold lines and Virasoro

It turn out that the boundary conditions in eq. (4.35) do not uniquely specify the string solution. We need to further specify a discrete set of data that specifies the behaviour of γ at the zeros of the stress-energy tensor [3]. In this subsection, we discuss how this additional data enters.

At zeros of the stress-energy tensor when we require a non-singular worldsheet metric in eq. (4.27), we find

$$\gamma \to \pm \frac{1}{2} \log T\bar{T} \qquad\qquad w \to z_i. \tag{4.62}$$

The field γ has singularities which we refer to as spikes. These spikes act as the sources for the reduced field γ in the sinh-Gordon eq. (4.28). Notice that it follows from eq. (4.28) that a closed $\gamma = 0$ contour contains either a zero of the stress-energy tensor or $\gamma = 0$ everywhere inside the contour.

Moreover we have a choice of sign in eq. (4.62). When we choose the plus sign, we call it a u-spike, and for minus sign we call it a d-spike. Before imposing the Virasoro constrains we have four different zeros, each of which can produce a u-spike or a d-spike. However, out of those 2^4 possibilities there are only two independent and allowed choices. Let us explain that. Redefining $\gamma \to -\gamma$, we can always choose one of the spikes to be a u-spike. We choose one of the spikes above the real axis to be a u-spike. Moreover, we can interpret $\gamma = 0$ contours as fold-lines. When $\gamma = 0$, eq. (4.27) gives

$$\left(\partial Y.\bar{\partial} Y\right)^2 = \partial Y.\partial Y\ \bar{\partial} Y.\bar{\partial} Y. \tag{4.63}$$

Therefore, there must be a direction on the worldsheet in which Y does not change, therefore, it is a fold-line. The converse is also true, when Y does not change in one direction then $\gamma = 0$ due to eq. (4.27). At the same time, a string embedded in AdS_2 must have a fold line that cyclically joins all operators. Finally, continuity dictates that we must have a $\gamma = 0$ contour between a u-spike and a d-spike. Conversely, eq. (4.27) implies that there must be spikes of the opposite kind on both sides of $\gamma = 0$ contour. Using these information we are left with two possible spike configurations. Either we have two u-spikes above the real axis and two d-spikes below, which we will call *uudd* spike configuration. The other alternative is a u-spike and a d-spike below the real axis and above the real axis with the opposite order below and above. The second configuration we will call *udud* spike configuration.

Imposing Virasoro constraint in section 4.3.5 we saw that the two roots above the real axis collide together. The same happens to the roots below the real axis, which are complex conjugates of those above real axis. When we collide all u-spikes with d-spikes, they cancel each other as sources of γ which leads to a trivial solution $\gamma = 0$ for all w. We further discuss the implication of this cancellation in section 4.4.

4.3.9 Chi coordinates

In this section, we use the triangulation in fig. 4.7 to form the Fock-Goncharov coordinates. We construct these coordinates by transporting small solutions defined in section 4.3.3 between the punctures as explained in section 4.3.4. For each edge E_{AB}, we take the two triangles in the triangulation that share this edge. These two triangles form a quadrilateral. We now restrict ourselves to transporting the solutions between the punctures only inside the quadrilateral. This way we can properly account for the monodromies and make $s_C \wedge s_D$ single valued, as long as we stay inside the quadrilateral. Subsequently, we form the coordinates χ from the wedge product of the small solutions

$$\chi_E = -\prod_{E'_{AB}\in\mathbb{E}} (s_A \wedge s_B)^{I(E,E'_{AB})}. \tag{4.64}$$

Taking care to properly include all monodromy factors coming from crossing the cuts indicated in fig. 4.7, we find

$$\begin{aligned}
\chi_{12} &= -\frac{(s_1 \wedge M_2 s_3)\,(s_2 \wedge s_4)}{(s_1 \wedge s_4)\,(s_2 \wedge M_2 s_3)}, \\
\chi_{34} &= -\frac{(s_3 \wedge M_4 s_1)\,(s_4 \wedge s_2)}{(s_3 \wedge s_2)\,(s_4 \wedge M_4 s_1)}, \\
\chi_{13} &= -\frac{\left(s_1 \wedge M_1^{-1} s_4\right)(M_2 s_3 \wedge s_2)}{(s_1 \wedge s_2)\left(M_2 s_3 \wedge M_1^{-1} s_4\right)}, \\
\chi_{24} &= -\frac{(s_2 \wedge s_3)\,(s_4 \wedge s_1)}{(s_2 \wedge s_1)\,(s_4 \wedge s_3)}, \\
\chi_{14} &= -\frac{(s_1 \wedge s_2)\left(s_4 \wedge M_4^{-1} s_3\right)}{\left(s_1 \wedge M_4^{-1} s_3\right)(s_4 \wedge s_2)}, \\
\chi_{23} &= -\frac{\left(s_2 \wedge M_2^{-1} s_1\right)(s_3 \wedge s_4)}{(s_2 \wedge s_4)\left(s_3 \wedge M_2^{-1} s_1\right)}.
\end{aligned} \tag{4.65}$$

Not all of the χ-functions are independent, and some products of the χ-functions trivialise. Using the above definitions, together with the fact that the four monodromy cuts cancel out at infinity, and the property $s_A \wedge M_C^{-1} s_B = M_C\, s_A \wedge s_B$, we can find that

$$\prod_{E \text{ meeting at A}} \chi_E = \mu_A^2, \tag{4.66}$$

where the μ_A were introduced in eq. (4.41). The product is over the edges of the WKB triangulation meeting at puncture A. Further, we notice that since the linear problem is $2\pi i$ periodic, so must be the solutions s_A, and the χ-functions must also inherit that property.

In section 4.3.4, we found the asymptotic expressions for $s_A \wedge s_B$ when $\theta \to \pm\infty$. Now, we can use these expressions to find the asymptotic expressions for the χ-functions in eq. (4.65). We notice that the line integrals for the asymptotics of the wedge products in eq. (4.48), that are along the edges of our quadrilaterals, now combine into a closed cycles. These closed cycles can be homotopically deformed. Each quadrilateral contains two zeros of the stress-energy tensor. Homotopically deforming the contour we cannot cross any of those zeros. Hence, we deform the closed cycle to go around the two zeros contained in the quadrilateral[6]. We will denote a cycle corresponding to χ_E by γ_E. The final result including up to next-to-leading order for both $\theta \to \pm\infty$ is

$$\chi_E(\theta) \sim \chi_E^0(\theta) \equiv \mathcal{S}_E \exp\left(\frac{Z_E}{2}\, e^{-\theta} + \frac{\bar{Z}_E}{2}\, e^{\theta}\right). \tag{4.67}$$

If cycle γ_E encloses even/odd number u-spikes, $\mathcal{S}_E = \pm 1$ respectively[7]. For *uudd* spike configuration we find that

$$\mathcal{S}_{\mathbb{E}} = \{\ -1,\ \ -1,\ \ +1,\ \ +1,\ \ -1,\ \ -1\ \}. \tag{4.68}$$

Whilst for *udud* spike configuration we find

$$\mathcal{S}_{\mathbb{E}} = \{\ +1,\ \ +1,\ \ -1,\ \ -1,\ \ -1,\ \ -1\ \}. \tag{4.69}$$

We define Z_E as the result of integrating ω over cycle γ_E

$$Z_E = \int_{\gamma_E} \omega. \tag{4.70}$$

We will refer to Z_E as the masses of the χ-functions. The path γ_E is a closed path in the double cover of the worldsheet. When we go around the zeros of the stress-energy tensor, we cross a branch cut and enter the other sheet. The two contributions, one from each of sheet, are equal. Therefore, Z_E is equal to twice the integral from one zero to the other through the path of γ_E on one of the sheets.

Not all Z_E are independent. Some combinations of the integrals for Z_E combine to form a closed contour on one of the sheets that goes around a singularity. We can find those combinations of Z_E with the residue theorem. For the case when the Virasoro limit is

[6] For this reason we do not need to include any monodromy factors in the asymptotics of the χ-functions.
[7] For a detailed derivation of the constant factor $\mathcal{S}_E$ we refer the reader to the appendix B.3 in [3]

imposed, we have only one zeros above the real axis and one below, we find

$$\begin{aligned} Z_{12} + Z_{14} &= -2\pi i\, \Delta_1 = -2\pi i\, \Delta\, (1+\ell), \\ Z_{12} + Z_{23} &= -2\pi i\, \Delta_2 = -2\pi i\, \Delta\, (1+\bar{\ell}), \\ Z_{23} + Z_{34} &= -2\pi i\, \Delta_3 = -2\pi i\, \Delta\, (1-\ell), \\ Z_{34} + Z_{14} &= -2\pi i\, \Delta_4 = -2\pi i\, \Delta\, (1-\bar{\ell}), \end{aligned} \tag{4.71}$$

For example, the integral for Z_{12} goes from the root above the real axis to the root below the real axis through the WKB line joining punctures one and two, whilst the integral for Z_{23} goes from the root below the real axis to the root above the real axis through the WKB line joining punctures two and three. Joining the two integrals together, we find that their sum is equal to $-2\pi i$ times the residue of the $\omega(w)$ at the second puncture.

From eq. (4.71) we notice that only one of the Z_E is independent. Moreover, because we integrate between complex conjugate points to find Z_E, they are all purely imaginary. For example, we can think of $iZ_{12} \in \mathbb{R}$ as an independent variable parametrising the single cross-ratio, and the other Z_E are given by solving eq. (4.71)[8].

4.3.10 Chi-system

The coordinates χ_E we have just defined are not all independent. Not only do they need to satisfy the monodromy conditions in eq. (4.66) but also a set of consistency conditions. In this section, we derive this set of consistency conditions that together with the asymptotics in eq. (4.67) uniquely define the full set of the χ-functions.

We will find these relations to be of the form

$$\chi_E\, \chi_E^{--} = S_E. \tag{4.72}$$

This set of equations we will call the χ-system. The right hand side, S_E, is a rational functions of χ_E. We denote the χ-functions shifted by $-i\pi/2$ with $\chi_E^{-} \equiv \chi_E(\theta - i\pi/2)$, similarly $\chi_E^{--} \equiv \chi_E(\theta - i\pi)$. The first step to find this system is to use the $\mathbb{Z}_2$ symmetry in eq. (4.39)

$$\chi_E\, \chi_E^{--} = \chi_E\, \tilde{\chi}_E, \tag{4.73}$$

[8] Z_{12} is a function of w_2, which can be explicitly found with eq. (4.70) and the stress-energy tensor in eq. (4.57); however, the analytic formula is particularly long and not particularly illuminating. As a result, we do not present it here.

where $\tilde{\chi}_E$ is just χ_E but with s_A replaced by $\tilde{s}_A$. Next, we use the Schouten identity

$$s_A \wedge s_B \; s_C \wedge s_D + s_A \wedge s_C \; s_D \wedge s_B \; + s_A \wedge s_D \; s_B \wedge s_C \; = 0 \tag{4.74}$$

to find that

$$\chi_E \, \chi_E^{--} = \chi_E \, \tilde{\chi}_E = \prod_{E' \in \mathbb{E}} (1 + A_{E'})^{I(E,E')}, \tag{4.75}$$

$$A_{E_{AB}} \equiv - \frac{s_A \wedge \tilde{s}_B \; s_B \wedge \tilde{s}_A}{s_B \wedge \tilde{s}_B \; s_A \wedge \tilde{s}_A}. \tag{4.76}$$

On the other hand, s_A and $\tilde{s}_A$ are linearly independent, as a result of which we can express s_B as

$$s_B = \frac{s_B \wedge \tilde{s}_A}{s_A \wedge \tilde{s}_A} s_A + \frac{s_A \wedge s_B}{s_A \wedge \tilde{s}_A} \tilde{s}_A. \tag{4.77}$$

Both s_A and $\tilde{s}_A$ are eigenvectors of M_A monodromy matrix eq. (4.41) thus

$$M_A s_B = \frac{s_B \wedge \tilde{s}_A}{s_A \wedge \tilde{s}_A} \, \mu_A \, s_A + \frac{s_A \wedge s_B}{s_A \wedge \tilde{s}_A} \, \mu_A^{-1} \, \tilde{s}_A. \tag{4.78}$$

Combining these two equations we find

$$\frac{M_A s_B \wedge s_B}{M_A s_B \wedge s_A} = (1 - \mu_A^2) \frac{s_B \wedge \tilde{s}_A}{s_A \wedge \tilde{s}_A}, \tag{4.79}$$

$$A_{E_{AB}} = - \, (1 - \mu_A^2)^{-1} \, (1 - \mu_B^2)^{-1} \, \frac{M_A s_B \wedge s_B}{M_A s_B \wedge s_A} \, \frac{M_B s_A \wedge s_A}{M_B s_A \wedge s_B}. \tag{4.80}$$

For the triangulation that we consider, we define

$$\Sigma(A, B) \equiv 1 + \chi_{E_{AC}} \, (1 + \chi_{E_{AD}}), \tag{4.81}$$

where E_{AC} is the edge that contains puncture A and $I(E_{AB}, E_{AC}) = -1$, whilst E_{AD} is the edge that contains puncture A and $I(E_{AB}, E_{AD}) = 1$. Using the Schouten identity we can show that

$$\Sigma(A, B) = \frac{s_A \wedge s_D}{s_B \wedge s_D} \frac{M_A s_B \wedge s_B}{M_A s_B \wedge s_A}, \tag{4.82}$$

where the puncture D is the aforementioned puncture on the edge E_{AD}. Therefore, we can write

$$A_{E_{AB}} = \chi_{E_{AB}} \, \frac{\Sigma(A, B) \, \Sigma(B, A)}{(1 - \mu_A^2) \, (1 - \mu_B^2)}. \tag{4.83}$$

Finally, we can use eq. (4.75, 4.81, 4.83) to express $\chi_E\,\chi_E^{--}$ in terms of unshifted χ_E only. Using the intersection matrix in eq. (4.61), we find the explicit expressions for A_E and S_E

$$\begin{aligned} S_{12} = S_{34} &= \frac{(1+A_{13})(1+A_{24})}{(1+A_{14})(1+A_{23})}, \\ S_{13} = S_{24} &= \frac{(1+A_{14})(1+A_{23})}{(1+A_{12})(1+A_{34})}, \\ S_{14} = S_{23} &= \frac{(1+A_{12})(1+A_{34})}{(1+A_{13})(1+A_{24})}, \end{aligned} \tag{4.84}$$

$$\begin{aligned} A_{12} &= \left(\frac{\chi_{12}\,(1+\chi_{23}\,(1+\chi_{24}))\,(1+\chi_{14}\,(1+\chi_{13}))}{(1-\mu_1^2)\,(1-\mu_2^2)}\right), \\ A_{34} &= \left(\frac{\chi_{34}\,(1+\chi_{23}\,(1+\chi_{13}))\,(1+\chi_{14}\,(1+\chi_{24}))}{(1-\mu_3^2)\,(1-\mu_4^2)}\right), \\ A_{13} &= \left(\frac{\chi_{13}\,(1+\chi_{12}\,(1+\chi_{14}))\,(1+\chi_{34}\,(1+\chi_{23}))}{(1-\mu_1^2)\,(1-\mu_3^2)}\right), \\ A_{24} &= \left(\frac{\chi_{24}\,(1+\chi_{12}\,(1+\chi_{23}))\,(1+\chi_{34}\,(1+\chi_{14}))}{(1-\mu_2^2)\,(1-\mu_4^2)}\right), \\ A_{14} &= \left(\frac{\chi_{14}\,(1+\chi_{13}\,(1+\chi_{12}))\,(1+\chi_{24}\,(1+\chi_{34}))}{(1-\mu_1^2)\,(1-\mu_4^2)}\right), \\ A_{23} &= \left(\frac{\chi_{23}\,(1+\chi_{13}\,(1+\chi_{34}))\,(1+\chi_{24}\,(1+\chi_{12}))}{(1-\mu_2^2)\,(1-\mu_3^2)}\right). \end{aligned} \tag{4.85}$$

We are now concerned with solving these consistency relations for the χ-functions in eq. (4.72, 4.84, 4.85) subject to prescribed asymptotics in eq. (4.67).

4.3.11 Inverting the chi-system

In section 4.3.10 we have derived a system of difference equations, that the χ-functions need to satisfy, which we dubbed the χ-system. Subsequently, using the asymptotic expressions for the χ-functions in eq. (4.67), we can invert the χ-system and write it as a system of integral equations for the χ-functions, see eq. (4.91). In this section, we will show how to find those integral equations by undoing the shifts in eq. (4.72) in the Fourier space.

First, we take the logarithm of eq. (4.72)

$$\log \chi_E(\theta) + \log \chi_E(\theta - i\pi) = \log S_E(\theta). \tag{4.86}$$

Now, we would like to take the Fourier transform of both sides, and undo the shift in the second term. To do that we need to control the asymptotics of the χ-functions as $\theta \to \pm\infty$ in the strip $-\pi < \mathrm{Im}(\theta) < 0$. This is possible if we choose to find the WKB lines at

$\mathrm{Im}(\theta) = -i\pi/2$, and the WKB analysis in section 4.3.4 is valid for $-\pi < \mathrm{Im}(\theta) < 0$. Noticing that, the asymptotic expressions satisfy

$$\chi^0(\theta)\ \chi^0(\theta - i\pi) = 1, \tag{4.87}$$

we can make left-hand side of eq. (4.86) explicitly convergent under the Fourier transform by writing

$$\log \frac{\chi_E}{\chi_E^0}(\theta) + \log \frac{\chi_E}{\chi_E^0}(\theta - i\pi) = \log S_E(\theta). \tag{4.88}$$

We need to assume that $s_A \wedge s_B(\theta)$ does not have zeros in the strip $-\pi < \mathrm{Im}(\theta) < 0$, such that the right-hand side of eq. (4.88) is also regular inside the strip. Finally, we take the Fourier transform of eq. (4.88), collect the χ_E to find

$$\log \frac{\chi_E}{\chi_E^0}(\theta) = \int \frac{d\omega}{2\pi} \frac{e^{i\,\omega\,\theta}}{1 + e^{\omega\,\pi}} \int d\theta'\ \log S(\theta')\ e^{-i\,\omega\,\theta'}. \tag{4.89}$$

Regularising with the $i\epsilon$-prescription and reversing the order of integration, we find the advertised system of integral equations

$$\log \chi_E(\theta) = \log \chi_E^0(\theta) - \int \frac{d\theta'}{2\pi i} \frac{\log S_E(\theta')}{\sinh(\theta' - \theta + i\epsilon)}. \tag{4.90}$$

We will refer to the $\log \chi_E^0(\theta)$ term as the source term, whilst the term with the integration sign we will call the kernel term. We derived eq. (4.90) for $-\pi < \mathrm{Im}(\theta) \leq \mathrm{Im}(\theta') \leq 0$. In particular, we can choose $\mathrm{Im}(\theta) = \mathrm{Im}(\theta') = -i\pi/2$ when all of the asymptotics decay the fastest as $\mathrm{Re}(\theta) \to \pm\infty$.

$$\log \chi_E^-(\theta) = \log \chi_E^{0\,-}(\theta) - \int_{\mathbb{R}} \frac{d\theta'}{2\pi i} \frac{\log S_E^-(\theta')}{\sinh(\theta' - \theta + i\epsilon)}. \tag{4.91}$$

In this case, both the left and the right hand side of eq. (4.91) decay as $\theta \to \pm\infty$. As a result, we can impose a cut-off for large θ, and the system of integral equations can be efficiently solved with iterations to find the χ-functions numerically. We can start with the asymptotics as the initial approximation of the χ-functions. Then, iteratively evaluating the right hand side of eq. (4.91) we find better approximations to the full χ-functions. Therefore, from now we will concentrate on the shifted $\chi_E^-(\theta)$ for $\theta \in \mathbb{R}$.

4.3.12 Cross-ratios

In this section, we show that evaluating the χ-functions at $\theta = 0, -i\pi$ we find the cross-ratios characterising the correlator. We start with two solutions to the linear problem $\psi_a(\theta)$, $a = 1, 2$, which can be decomposed as

$$\psi_a(\theta) = c_a \; s_A + \tilde{c}_a \; \tilde{s}_A. \tag{4.92}$$

We normalise $s_A \wedge \tilde{s}_A = 1$ so that

$$\psi_a = (\psi_a \wedge \tilde{s}_A) \; s_A + (s_A \wedge \psi_a) \; \tilde{s}_A. \tag{4.93}$$

We transform into the AdS_2 Poincaré coordinates

$$\frac{1}{z} = Y^2 - Y^1, \qquad x = \frac{Y^3}{Y^2 - Y^1}. \tag{4.94}$$

Close to the A^{th} puncture the solution $\tilde{s}_A$ dominates when $\theta = 0$; therefore, using of eq. (4.34) and eq. (4.93), we find that for the A^{th} insertion

$$x_A = \frac{\psi_2 \wedge s_A}{\psi_1 \wedge s_A}(\theta = 0), \tag{4.95}$$

which together with the Schouten identity gives

$$x_A - x_B = \frac{s_A \wedge s_B}{\psi_2 \wedge s_A \; \psi_2 \wedge s_B}(\theta = 0). \tag{4.96}$$

We can repeat the same exercise for $\theta = -i\pi$ and find the same is true. The special values of spectral parameter $\theta = 0, -i\pi$ we will call the physical values and denote by θ^*. For these values the monodromy matrices become $M_P|_{\theta^*} = \mathbb{1}$. Taking the definitions of the χ-functions in eq. (4.65), and using eq. (4.96), we find

$$\begin{aligned} \chi_{12}(\theta^*) = \chi_{34}(\theta^*) &= -\frac{x_{13}\, x_{24}}{x_{14}\, x_{23}}, \\ \chi_{13}(\theta^*) = \chi_{24}(\theta^*) &= \frac{x_{14}\, x_{23}}{x_{12}\, x_{34}}, \\ \chi_{14}(\theta^*) = \chi_{23}(\theta^*) &= -\frac{x_{12}\, x_{34}}{x_{13}\, x_{24}}. \end{aligned} \tag{4.97}$$

We conclude that evaluating the χ-functions at the physical values we find the cross-ratios. However, they are not all independent. We use conformal symmetry to put $x_1 = 0$, $x_2 \in$

$\mathbb{R}$, $x_3 = 1$, $x_4 = \infty$, and parametrise the cross-ratios by x_2. This gives

$$\begin{aligned}\chi_{12}(\theta^*) = \chi_{34}(\theta^*) &= -\frac{1}{1-x_2},\\ \chi_{13}(\theta^*) = \chi_{24}(\theta^*) &= \frac{1-x_2}{x_2},\\ \chi_{14}(\theta^*) = \chi_{23}(\theta^*) &= -x_2.\end{aligned} \tag{4.98}$$

4.3.13 Area

In this section, we summarize how to find the area of the worldsheet from the χ-functions, and how to find the corresponding contribution to the four point function. The authors of [3] consider the regularised area of the string and find

$$G_4(x_1, x_2, x_3, x_4) = \left(f_{fin}^{AdS} f_{div}^{AdS\times S} f_{fin}^{S}\right) \prod_{A<B}^{4} (x_{AB})^{\sqrt{\lambda}\,\Delta_{AB}}\,, \tag{4.99}$$

where

$$\begin{aligned} f_{fin}^{AdS} &\equiv e^{-\frac{\sqrt{\lambda}}{\pi}\int_\Sigma d^2w\left(\mathcal{L}_{AdS}-\sqrt{T_{AdS}\,\overline{T}_{AdS}}\right)} = e^{-\frac{\sqrt{\lambda}}{\pi}A_{fin}},\\ f_{fin}^{S} &\equiv e^{-\frac{\sqrt{\lambda}}{\pi}\int_\Sigma\left(S^5\text{ contribution}-\sqrt{T_{AdS}\,\overline{T}_{AdS}}\right)}\,,\\ f_{div}^{AdS\times S} &\equiv e^{-2\frac{\sqrt{\lambda}}{\pi}\int_{\Sigma\setminus\{\epsilon_A\}} d^2w\sqrt{T_{AdS}\,\overline{T}_{AdS}}} = e^{-2\frac{\sqrt{\lambda}}{\pi}A_{reg}}\prod_{A>B}^{4}\left(|s_A\wedge s_B|_0\right)^{-\sqrt{\lambda}\,\Delta_{AB}}\,, \end{aligned} \tag{4.100}$$

where S^5 contribution stands for the S^5 Lagrangian together with the contributions from the wavefunctions of the operators [144]. Both contributions are discussed in the following subsection. Further, using the Riemann Bilinear Identity on the double cover of the worldsheet one finds

$$A_{fin} = 4\times\frac{\pi}{12} + \frac{i}{2}\sum_{E\in\mathbb{E}} Z_E\eta_E. \tag{4.101}$$

It receives a contribution of $\frac{\pi}{12}$ for each zero of the stress-energy tensor. The regular part of the area can be evaluated as

$$A_{reg} = \int_{\Sigma\setminus\{\epsilon_a\}} d^2w\,\sqrt{T_{AdS}\,\overline{T}_{AdS}} + \frac{\pi}{2}\sum_A \Delta_A^2\log\epsilon_A, \tag{4.102}$$

$$s_A\wedge s_B(\theta=0) = \exp\left(\mathrm{Re}\,\varpi_{AB} + \int_{\mathbb{R}}\frac{d\theta}{2\pi}\frac{\log\left(1+A_{AB}^{-}\right)}{\cosh\theta}\right). \tag{4.103}$$

Sphere contribution and regular part of area

In this section, we simplify the formulas summarised in the previous section. First, we show that for the correlator we consider $f^S_{fin} = 1$. For correlators involving only Z and $\overline{Z}$, it is known how to calculate the sphere contribution to the area [101]. In particular, the operators $\mathrm{Tr}\, Z^{\sqrt{\lambda}\,\Delta_A}(x_A)$ and $\mathrm{Tr}\, \overline{Z}^{\sqrt{\lambda}\,\Delta_A}(x_A)$ have wave functions

$$\Psi_A = e^{i\sqrt{\lambda}\,\sigma_A\,\Delta_A\,\varphi(w_A,\overline{w}_A)}, \tag{4.104}$$

where φ is the azimuthal angle on the sphere. The string dual of these operators corresponds geometrically to a string that is point-like in the sphere and rotates around an equator. Their wave-function scales exponentially with $\sqrt{\lambda}$, and they will act as sources for the equations of motion for φ. Hence, the regularised sphere contribution is

$$f^S_{fin} = \exp\left(-\frac{\sqrt{\lambda}}{\pi}\left(\int d^2w\,\partial\varphi\,\overline{\partial}\varphi - i\pi\sum_A \sigma_A\,\Delta_A\,\varphi(w_A)\right) + \frac{\sqrt{\lambda}}{\pi}\int d^2w\,\sqrt{T_{AdS}\,\overline{T}_{AdS}}\right). \tag{4.105}$$

The resulting equation of motion for φ are equivalent to the equations for the electrostatic potential of point charges on the sphere, with charges proportional to $\sigma_A\,\Delta_A$. For a solution to exist we must have R-charge conservation $\sum_A \sigma_A\,\Delta_A = 0$. Given that this constraint is satisfied, the solution exists and is given by[9]

$$\varphi(w,\overline{w}) = -i\sum_A \sigma_A\,\Delta_A \log|w - w_A|. \tag{4.106}$$

We now plug eq. (4.106) into eq. (4.105). Although the full contribution to the exponent in (4.105) is finite, the individual parts are not finite, and we need to introduce cut-off around each puncture. From the sphere action we have $T_S = (\partial\varphi)^2$, $\overline{T}_S = (\overline{\partial}\overline{\varphi})^2$. Since φ is purely imaginary

$$-\partial\varphi\,\overline{\partial}\varphi = \sqrt{T_S\,\overline{T}_S} = \sqrt{T_{AdS}\,\overline{T}_{AdS}}. \tag{4.107}$$

In the last step we have used the Virasoro constraint $T = T_{AdS} + T_S = 0$. Using eq. (4.107) to simplify eq. (4.105) we find

$$f^S_{fin} = \exp\left(\frac{\sqrt{\lambda}}{\pi}\left(2\int_{\Sigma\setminus\{\epsilon_A\}} d^2w\,\sqrt{T_{AdS}\,\overline{T}_{AdS}} + i\pi\sum_A \sigma_A\,\Delta_A\,\varphi(w_A)\right)\right), \tag{4.108}$$

[9] Without the R-charge neutrality there would be an additional singularity at infinity.

where φ_A is evaluated a distance ϵ_A away from the puncture. Because the stress-energy tensor is a perfect square, one can evaluate the integral $\int d^2w \sqrt{T_{AdS}\,\overline{T}_{AdS}}$ and find

$$\frac{2}{\pi}\int_{\Sigma\setminus\{\epsilon_A\}} d^2w\,\sqrt{T_{AdS}\,\overline{T}_{AdS}} = -i\sum_A \sigma_A\Delta_A\varphi(w_A) = -\sum_A \Delta_A^2\log\epsilon_A - \sum_{A\neq B}\sigma_A\sigma_B\Delta_A\Delta_B\log|w_A-w_B|.$$

Therefore, $f^S_{fin}=1$ for a correlator of BMN operators. Note, that this does not mean the sphere does not contribute, as the sphere contribution is precisely equal to the integral of $\sqrt{T_{AdS}\,\overline{T}_{AdS}}$, which we included in $f^{AdS\times S}_{div}$.

The second observation we would like to describe we have only observed numerically. Evaluating A_{reg} by numerically integrating $\sqrt{T_{AdS}\,\overline{T}_{AdS}}$ with small circular disks cut out around the punctures, we found that

$$\sum_{A>B}^{4}\Delta_{AB}\,\mathrm{Re}\,\varpi_{AB} + \frac{2}{\pi}A_{reg} = 0. \tag{4.109}$$

Correlator in terms of string area

Here we would like to summarise the formulas that we use to find the contribution from the saddle point to the correlator we study

$$G_4(x_1,x_2,x_3,x_4) = e^{-\frac{\sqrt{\lambda}}{\pi}(A_{fin}+A_\kappa)}\prod_{A>B}^{4}(x_{AB})^{\sqrt{\lambda}\Delta_{AB}}, \tag{4.110}$$

where

$$A_{fin} = \frac{\pi}{3} + \frac{i}{2}\sum_{E\in\mathbb{E}} Z_E\,\eta_E, \qquad A_\kappa = \pi\sum_{E\in\mathbb{E}}\Delta_E\,\kappa_E,$$
$$\eta_E = \int_{\mathbb{R}}\frac{d\theta}{\pi}e^{-\theta-i\phi}\log\left(1+A_E^-(\theta+i\phi)\right), \qquad \kappa_E = \int_{\mathbb{R}}\frac{d\theta}{2\pi}\frac{\log(1+A_E^-)}{\cosh\theta},$$
$$\Delta_{E_{AB}} = \Big(\sum_C\frac{\Delta_C}{3}\Big) - \Delta_A - \Delta_B.$$

Area is real

The area of the string worldsheet must be a real number; however, the formula in eq. (4.110) does not make this explicit as the χ-functions are in general complex. In order to show that eq. (4.110) gives a real area, we assume that the integral equation in eq. (4.91) converges *i.e.* we can find the full χ-functions by starting with asymptotics, and by iteratively evaluating the left hand side in eq. (4.91) we converge to the full χ-functions. The asymptotics in

eq. (4.67) have their real part even function of θ, whilst their imaginary part is an odd function of θ. Moreover, this property is preserved when we iterate eq. (4.91) to find the full χ-functions. Consequently, the real components of the χ-functions are even functions of θ, whilst the imaginary components are odd

$$\chi_E(\theta)^* = \chi_E(-\theta). \tag{4.111}$$

Therefore, η_E and κ_E are purely real as the imaginary part integrates to zero. Furthermore, when we impose the Virasoro constraint, the masses Z_E become purely imaginary. As we have noticed in section 4.3.6, in the Virasoro limit we have only one complex conjugate pair of zeros of the stress-energy tensor. The contours of integration γ_E go between the two zeros. Therefore, eq. (4.70) for the stress-energy tensor in eq. (4.57) with only real coefficients ensures that the masses Z_E are purely imaginary. As a result the area we find in eq. (4.110) is a real number.

4.4 Imposing the Virasoro constraint

In section 4.3.5 on the stress-energy tensor, we have shown that imposing the Virasoro constraint amounts to colliding two pairs of zeros. These zeros collide on the WKB lines joining w_1 with w_3, and w_2 with w_4. As a result, the two corresponding γ_E cycles that go around those two pairs of zeros vanish. This leads to

$$Z_{13} \to 0, \qquad\qquad Z_{24} \to 0. \tag{4.112}$$

The χ_{AB}-functions, for A and B corresponding to two Z operators or two $\bar{Z}$, are distinguished by becoming massless in the Virasoro limit[10]. In this section, we will use the high temperature procedure to impose the Virasoro limit at the level of the χ-system.

4.4.1 Virasoro plateau for uudd spike configuration

In this section, we are going to take $Z_{13} \to 0, Z_{24} \to 0$ and see what effect it produces on the integrable system presented in the previous section in the *uudd* spike configuration.

We concentrate on the case when $w_2^- < w_2 < w_2^+$ and the zeros of the stress-energy

[10]The authors have observed that having no Wick contractions between two operators at weak coupling directly translates at strong coupling to having two zeros colliding on a WKB line joining these two operators, and the corresponding χ-function becoming massless.

tensor come in complex conjugate pairs. In the Virasoro limit eq. (4.70, 4.71) ensure that the masses Z_E are purely imaginary, with negative imaginary part. Looking at the asymptotic expressions of the χ-functions in eq. (4.67), we observe that far enough from the origin the χ-functions with finite masses, $\chi_{12}, \chi_{34}, \chi_{14}, \chi_{23}$, are exponentially small

$$\chi_E^-(\theta) \propto e^{-|Z_E|\cosh(\theta)}.$$

Only χ_{13}, χ_{24} that become massless in this limit survive. In this region, the χ-system in eq. (4.72) reduces to

$$\chi_{12}\,\chi_{12}^{--} = (1+\chi_{13})(1+\chi_{24}), \tag{4.113}$$

$$\chi_{34}\,\chi_{34}^{--} = (1+\chi_{13})(1+\chi_{24}), \tag{4.114}$$

$$\chi_{13}\,\chi_{13}^{--} = 1, \tag{4.115}$$

$$\chi_{24}\,\chi_{24}^{--} = 1, \tag{4.116}$$

$$\chi_{14}\,\chi_{14}^{--} = 1/(1+\chi_{13})(1+\chi_{24}), \tag{4.117}$$

$$\chi_{23}\,\chi_{23}^{--} = 1/(1+\chi_{13})(1+\chi_{24}). \tag{4.118}$$

We notice that eq. (4.115, 4.116) are solved by the asymptotic expressions of χ_{13}, χ_{24}. Therefore, far enough from the origin the full χ-functions in the *uudd* spike configuration are just

$$\chi_{13}(\theta) = \chi_{13}^0(\theta) = e^{\frac{1}{4}(Z_{13}\,e^{-\theta}+\overline{Z}_{13}\,e^{\theta})}, \tag{4.119}$$
$$\chi_{24}(\theta) = \chi_{24}^0(\theta) = e^{\frac{1}{4}(Z_{24}\,e^{-\theta}+\overline{Z}_{24}\,e^{\theta})}.$$

For $|\theta| \ll -\log(\mathrm{Max}(\mathrm{Im}(Z_{13}, Z_{24})))$, we have $\chi_{13} = 1$ and $\chi_{24} = 1$. This region, far enough from the origin such that $\chi_{12}, \chi_{34}, \chi_{14}, \chi_{23}$ can be neglected, but not far enough for Z_{13}, Z_{24} to have an effect on χ_{13}, χ_{24}, will be called the Virasoro plateau. In this region, eq. (4.113-4.114, 4.117-4.118) together with $\chi_{13} = 1$ and $\chi_{24} = 1$ imply that the asymptotic expressions of $\chi_{12}, \chi_{34}, \chi_{14}, \chi_{23}$ get corrected

$$\frac{\chi_{12}(\theta)}{\chi_{12}^0(\theta)} = \frac{\chi_{34}(\theta)}{\chi_{34}^0(\theta)} = 2 \qquad \text{for large } \theta, \tag{4.120}$$
$$\frac{\chi_{14}(\theta)}{\chi_{14}^0(\theta)} = \frac{\chi_{23}(\theta)}{\chi_{23}^0(\theta)} = \frac{1}{2} \qquad \text{for large } \theta.$$

4.4.2 Virasoro kink

The plateau region ends around $|\theta| \approx -\log(\mathrm{Max}(\mathrm{Im}(Z_{13}, Z_{24})))$. The transition between the Virasoro Plateau and the $|\theta| \gg -\log(\mathrm{Max}(\mathrm{Im}(Z_{13}, Z_{24})))$ regions, will be called the Virasoro

kink. It contributes a finite amount to A_{fin}, which we determine in this subsection.

When $\chi_{12}, \chi_{34}, \chi_{14}, \chi_{23}$ are exponentially small, the A-functions in eq. (4.85) simplify to

$$A_{12} = A_{34} = 0, \qquad A_{13} = \chi_{13}, \qquad A_{24} = \chi_{24}, \qquad A_{14} = A_{23} = 0. \tag{4.121}$$

The finite contribution to A_{fin} from this region is

$$\begin{aligned} \Delta A_{fin} &= \sum_{E\in\mathbb{E}} iZ_E \int_{\text{Kink}} \frac{d\theta}{2\pi}\, e^{-\theta}\, \log\left(1 + A_E^-(\theta)\right) \\ &= \int_{\text{Kink}} \frac{d\theta}{2\pi}\, \cosh\theta \left(iZ_{13} \log(1+\chi_{13}^-(\theta)) + iZ_{24}\log(1+\chi_{24}^-(\theta))\right). \end{aligned} \tag{4.122}$$

We notice that since $Z_{13} \to 0, Z_{24} \to 0$ only the large θ region contributes, as only for large enough θ the factor of $\cosh(\theta)$ wins over the vanishing Z_{13}, Z_{24} prefactor. For iZ_{13}, $iZ_{24} \in \mathbb{R}$ eq. (4.119) becomes

$$\begin{aligned} \chi_{13}^-(\theta) &= \chi_{13}^0(\theta - i\pi/2) = e^{-\frac{1}{2}Z_{13}\cosh(\theta)}, \\ \chi_{24}^-(\theta) &= \chi_{24}^0(\theta - i\pi/2) = e^{-\frac{1}{2}Z_{24}\cosh(\theta)}. \end{aligned} \tag{4.123}$$

We extend the range of integration from just the kink region to all θ. All the other contributions from outside $|\theta| \approx -\log(\text{Max}(\text{Im}(Z_{13}, Z_{24})))$ vanish in this limit. This enables us to evaluate the contribution from the Virasoro kink[11]

$$\begin{aligned} \Delta A_{fin} &= -\frac{1}{\pi}\int_0^\infty d\theta \left(-\frac{i}{4} Z_{13}\, e^{\theta}\, \log(1 + e^{-\frac{i}{4}Z_{13}e^{\theta}}) - \frac{i}{4} Z_{24}\, e^{\theta}\, \log(1+e^{-\frac{i}{4}Z_{24}e^{\theta}})\right) \\ &= -\frac{2}{\pi}\int_1^0 \frac{df}{f}\, \log(1+f) = \frac{\pi}{6}. \end{aligned} \tag{4.124}$$

From now we are going to strictly impose the Virasoro constraint and set $Z_{13} = 0$ and $Z_{24} = 0$. It amounts to moving the Virasoro kink outside the range of θ that we consider. As a result, we never move outside the Virasoro plateau. The asymptotics of χ_{12} and χ_{34} get multiplied by a factor of 2, and the asymptotics of χ_{14} and χ_{23} by a factor of $1/2$. Moreover, in order to find A_{fin} instead of eq. (4.110) we use

$$A_{fin} = \frac{\pi}{2} + \sum_{E\in\mathbb{E}} iZ_E \int \frac{d\theta}{2\pi}\, e^{-\theta}\, \log\left(1 + A_E^-(\theta)\right), \tag{4.125}$$

which includes the contribution from the kink.

Finally, we notice that because $S_{13} = S_{24}$ and χ_{13}, χ_{24} have the same asymptotics, $Z_{13} = Z_{24} = 0$, eq. (4.91) implies that $\chi_{13} = \chi_{24}$ in the Virasoro limit.

[11] We have found that this result perfectly agrees with our numerical tests of the χ-system.

4.4.3 udud spike configuration

In the Virasoro limit of *udud* spike configuration we collide the u-spikes with d-spikes. They cancel as sources of the γ field defined in eq. (4.27). The minimal surface must be collapsed, and it is natural to hypothesise that this spike configuration gives a geodesic configuration described thoroughly in section 4.2. In this section we discuss this hypothesis.

First, let us consider the range $w_2^- < w_2 < w_2^+$. Just as for the *uudd* case the masses Z_E are purely imaginary, and provided we are far enough from the origin, the eq. (4.113-4.118) are still valid. In this region χ_{13} and χ_{24} are once again equal to their asymptotics. However, in the *udud* case the new asymptotics have a different sign

$$\begin{aligned}
\chi^0_{13}(\theta) = &\quad e^{\frac{1}{4}(Z_{13}\, e^{-\theta}+\overline{Z}_{13}\, e^{\theta})},\\
\chi^0_{24}(\theta) = &\quad e^{\frac{1}{4}(Z_{24}\, e^{-\theta}+\overline{Z}_{24}\, e^{\theta})},\\
\chi_{13}(\theta) = \chi^0_{13}(\theta) = &-e^{\frac{1}{4}(Z_{13}\, e^{-\theta}+\overline{Z}_{13}\, e^{\theta})},\\
\chi_{24}(\theta) = \chi^0_{24}(\theta) = &-e^{\frac{1}{4}(Z_{24}\, e^{-\theta}+\overline{Z}_{24}\, e^{\theta})},\\
\chi^0_{13}(\theta) = &-e^{\frac{1}{4}(Z_{13}\, e^{-\theta}+\overline{Z}_{13}\, e^{\theta})},\\
\chi^0_{24}(\theta) = &-e^{\frac{1}{4}(Z_{24}\, e^{-\theta}+\overline{Z}_{24}\, e^{\theta})}.
\end{aligned} \tag{4.126}$$

In the plateau region $|\theta| \ll -\log(\mathrm{Max}(\mathrm{Im}(Z_{13}, Z_{24})))$, we have $\chi_{13} = -1$ and $\chi_{24} = -1$. This difference of sign compared to the *uudd* spike configuration leads to a considerable difference in eq. (4.113-4.118). In the Virasoro plateau the asymptotics χ_{12} and χ_{34} vanish

$$\begin{aligned}
\chi^0_{13}(\theta) = 0\, e^{\frac{1}{4}(Z_{13}\, e^{-\theta}+\overline{Z}_{13}\, e^{\theta})},\\
\chi^0_{24}(\theta) = 0\, e^{\frac{1}{4}(Z_{24}\, e^{-\theta}+\overline{Z}_{24}\, e^{\theta})},
\end{aligned} \tag{4.127}$$

whilst the asymptotics of χ_{14} and χ_{23} diverge

$$\begin{aligned}
\chi^0_{13}(\theta) = -\infty\, e^{\frac{1}{4}(Z_{13}\, e^{-\theta}+\overline{Z}_{13}\, e^{\theta})},\\
\chi^0_{24}(\theta) = -\infty\, e^{\frac{1}{4}(Z_{24}\, e^{-\theta}+\overline{Z}_{24}\, e^{\theta})}.
\end{aligned} \tag{4.128}$$

When we take these asymptotics as approximate χ-functions and iterate with eq. (4.91), we notice that the factors of zero or infinity do not change with iterations. Therefore, we are tempted to conclude that the corrected asymptotics are the full χ-functions and read off the cross-ratio $x_2 = \infty$ using eq. (4.8). However, if we introduce an ϵ parameter such that in the

limit $\epsilon \to 0$ the factors of 0 and ∞ in eq. (4.127, 4.128) are reproduced, we find that these asymptotics do not solve the χ-system even in the limit as $\epsilon \to 0$. The interpretation is that the system of integral equations in eq. (4.91) diverges in the Virasoro limit for the *udud* spike configuration in the triangulation we presented in this chapter. In order to regularise this limit we will consider this limit in a different triangulation.

Symmetric configuration

In this subsection we will briefly explain how to regularise the *udud* spike configuration. We regularise by going to a different triangulation considered in [3]. There are quite a few differences between the two triangulations. First, we have a different set of WKB lines

$$\mathbb{E} = \{E_{12}, E_{34}, E_{24}, E_{\hat{24}}, E_{14}, E_{23}\}. \tag{4.129}$$

Moreover, the forms of the χ-functions, the A-functions, the S-functions and the χ-system are different and summarised in eq. (145-158) in [3]. However, we assume that the formulas for the areas in eq. (4.110) stay the same. In this subsection we specialise to the symmetric configuration when $w_2 = 1/2$ and $\overline{\ell} = 0$. For this configuration in section 4.6.2 we find the masses of the χ-functions to be

$$\begin{aligned} Z_{12} &= Z_{14} = -i\pi\,\Delta\,(1-\ell), \\ Z_{24} &= Z_{\hat{24}} = 0, \\ Z_{23} &= Z_{34} = -i\pi\,\Delta\,(1+\ell). \end{aligned} \tag{4.130}$$

These produce the following asymptotics

$$\begin{aligned} \chi_{12}^{-} &= \chi_{14}^{-} = -\,e^{-\pi\,\Delta\,(1-\ell)\cosh(\theta)}, \\ \chi_{24}^{-} &= \chi_{\hat{24}}^{-} \to -\,1, \\ \chi_{23}^{-} &= \chi_{34}^{-} = -\,e^{-\pi\,\Delta\,(1+\ell)\cosh(\theta)}. \end{aligned} \tag{4.131}$$

These asymptotics turn out to solve the χ-system presented in [3] in eq. (151-152). We read off the cross-ratio with[12]

$$\chi_{24}(\theta^*) = \frac{x_{14}x_{23}}{x_{12}x_{34}} \tag{4.132}$$

[12]This is the only equation valid among eq. (4.97 in the [3] triangulation.

we find that $x_2 = \infty$. In order to find the area of this configuration, we need to find the Virasoro kink contribution first. Analogously to eq. (4.124) we find that

$$\Delta A_{fin} = -\frac{2}{\pi}\int_{-1}^{0}\frac{df}{f}\,\log(1+f) = -\frac{\pi}{3}.$$

Taking into account this contribution we find

$$A_{fin} = \sum_{E\in\mathbb{E}} iZ_E \int \frac{d\theta}{2\pi}\, e^{-\theta}\,\log\left(1+A_E^-(\theta)\right) = 0, \tag{4.133}$$

where in the final equality we have used that $A_{12} = A_{34} \to 0$, $Z_{24} = Z_{\hat{24}} = 0$ and $A_{14} = A_{23} \to 0$. Moreover, these also imply that

$$\kappa_{12} = \kappa_{34} = \kappa_{14} = \kappa_{23} = 0 \tag{4.134}$$

On the other hand, other $\kappa_2 4$ diverges

$$\kappa_{24} = \int_{\mathbb{R}} \frac{d\theta}{2\pi}\frac{\log(1+A_{24}^-)}{\cosh\theta} = \lim_{\epsilon\to 0}\int_{\mathbb{R}}\frac{d\theta}{2\pi}\frac{\log(1+e^{-\epsilon\cosh(\theta)})}{\cosh\theta} \to \infty. \tag{4.135}$$

In order to find A_κ part of the area, we still need to find κ_{13}. For this purpose we use the Schouten identity to obtain

$$s_1\wedge s_3 = \left(\frac{1}{\sqrt{u}}+\sqrt{u}\right)\frac{\sqrt{s_1\wedge s_2\; s_2\wedge s_3\; s_3\wedge s_4\; s_1\wedge s_4}}{s_2\wedge s_4}, \tag{4.136}$$

$$\log\kappa_{13} = \log\left(\frac{1}{\sqrt{u}}+\sqrt{u}\right) - \log\kappa_{24}. \tag{4.137}$$

We see that the infinite contribution of κ_{24} cancels out and we obtain

$$G_4^{udud}(x_1,x_2,x_3,x_4) = \frac{1}{x_{12}^{2\mathbf{\Delta}(1+\ell)}x_{23}^{2\mathbf{\Delta}(1-\ell)}} \qquad \text{for } x_2\to x_4 \tag{4.138}$$

which corresponds to a geodesic string configuration.

Geodesic hypothesis

In this subsection we explain why we conjecture that the *udud* spike configuration gives the geodesic configuration described in section 4.2 for all cross-ratios.

Finding that the *udud* spike configuration gives a geodesic string for just $x_2 \to \infty$, might not seem a particularly persuasive argument for the conjecture. However, from the perspective of the worldsheet there seems to be nothing special about the $w_2 = 1/2$ configuration

we have studied. The field γ stays trivially zero for all w_2. The only feature that distinguishes $w_2 = 1/2$ is additional symmetry that enables us to solve this configuration. Notice that even for $\bar{\ell} \neq 0$ we cannot solve the $x_2 \to \infty$ case, even though we expect the string configuration not to change with $\bar{\ell}$. Therefore, there are situations when we cannot solve the χ-system, even though we know that the string is geodesic. We suspect that in a similar way the *udud* spike configuration gives the geodesic configuration described in section 4.2 for all cross-ratios, even though it is particularly hard to solve the χ-system outside the symmetric configuration[13].

Further, we would like to draw attention to the similarity of the symmetric configuration, we have just solved, and the extremal limit considered by the authors of [3]

$$\langle \mathcal{O}^{\mathbf{\Delta}_1}(x_1)\, \mathcal{O}^{\mathbf{\Delta}_2}(x_2)\, \mathcal{O}^{\mathbf{\Delta}_3}(x_3)\, \overline{\mathcal{O}}^{\mathbf{\Delta}_1+\mathbf{\Delta}_2+\mathbf{\Delta}_3}(x_4) \rangle. \tag{4.139}$$

There the authors showed that the string degenerates to three geodesic strings for the $w_2 = 1/2$ symmetric configuration, for all other values of the cross-ratio the limit was not accessible with analytic methods.

4.5 Crossing symmetry

In section 4.2, we have argued that when $\ell = 0$ or $\bar{\ell} = 0$ the four-point correlator has an extra crossing symmetry.[14] For example, the first and the third operator are identical when $l = 0$, thus switching $x_1 \leftrightarrow x_3$ should leave the correlator invariant. Subsequently, we used x_2 to parametrise the cross-ratios, and used conformal transformations to put $x_1 = 0,\ x_3 = 1,\ x_4 = \infty$. In that parametrisation, the crossing transformation is achieved with $x_2 \to 1 - x_2$ transformation. This section is dedicated to how the crossing symmetry is realised for the integrable system presented in section 4.3.

Let us start with a set of χ-functions that are solutions to the χ-system in eq. (4.72). We

[13] In order to check this conjecture, one would have to have a numerical code to solve for the χ-functions outside the Virasoro limit for the *udud* configuration and extrapolate the results to the Virasoro limit.

[14] In section 4.2, we have taken $\ell \geq \bar{\ell}$; therefore, we have only seen the symmetry when $\bar{\ell} = 0$. When we consider the integrable system, we do not need to take $\ell \geq \bar{\ell}$, and the symmetry under $Z \leftrightarrow \overline{Z}$ exchange ensures that we have the crossing symmetry when $\ell = 0$ as well.

can construct a new set of χ'-functions

$$\begin{aligned}
\chi'_{12} &= (1+\chi_{13})^2\,\chi_{14}, \\
\chi'_{34} &= (1+\chi_{13})^2\,\chi_{23}, \\
\chi'_{13} &= \chi'_{24} = 1/\chi_{13} = 1/\chi_{24}, \\
\chi'_{14} &= \frac{\chi_{12}\,\chi_{13}^2}{(1+\chi_{13})^2}, \\
\chi'_{23} &= \frac{\chi_{34}\,\chi_{13}^2}{(1+\chi_{13})^2}.
\end{aligned} \tag{4.140}$$

These turn out to be a solutions to the χ-system as well. A simple way to see that eq. (4.140) describes a new solution to the χ-system is to define $h \equiv (1+\chi_{13})^2$, and use eq. (4.72, 4.84, 4.85) to find

$$h\,h^{--} = (1+\chi_{13})^2\,(1+\chi_{13}^{--})^2 = (1+\chi_{13})^2\,(1+\frac{S_{13}}{\chi_{13}})^2 = \frac{S'_{12}}{S_{14}} = S_{13}^2\,\frac{S_{12}}{S'_{14}}. \tag{4.141}$$

There are two interesting properties of this solution. First, by virtue of $Z_{13} = 0$, from eq. (4.140) we can read off the new masses

$$\begin{aligned}
Z'_{12} &= Z_{14}, & Z'_{13} &= 0, & Z'_{14} &= Z_{12}, \\
Z'_{34} &= Z_{23}, & Z'_{24} &= 0, & Z'_{23} &= Z_{34}.
\end{aligned} \tag{4.142}$$

Such a transformation amounts to replacing $w_2 \to 1-w_2$ on the worldsheet. We prove it, by first observing that the masses Z_E defined in eq. (4.70) involve only closed contours, and as a result they are invariant under conformal transformations on the worldsheet. Further, we notice that the transformation in eq. (4.142) corresponds to switching the second and the fourth puncture. However, switching second and fourth puncture and then performing conformal transformation

$$w \to \frac{(1-w_2)\,w}{w-w_2} \tag{4.143}$$

is equivalent to replacing w_2 with $1-w_2$. Therefore, the transformation of masses in eq. (4.142) is equivalent to replacing $w_2 \to 1-w_2$. Second, if we parametrise the χ-functions at $\theta^* = 0, i\pi$ with x_2 as in eq. (4.98)

$$\begin{aligned}
\chi_{12}(\theta^*) = \chi_{34}(\theta^*) &= -\frac{1}{1-x_2}, \\
\chi_{13}(\theta^*) = \chi_{24}(\theta^*) &= \frac{1-x_2}{x_2}, \\
\chi_{14}(\theta^*) = \chi_{23}(\theta^*) &= -x_2.
\end{aligned} \tag{4.144}$$

Then the χ'-functions evaluated at θ^* give

$$\begin{aligned}\chi_{12}(\theta^*) = \chi_{34}(\theta^*) &= -\frac{1}{x_2},\\ \chi_{13}(\theta^*) = \chi_{24}(\theta^*) &= \frac{x_2}{1-x_2},\\ \chi_{14}(\theta^*) = \chi_{23}(\theta^*) &= -(1-x_2),\end{aligned} \tag{4.145}$$

Eq. (4.144) and eq. (4.145) are related by $x_2 \to 1 - x_2$, which we argued in section 4.2.3 is the crossing transformation.

For the four-point function to be invariant under the crossing transformation, the area of these two solutions must be the same. First step is to notice that some of the A-functions defined in eq. (4.85) have simple transitions under the crossing in eq. (4.140), namely

$$\begin{aligned} A'_{12} &= A_{14}, & A'_{14} &= A_{12},\\ A'_{34} &= A_{23}, & A'_{23} &= A_{34}. \end{aligned} \tag{4.146}$$

The consequence of eq. (4.142) and eq. (4.146) is that the $A_{fin} = \frac{\pi}{2} + \frac{i}{2}\sum_{e\in\mathbb{E}} Z_e\,\eta_e$ part for the area is invariant. However, we still need to find how A_κ transforms. Now, we will now concentrate on the transformation of A_{13} and prove that $A'_{13} = A^*_{13}$.

We are dealing with an operator on a line, thus we can put the punctures w_1, w_2, w_3, w_4 on the real axis. When we transport solutions to the linear problem defined in section 4.3.1 between consecutive punctures, we move only along the real line, and the connection defined in eq. (4.30) is purely real. Consequently, some of the A-functions defined in eq. (4.85) that involve only transporting solutions along the real lines are real

$$A_{12} = -\frac{(s_1 \wedge \widetilde{s}_2)(s_2 \wedge \widetilde{s}_1)}{(s_1 \wedge \widetilde{s}_1)(s_2 \wedge \widetilde{s}_2)} \in \mathbb{R}, \qquad A_{14} = -\frac{(s_1 \wedge \widetilde{s}_4)(s_4 \wedge \widetilde{s}_1)}{(s_1 \wedge \widetilde{s}_1)(s_4 \wedge \widetilde{s}_4)} \in \mathbb{R}, \tag{4.147}$$

$$A_{34} = -\frac{(s_3 \wedge \widetilde{s}_4)(s_4 \wedge \widetilde{s}_3)}{(s_3 \wedge \widetilde{s}_3)(s_4 \wedge \widetilde{s}_4)} \in \mathbb{R}, \qquad A_{23} = -\frac{(s_2 \wedge \widetilde{s}_3)(s_3 \wedge \widetilde{s}_2)}{(s_2 \wedge \widetilde{s}_2)(s_3 \wedge \widetilde{s}_3)} \in \mathbb{R}, \tag{4.148}$$

We can combine these to form S_{13}, which also must be real

$$\chi_{13}\,\chi^{--}_{13} = S_{13} = \frac{(1+A_{14})(1+A_{23})}{(1+A_{12})(1+A_{34})} \in \mathbb{R}. \tag{4.149}$$

Combing eq. (4.149, 4.142, 4.91), and taking care of the residues, we find

$$\chi^{--}_{13} = \chi^*_{13}, \tag{4.150}$$

which we use to prove that both sides of eq. (4.141) are real

$$h\,h^{--} = \frac{S'_{12}}{S_{14}} = S_{13}^2\,\frac{S_{12}}{S'_{14}} \in \mathbb{R}. \tag{4.151}$$

Together with the definitions of S-functions in eq. (4.84), we get

$$(1+A_{13})(1+A_{24})(1+A'_{13})(1+A'_{24}) \in \mathbb{R}. \tag{4.152}$$

A_{13} and A_{24} are independent, as a result

$$(1+A_{13})(1+A'_{13}) \in \mathbb{R}, \qquad (1+A_{24})(1+A'_{24}) \in \mathbb{R}. \tag{4.153}$$

Eq. (4.153) must hold any value of θ and all possible masses $Z_{12}, Z_{34}, Z_{14}, Z_{23}$ hence

$$A'_{13} = A^*_{13}, \qquad A'_{24} = A^*_{24}, \qquad S'_{12} = \frac{1}{S^*_{14}}, \qquad S'_{14} = \frac{1}{S^*_{12}}. \tag{4.154}$$

We conclude that only the imaginary part of A_{13} and A_{24} changes. However, in section 4.3.13 we have argued that the imaginary part is odd and gets integrated to zero when we evaluate κ_{13}, κ_{24}.

$$\kappa'_{13} = \kappa_{13} = \int \frac{d\vartheta}{\pi}\frac{\log(1+A^-_{13})}{\cosh(\vartheta)}, \qquad \kappa'_{24} = \kappa_{24} = \int \frac{d\vartheta}{\pi}\frac{\log(1+A^-_{24})}{\cosh(\vartheta)}. \tag{4.155}$$

Now, let us look at how A_κ, defined in eq. (4.110), transforms. For $\bar{l} = 0$ we have $\Delta_{12} = \Delta_{14}$ and $\Delta_{34} = \Delta_{23}$. Therefore, the area does not change when we exchanging $\kappa_{12} \leftrightarrow \kappa_{14}$ and $\kappa_{34} \leftrightarrow \kappa_{23}$, as a result of eq. (4.146). Hence, the area of the minimal surface is invariant under crossing symmetry when $\bar{l} = 0$.

On the other hand, when $l = 0$, we find $\Delta_{12} = \Delta_{23}$ and $\Delta_{34} = \Delta_{14}$, and exchanging $\kappa_{12} \leftrightarrow \kappa_{23}$ and $\kappa_{34} \leftrightarrow \kappa_{14}$ does not change the area. In this case, we rewrite eq. (4.140-4.146) with $14 \leftrightarrow 23$ interchanged, and we conclude that our four-point function is also invariant under crossing symmetry. When $l \neq 0$ and $\bar{l} \neq 0$, A_κ is clearly not invariant under the symmetry. We conclude that the area of the minimal surface is invariant under crossing symmetry if and only if $l = 0$ or $\bar{l} = 0$. This exactly matches the crossing symmetry.

The content of this section was confirmed by numerically implementing integral equations in eq. (4.91). In fact, all equations in this section were first observed numerically, and then proved analytically.

4.5.1 Inverted cross-ratio problem

The integrable system we have presented in the last two sections introduced by the authors of [3] suffers from an artefact. The numerical studies of this integrable model revealed that if the second puncture w_2 approaches the third puncture w_3 on the worldsheet, then, in the space-time, the second puncture x_2 approaches the first puncture x_1. It is as if the worldsheet cross-ratio is "inverted" with respect to the space-time cross-ratio. In fact, this property could have been noticed in the numerics in section 6.2 of [3].

At the same time, the results we present in section 4.6 are self-consistent if and only if the two punctures that get close on the worldsheet are the same as the ones getting close in the space-time. For example in section 4.6.1 we look at the collisions of zeros of stress energy tensor. They follow the expected pattern if and only if the two punctures that approach each other on the worldsheet also do so in the space-time.

Although the authors are not certain what the reason for this artefact is, there are two ways to correct it. One is to replace

$$x_2 \to 1 - x_2 \tag{4.156}$$

for $0 < x_2 < 1$ at the end of the calculations. The second is to distinguish between the conformal weights on the worldsheet and in the space-time

$$\begin{aligned} \ell^{\text{worldsheet}} &= -\ell, \\ \bar{\ell}^{\text{worldsheet}} &= \bar{\ell}, \end{aligned} \tag{4.157}$$

and replace

$$w_2 \to 1 - w_2. \tag{4.158}$$

When we perform both transformations eq. (4.157, 4.158) the masses of the χ-functions change in the following way

$$\begin{aligned} &Z_{12} \to Z_{23}, && Z_{13} = 0, && Z_{14} \to Z_{34}, \\ &Z_{34} \to Z_{14}, && Z_{24} = 0, && Z_{23} \to Z_{12}. \end{aligned} \tag{4.159}$$

In the following sections we will be correcting the cross-ratio artefact by performing the transformation in eq. (4.156).

4.6 Particular limits

In this section, we will consider the analytically available limits of the integrable system. First, we present some intuition behind the behaviour of the zeros of stress energy tensor. Then we present the symmetric configuration at $w_2 = 1/2$ that is invariant under the crossing symmetry. Finally, we will consider going as far away from the symmetric configuration as possible *i.e.* $w_2 \to w_2^{\pm}$ and investigate the OPE limit.

4.6.1 Colliding zeros of the stress-energy tensor

In section 4.3.6, we have discussed that for $w_2^- < w_2 < w_2^+$ all four roots are distinct and complex. Two zeros are above the real axis and the two others are complex conjugates of the first two. In this subsection, we discuss what happens when w_2 reaches $w_2^{\pm}$ and the zeros of the stress-energy tensor collide on the real axis.

The values of $w_2^{\pm}$ are always between 0 and 1 for $\ell < 1$, $\bar{\ell} < 1$. They reach these bounds when $\ell = \bar{\ell} \Leftrightarrow w_2^- = 0$ and when $\ell = -\bar{\ell} \Leftrightarrow w_2^+ = 1$. The χ-system for these special cases are considered in detail in section 4.6.3 and 4.7.3.

When $w_2 = w_2^{\pm}$, all the zeros collide at

$$w = w^{\pm}_{collide} \equiv \frac{1}{2}\left(1+\ell\right) \pm \frac{\sqrt{\left(1-\ell^2\right)\left(1-\bar{\ell}^2\right)}}{2\left(1-\bar{\ell}\right)} \in \mathbb{R}. \tag{4.160}$$

The plus or minus we choose depending on whether $w_2 = w_2^+$ or $w_2 = w_2^-$ respectively. From eq. (4.160) we notice that $w^-_{collide}$ can be either between $0 < w^-_{collide} < 1$ or $w^-_{collide} < 0$ depending on whether $\ell > \bar{\ell}$ or $\ell < \bar{\ell}$. Similarly, $w^+_{collide}$ can be either between $0 < w^+_{collide} < 1$ or $1 < w^+_{collide}$ depending on whether $\ell < -\bar{\ell}$ or $\ell > -\bar{\ell}$. Furthermore, when $0 < w^-_{collide} < 1$ we have $0 < w_2^- < w^-_{collide}$, whilst when $0 < w^+_{collide} < 1$ we have $w^+_{collide} < w_2^+ < 1$.

These results have a nice physical interpretation. In next sections, we consider taking $w_2 \to w_2^-$ and show it corresponds to the first and the second operator coming close. In this limit, these two operators prefer to Wick contract between themselves. Similarly, this happens to the third and the fourth. When $\ell = \bar{\ell}$ there are no other contractions we need to do, we will usually refer to it as the special case. Whilst when $\ell > \bar{\ell}$ the first and the fourth operators need to form additional Wick contractions between themselves. On the other hand, the second and the third are fully contracted, so there are no contractions between

them. In our worldsheet picture, two zeros collide on a WKB line that connects the two punctures that have no Wick contractions. The same logic can described all the other cases.

We consider the limit $w_2 \to w_2^-$ of the χ-system for $\ell = \bar{\ell}$ in section 4.6.3 and for $\ell \neq \bar{\ell}$ in section 4.6.4.

Triangulation changes

In section 4.3.7, we have plotted the separating WKB lines and found the triangulation to be a tetrahedron. The rest of the content of this and the next sections depend on the assumption that the triangulation does not change for the particular operators and value of w_2 that we consider. Here we would like to justify this assumption.

In section 4.3.7 we have noticed that it is the separating WKB lines that carry all the information about the triangulation. They are the WKB lines that connect one of the zeros and one of the punctures. Like all other WKB lines they cannot cross each other. Therefore, the only way for them to change their topology is when one of the regions enclosed by separating WKB lines shrinks to a curve, see fig. 4.8. When this region shrinks into a curve,

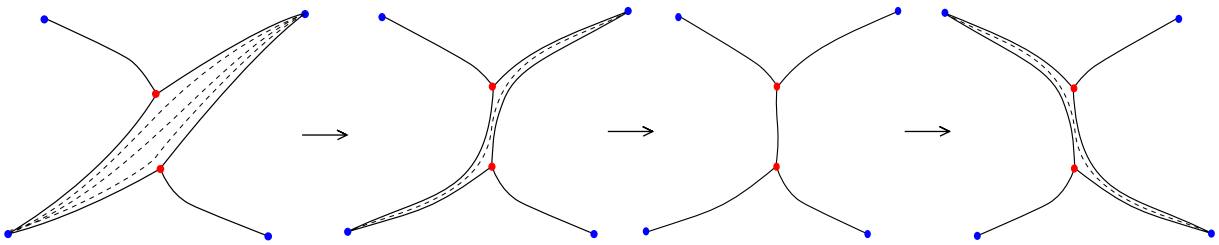

Figure 4.8: The process of a triangulation change. Schematic plot of separating WKB lines represented by solid black curves. The dashed curves are the generic WKB lines. Blue/red dots represent poles/zeros of the stress-energy tensor. Notice that, as a result of the triangulation change, the presented generic WKB lines join different operators before and after the transition.

two separating WKB lines join to form a curve joining two zeros of stress energy tensor. Afterwards, the two other separating WKB lines open up, and a new region appears joining two different punctures see fig. 4.8. In the Virasoro limit, when the two zeros of the stress-energy tensor above the real axis are very close together, it is particularly easy to check if there is a separating WKB line joining the two zeros indicating a triangulation change. It is enough to find the phase of $\sqrt{T}$ between the two zeros. Plotting this phase for different

w_2, Δ, ℓ, $\bar{\ell}$, we have not found any phase transitions in the range $w_2^- < w_2 < w_2^+$.

On the other hand, when the zeros collide for $w_2 = w_2^{\pm}$, we would expect a triangulation change in the way we present in fig. 4.9. We have plotted the separating lines for several values of w_2 outside the range $w_2^- < w_2 < w_2^+$ and have found that the new triangulation, that opens up, is another tetrahedral triangulation equivalent to the one described in section 4.3. Therefore, we use the same triangulation for all w_2.

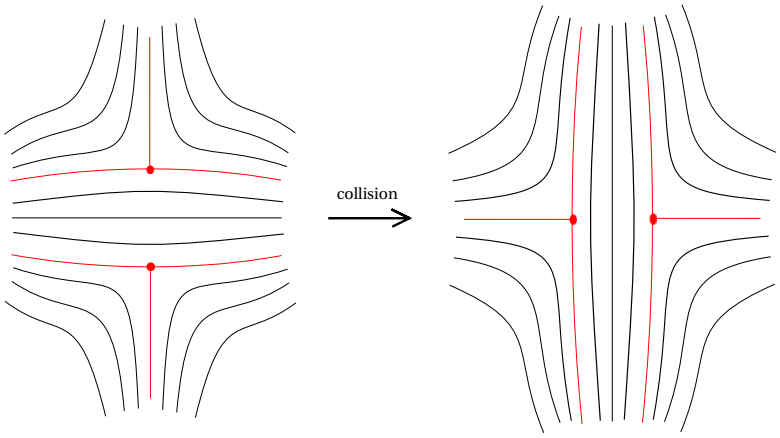

Figure 4.9: Two zeros of the stress-energy tensor (marked as the red dots) colliding and leading to a triangulation change. Solid black curves represent WKB lines, and solid red curves represent separating WKB lines that pass through zeros.

4.6.2 Self dual configuration

In section 4.5, we have shown that when $\ell = 0$ or $\bar{\ell} = 0$ the area of the minimal surface is invariant under the crossing symmetry. The crossing transformation amounts to $x_2 \to 1 - x_2$ and $w_2 \to 1 - w_2$. Clearly, $x_2 = w_2 = 1/2$ is a self-dual configuration under crossing symmetry. In this section, we will solve it analytically.

We choose to consider the $\bar{\ell} = 0$ case. We start by finding the asymptotic expressions for the χ-functions. From eq. (4.142) we see that $Z_{12} = Z_{14}$ and $Z_{34} = Z_{23}$, which together with eq. (4.71, 4.112) determines all the masses

$$\begin{aligned} Z_{12} &= Z_{14} = -i\pi\,\Delta\,(1+\ell), \\ Z_{13} &= Z_{24} = 0, \\ Z_{23} &= Z_{34} = -i\pi\,\Delta\,(1-\ell). \end{aligned} \tag{4.161}$$

Therefore, the asymptotic values of the χ-functions (4.67) for $w_2 = 1/2$, corrected by imposing the Virasoro constraint, as described in section 4.4, are given by

$$\begin{aligned} &\chi_{12} = -2\, e^{-\pi\Delta\,(1+\ell)\cosh\theta}, \qquad &&\chi_{13} = 1, \qquad &&\chi_{14} = -\frac{1}{2}\, e^{-\pi\Delta\,(1+\ell)\cosh\theta}, \\ &\chi_{34} = -2\, e^{-\pi\Delta\,(1-\ell)\cosh\theta}, \qquad &&\chi_{24} = 1, \qquad &&\chi_{23} = -\frac{1}{2}\, e^{-\pi\Delta\,(1-\ell)\cosh\theta}. \end{aligned} \tag{4.162}$$

We evaluate the S-functions in eq. (4.84) for these χ-functions

$$\begin{aligned} S_{12} &= S_{14} = 4, \\ S_{24} &= S_{13} = 1, \\ S_{14} &= S_{23} = \frac{1}{4}. \end{aligned} \tag{4.163}$$

We see that the asymptotic values of the χ-functions in eq. (4.162) satisfy the χ-system in eq. (4.72), thus they are the full interacting χ-functions for $x_2 = w_2 = 1/2$. We proceed to find the area. First, we evaluate A-function in eq. (4.85)

$$\begin{aligned} A_{12} &= A_{14} = -1 + \coth(\pi\Delta\cosh\theta)\tanh\left(\frac{\pi\Delta\,(1+\ell)}{2}\cosh\theta\right), \\ A_{13} &= \tanh(\pi\Delta\,(1+\ell)\cosh\theta)\tanh(\pi\Delta\,(1-\ell)\cosh\theta)\,, \\ A_{23} &= A_{34} = -\mathrm{csch}(\pi\Delta\cosh\theta)\,\mathrm{sech}\left(\frac{\pi\Delta\,(1-\ell)}{2}\cosh\theta\right)\sinh\left(\frac{\pi\Delta\,(1+\ell)}{2}\cosh\theta\right), \\ A_{24} &= \frac{\left(1+e^{2\Delta\pi\cosh(\theta)}-2e^{\Delta\,(1-\ell)\,\pi\cosh(\theta)}\right)\left(1+e^{2\Delta\pi\cosh(\theta)}-2e^{\Delta\,(1+\ell)\,\pi\cosh(\theta)}\right)}{\left(e^{2\Delta\pi\cosh(\theta)}-1\right)^2}. \end{aligned} \tag{4.164}$$

We can use these expressions to find A_{fin} and A_κ defined in eq. (4.110). As a result, we can find the area of the minimal surface in terms of integrals over spectral parameter. These integrals involve logarithms and hyperbolic functions and can be readily evaluated numerically. We present the numerical results in section 4.7.2.

In the special case when $\ell = 0$, the A-functions simplify, and the area in eq. (4.110) becomes

$$\begin{aligned} A_{fin} &= \frac{\pi}{2} + 2\Delta\int_{-\infty}^{\infty} d\theta\,\cosh\theta\,\log\left(1-\frac{1}{2}\,\mathrm{sech}^2\left(\frac{\pi\Delta}{2}\cosh\theta\right)\right), \\ A_\kappa &= -\frac{2\Delta}{3}\left(4\int_{-\infty}^{\infty} d\theta\,\frac{1}{\cosh\theta}\log\left(1-\frac{1}{2}\,\mathrm{sech}^2\left(\frac{\pi\Delta}{2}\cosh\theta\right)\right)\right. \\ &\qquad \left. + 2\int_{-\infty}^{\infty} d\theta\,\frac{1}{\cosh\theta}\log\left(1+\tanh^2\left(\frac{\pi\Delta}{2}\cosh\theta\right)\right)\right). \end{aligned} \tag{4.165}$$

The above integrals can be expanded for both small and large Δ. For example, for large Δ we can expand A_{fin} in terms of the modified Bessel functions of the second kind

$$A_{fin} = \frac{\pi}{2} - 4\,\Delta \sum_{i,j=1}^{\infty} \frac{(-2j)^i (-1)^{i\,j}}{i} K_1(i\,j\,\pi\,\Delta) + \dots . \tag{4.166}$$

4.6.3 OPE limit: special case

In this and the next subsection we study the limit of the integrable system presented in section 4.3 when $w_2 \to w_2^{\pm}$. First, we will deal with the special case when $\ell = -\bar{\ell}$ which makes $w_2^+ = 1$. We argue that this limit corresponds to the OPE limit when the space-time locations of two operators come close. The more general case when $\ell \neq \pm\bar{\ell}$ we leave for the next subsection.

Decoupling of massive modes

When $\ell = -\bar{\ell}$, it is interesting to look at the roots in eq. (4.58) around $w_2 \to 1$

$$w_\pm = 1 + \frac{1-w_2}{1-l} \pm i\sqrt{\frac{1+\ell}{1-\ell}\,(1-w_2)} + \mathcal{O}\big((1-w_2)^{3/2}\big)\,. \tag{4.167}$$

We can set $\delta U \to 0$. We notice that the imaginary part is proportional to $\sqrt{1-w_2}$, whilst the real part is linear in $(1-w_2)$. As a result, when $w_2 \to 1$, the roots are much further above or below the real axis than the two poles of the stress-energy tensor, at $w = 1$ and w_2, are apart. From the perspective of the cycle Z_{12} these two poles cancel each other in the limit as $w_2 \to 1$ making Z_{12} vanish. In order to find the other Z_E masses we use eq. (4.71)

$$\begin{aligned} Z_{23} &\to -2\pi\,i\,\Delta\,(1+\ell), \\ Z_{14} &\to -2\pi\,i\,\Delta\,(1-\ell), \\ Z_{12} = Z_{34} &\to 0, \\ Z_{13} = Z_{24} &= 0. \end{aligned} \tag{4.168}$$

Both χ_{14} and χ_{23} are massive, and as a result far enough from the origin

$$\chi_{14}^{-}(\theta) \propto e^{-2\pi\,\Delta\,(1-\ell)\cosh(\theta)},$$

they are exponentially small, and we can set them to zero. Furthermore, as $S_{12} = S_{34}$, $S_{13} = S_{24}$ and $Z_{12} = Z_{34}$, $Z_{13} = Z_{24}$ from eq. (4.67-4.91), we have $\chi_{12} = \chi_{34}$ and $\chi_{13} = \chi_{24}$.

These observations reduce the χ-system in eq. (4.72) considerably

$$\begin{aligned} \chi_{12}\,\chi_{12}^{--} &= (1+(1+\chi_{12})^2\,\chi_{13})^2, \\ \chi_{13}\,\chi_{13}^{--} &= \frac{1}{(1+\chi_{12})^2}, \\ \chi_{14}\,\chi_{14}^{--} = \chi_{23}\,\chi_{23}^{--} &= \frac{(1+\chi_{12})^2}{(1+(1+\chi_{12})^2\,\chi_{13})^2}. \end{aligned} \tag{4.169}$$

Notice that the massless modes χ_{12} and χ_{13} do not couple to massive modes modes χ_{14}, χ_{23}. We define

$$\begin{aligned} f &\equiv \chi_{12}, \\ h &\equiv (1+\chi_{12})^2\,\chi_{13}. \end{aligned} \tag{4.170}$$

Using eq. (4.169) we find that h satisfies a simple difference equation

$$h\,h^{--} = (1+\chi_{12})^2\,\chi_{13}\,(1+\chi_{12}^{--})^2\,\chi_{13}^{--} = (1+f^{--})^2. \tag{4.171}$$

In the above equation, we shift the spectral parameter by $i\pi$ and use the fact that the χ-functions are $2\pi i$ periodic. We find that f and h satisfy the following set of equations

$$\begin{aligned} f\,f^{--} &= (1+h)^2, \\ h\,h^{--} &= (1+f)^2. \end{aligned} \tag{4.172}$$

The region far enough from the origin such that χ_{14}, χ_{23} are small enough, but

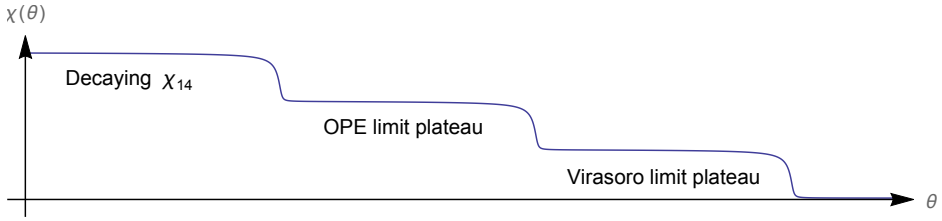

Figure 4.10: Imposing the Virasoro constraint first and the OPE limit second we find that the χ-functions form two plateaux. The figure indices the relative order of limits.

$|\theta| \ll -\log(\text{Max}(\text{Im}(Z_{12}, Z_{34})))$, such that χ_{12} is still a constant is called the OPE plateau region, see fig. 4.10. In this region, all χ-functions are either zero or constant. Therefore, their value has to be given by an algebraic solution to eq. (4.172) with $f^{--} = f$ and $h^{--} = h$. There is only one algebraic solution to the χ-system in eq. (4.172) $h = -1 - f$. This one

parameter family of solutions can be conveniently parameterised with x_2

$$\begin{aligned} \chi_{12} &= -\frac{1}{1-x_2}, & \chi_{13} &= \frac{1-x_2}{x_2}, \\ \chi_{14} &= -x_2\, e^{-2\pi\,\Delta\,(1-\ell)\,\cosh(\theta)}, & \chi_{23} &= -x_2\, e^{-2\pi\,\Delta\,(1+\ell)\,\cosh(\theta)}. \end{aligned} \tag{4.173}$$

A few comments are in order:

- So far we have found an algebraic solution for the region where the exponentials in eq. (4.173) make χ_{14} and χ_{23} negligible. Unexpectedly, the algebraic solution together with the asymptotics of χ_{14} and χ_{23} presented in eq. (4.173) satisfies the χ-system in eq. (4.72) for all $|\theta| \ll -\log(\text{Max}(\text{Im}(Z_{12}, Z_{34})))$. Therefore, eq. (4.173) describes the χ-functions including the region where χ_{14} and χ_{23} are not small.

- We have chosen the parametrisation of the solution, such that, evaluating the χ-functions at $\theta^* = 0, i\pi$ gives

  $$\chi_{12}(\theta^*) = -\frac{1}{1-x_2}, \qquad \chi_{13}(\theta^*) = \frac{1-x_2}{x_2}, \qquad \chi_{14}(\theta^*) = \chi_{23}(\theta^*) = -x_2.$$

  Notice, that this is equivalent to parametrising the cross-ratios in eq. (4.98) with x_2 by setting $x_1 = 0$, $x_3 = 1$, $x_3 = \infty$ with a conformal transformation.

- The plateau region is followed by a region with $|\theta| \approx -\log(\text{Max}(\text{Im}(Z_{12}, Z_{34})))$ where we cannot assume that χ_{12}, χ_{34} are massless. χ_{12}, χ_{34}, χ_{13}, χ_{24} all interact and are described by the system in eq. (4.172). This region we will call the kink.

Kink free energy

In the kink region χ_{12}, χ_{34}, χ_{13}, χ_{24} all interact, producing a contribution to A_{fin} in eq. (4.125). In this section, we will show that this contribution exactly cancels the factor of $\pi/2$ and $A_{fin} = 0$. We start by evaluating the A-functions in eq. (4.85). Once again, far enough from the origin we can set χ_{14}, χ_{23} to zero and use eq. (4.170)

$$\begin{aligned} A_{12} &= A_{34} = f, \\ A_{13} &= A_{24} = h, \\ A_{14} &= A_{23} = 0. \end{aligned} \tag{4.174}$$

Evaluating A_{fin} with $Z_{13}=0$, $Z_{24}=0$ we get

$$\begin{aligned} A_{fin} &= \frac{1}{2} - \sum_{E\in\mathbb{E}} Z_E \int \frac{d\theta}{2\pi^2} e^{\theta} \log\left(1+A_E(\theta)\right) \\ &= \frac{1}{2} - Z_f \int_{-\infty}^{\infty} \frac{d\theta}{\pi^2}\, e^{\theta} \log(1+f(\theta)) \\ &= \frac{1}{2} - 2\, Z_f \int_{0}^{\infty} \frac{d\theta}{\pi^2}\, \cosh(\theta) \log(1+f(\theta)), \end{aligned} \tag{4.175}$$

where in the last step we have used that $f(\theta)=f(-\theta)$. We will now follow the high temperature expansion procedure to evaluate the integrals. We start with the integral equation for $f=\chi_{12}$ from eq. (4.91)

$$\begin{aligned} \log(f(\theta)) &= \frac{1}{2}\left(Z_f\, e^{-\theta} + \overline{Z}_f\, e^{\theta}\right) + \int \frac{d\theta'}{2\pi i} \frac{\log[(1+h(\theta))^2]}{\sinh(\theta'-\theta+i0)} \\ &= -Z_f \sinh(\theta) + \int \frac{d\theta'}{2\pi i} \frac{\log[(1+h(\theta))^2]}{\sinh(\theta'-\theta+i0)}. \end{aligned} \tag{4.176}$$

We have used $iZ_{12}=iZ_f\in\mathbb{R}$. Then we solve for the source and take the derivative of the whole equation

$$Z_f \cosh(\theta) = -\partial_\theta \log(f) + \int \frac{d\theta'}{2\pi i} \left(\partial_\theta \frac{1}{\sinh(\theta'-\theta+i0)}\right) \log[(1+h(\theta'))^2] \tag{4.177}$$

$$= -\partial_\theta \log(f) - \int \frac{d\theta'}{2\pi i} \left(\partial_{\theta'} \frac{1}{\sinh(\theta'-\theta+i0)}\right) \log[(1+h(\theta'))^2] \tag{4.178}$$

$$= -\partial_\theta \log(f) + \int \frac{d\theta'}{2\pi i} \frac{\partial_{\theta'} \log[(1+h(\theta'))^2]}{\sinh(\theta'-\theta+i0)}.$$

We use this expression to eliminate Z_f in the integral for A_{fin} in eq. (4.175)

$$\begin{aligned} A_{fin} &= \frac{1}{2} + 2\int_0^{\infty} \frac{d\theta}{\pi^2} \frac{\partial_\theta f}{f} \log(1+f(\theta+i\pi/2)) \\ &\quad - 2\int_0^{\infty} \frac{d\theta}{\pi^2}\ \log(1+f(\theta+i\pi/2)) \int \frac{d\theta'}{2\pi i} \frac{\partial_{\theta'} \log[(1+h(\theta'))^2]}{\sinh(\theta'-\theta+i0)} \\ &\equiv \frac{1}{2} - I_1 - I_2, \end{aligned} \tag{4.179}$$

where in the last line we have named the two integrals I_1, I_2. We assume that $f(\theta)$ monotonically increases from the plateau value $f(0)=-\dfrac{1}{1-x_2}$ to $f(\infty)=0$ *i.e.* it is exponentially small for $|\theta| \gg -\log(\mathrm{Max}(\mathrm{Im}(Z_{12}, Z_{34})))$.

$$\begin{aligned} I_1 &= \frac{2}{\pi^2}\int_0^{\infty} d\theta\, \frac{\partial_\theta f}{f}\, \log\left(1+f\right) = \frac{2}{\pi^2}\int_{f(0)}^{f(\infty)} df\, \frac{\log(1+f)}{f} = \frac{2}{\pi^2}\int_{\frac{1}{x_2-1}}^{0} df\, \frac{\log(1+f)}{f} \\ &= \frac{2}{\pi^2}\left(\frac{\pi^2}{3} - 2i\pi \log\left(\frac{1}{1-x_2}\right) - \frac{1}{2}\log\left(\frac{1}{1-x_2}\right)^2 - \mathrm{Li}_2\left(1-x_2\right)\right) \\ &= \frac{1}{3} + \frac{2}{\pi^2}(1 - i\pi - \log(x_2))x_2 + \mathcal{O}(x_2^2). \end{aligned} \tag{4.180}$$

In the last step we have expanded the result around the OPE limit $x_2 = 0$. In order to evaluate I_2 we need to find a corresponding integral equation for $h = (1+\chi_{12})^2\,\chi_{13}$. We notice that $h(\theta)$ is massless. Inverting eq. (4.172) we find

$$\log(h^-(\theta)) = \int_{-\infty}^{\infty} \frac{d\theta'}{2\pi i} \frac{\log[(1+f^-(\theta'))^2]}{\sinh(\theta'-\theta+i0)}, \tag{4.181}$$

Once again we assume that $h(\theta)$ changes monotonically from $h(0) = \frac{x_2}{1-x_2}$ (see eq. (4.173)) to $h(\infty) = 1$ (see eq. (4.120)).

$$\begin{aligned}
I_2 &= +\frac{2}{\pi^2} \int_0^{\infty} d\theta \;\; \log(1+f(\theta)) \int_{-\infty}^{\infty} \frac{d\theta'}{2\pi i} \frac{\partial_{\theta'} \log[(1+h(\theta'))^2]}{\sinh(\theta'-\theta+i0)} \\
&= -\frac{2}{\pi^2} \int_0^{\infty} d\theta \;\; \partial_\theta \log(1+h(\theta)) \int_{-\infty}^{\infty} \frac{d\theta'}{2\pi i} \frac{\log[(1+f(\theta'))^2]}{\sinh(\theta'-\theta+i0)} \\
&= -\frac{2}{\pi^2} \int_0^{\infty} d\theta \;\; \log(h(\theta))\, \partial_\theta \log(1+h(\theta)) \\
&= \frac{2}{\pi^2} \int_{h(0)}^{h(\infty)} \frac{dh}{h} \;\; \log(1+h) + \frac{2}{\pi^2} \log(\frac{x_2}{1-x_2}) \log(\frac{1}{1-x_2}) \\
&= \frac{1}{6} + \frac{2}{\pi^2} \mathrm{Li}_2\left(\frac{x_2}{-1+x_2}\right) \\
&= \frac{1}{6} - \frac{2}{\pi^2} (1+\log x_2)\, x_2 + \mathcal{O}(x_2^2).
\end{aligned} \tag{4.182}$$

Combining these results we find

$$\lim_{x_2 \to 0} A_{fin} = 0. \tag{4.183}$$

Notice that I_2 cancels exactly the contribution from the Virasoro kink found in section 4.4. This contribution arises only when we impose the Virasoro constraint *i.e.* when χ_{13}, χ_{24} are massless. On the other hand, I_1 exactly cancels the constant term in A_{fin} from before imposing the Virasoro constraint. Authors of [3] show that this contribution comes from the zeros of the stress-energy tensor which enter when using the Riemann Bilinear Identity.

Relation between worldsheet and space-time

In the previous subsection we have not discussed the connection between w_2 and x_2. Even though we have found the χ-functions in the limit when $w_2 \to 1$, we were not able to deduce the corresponding value of x_2. The space-time cross-ratio x_2 remains a free parameter, although the worldsheet cross-ratio has a concentrate value. Only at the end of the calculation we have artificially set $x_2 \to 0$. On the other hand, we know that in the limit when $w_2 \to 1$

the zeros of the stress-energy tensor collide at $w = 0$. Therefore, the spikes that source the field γ cancel out and, as a result, $\gamma = 0$ for all w and $A_{fin} = 0$. On the other hand, from section 4.6.3 we know A_{fin} as a function of x_2. In the range we consider, A_{fin} vanishes only for $x_2 \to 0$. Hence, we can deduce that the limit when $w_2 \to 1$ corresponds to $x_2 \to 0$. This illustrates the artefact we described in section 4.5.1. We correct it by replacing $x_2 \to 1 - x_2$. Therefore, the limit described in this section corresponds to $x_2 \to 1$. It is an OPE limit when we collide two operators with the same magnitude but opposite sign of R-charge as $\ell = -\bar{\ell}$.

Kappa terms

In this section, we compute the remaining part of the area in the OPE limit. We start by evaluating the A-functions in eq. (4.85). For $|\theta| \ll -\log(\text{Max}(\text{Im}(Z_{12}, Z_{34})))$ we use the solution in eq. (4.173) to find

$$\begin{aligned} A_{12} &= A_{34} = \frac{1}{x_2 - 1}, \\ A_{13} &= A_{24} = \frac{x_2}{1 - x_2}, \\ A_{14} &= A_{23} = 0. \end{aligned} \tag{4.184}$$

We use these to evaluating A_κ in eq. (4.110)

$$\begin{aligned} A_\kappa &= \sum_{e \in \mathbb{E}} \Delta_e \, \kappa_e = \sum_{e \in \mathbb{E}} \Delta_e \int_{-\infty}^{\infty} d\theta \, \frac{1}{2\pi \cosh\theta} \log(1 + A_e) \\ &= -\frac{2\Delta}{3} \left(\log(1 + \frac{x_2}{1 - x_2}) + \log(1 - \frac{1}{1 - x_2}) \right) \\ &= -\frac{2\Delta}{3} \log x_2 + \mathcal{O}(x_2 \log x_2), \end{aligned} \tag{4.185}$$

where in the last step we have expanded around $x_2 = 0$ and kept only the leading term. Finally, taking into account the $x_2 \to 1 - x_2$ correction, we find that in the OPE limit when we collide the two operators, $x_2 \to 1$, with the same magnitude but the opposite sign of R-charge, $\ell = -\bar{\ell}$, the saddle point gives

$$\lim_{x_2 \to 1} G^{uudd}_{(x_1, x_2, x_3, x_4)} = \lim_{x_2 \to 1} e^{\frac{2\sqrt{\lambda}\Delta}{3} \log(1 - x_2)} \prod_{A > B} (x_{AB}^2)^{\sqrt{\lambda} \Delta_{AB}}. \tag{4.186}$$

The superscript *uudd* indicates that this result corresponds to the *uudd* spike configuration. In the next section we will consider taking two operators with a non-zero net R-charge close together.

4.6.4 Generic case

In section 4.3.6 we have looked at the roots of the stress-energy tensor. We have observed that when $w_2 \to w_2^{\pm}$ the roots collide on the real axis. In this section we would like to study what happens in these limits for $\ell \neq \pm\bar{\ell}$.

Decoupling of massive modes

We choose to study the limit as $w_2 \to w_2^{+}$ when $\ell < -\bar{\ell}$. As discussed in the section 4.3.6, it is the limit when the zeros collide on WKB line E_{12}. As a result, the cycle corresponding to Z_{12} vanishes. The other cycles responsible for the masses of the χ-functions become closed contour integrals, see fig. 4.11. Consequently, we can just read off the values of Z_E using eq. (4.71).

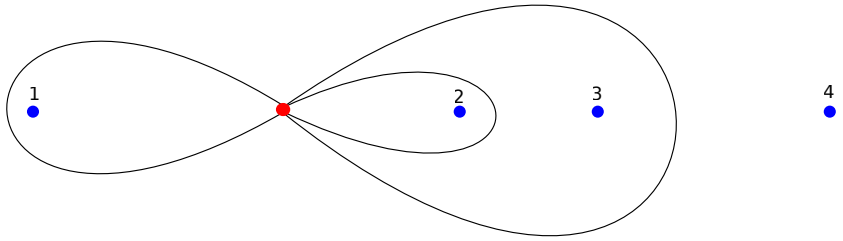

Figure 4.11: Cycles corresponding to masses of each coordinate χ in the OPE limit when all roots collide on the real axis. Cycle corresponding to Z_{12} vanishes. The other cycles become a closed contour integrals. Zeros and double poles of the stress-energy tensor are marked red and blue respectively.

$$
\begin{aligned}
Z_{12} &\to 0, \\
Z_{34} &\to \quad 2\pi\, i\, \Delta\, (\ell + \bar{\ell}), \\
Z_{14} &\to -2\pi\, i\, \Delta\, (1 + \ell), \\
Z_{23} &\to -2\pi\, i\, \Delta\, (1 + \bar{\ell}), \\
Z_{13} &= Z_{24} = 0.
\end{aligned}
\tag{4.187}
$$

Therefore, $\chi_{34}, \chi_{14}, \chi_{23}$ have finite masses and far enough from the origin they are exponentially small and we can set them to zero. Furthermore, as $S_{13} = S_{24}$ and $Z_{13} = Z_{24} = 0$ from eq. (4.67,4.91) we have that $\chi_{13} = \chi_{24}$. These observations reduce the chi-system in

eq. (4.72) considerably

$$\begin{aligned}\chi_{12}\,\chi_{12}^{--} &= (1+(1+\chi_{12})\,\chi_{13})^2, \\ \chi_{13}\,\chi_{13}^{--} &= \frac{1}{1+\chi_{12}}, \\ \chi_{14}\,\chi_{14}^{--} = \chi_{23}\,\chi_{23}^{--} &= \frac{(1+\chi_{12})^2}{(1+(1+\chi_{12})\,\chi_{13})^2}.\end{aligned} \tag{4.188}$$

Notice that the massless modes χ_{13} and χ_{23} do not couple to massive modes $\chi_{12}, \chi_{34}, \chi_{14}$. We define

$$\begin{aligned} f &\equiv \chi_{12}, \\ h &\equiv (1+\chi_{12})\,\chi_{13}, \\ h\,h^{--} &= (1+\chi_{12})\,\chi_{13}\,(1+\chi_{12}^{--})\,\chi_{13}^{--} = (1+f^{--}). \end{aligned} \tag{4.189}$$

In the last equality we have used eq. (4.188). From the above we find that h and g satisfy the following simple set of equations

$$\begin{aligned} f\,f^{--} &= (1+h)^2, \\ h\,h^{--} &= (1+f). \end{aligned} \tag{4.190}$$

Plateau region

We will now concentrate on the region far enough from the origin such that $\chi_{34}, \chi_{14}, \chi_{23}$ are small enough, but $|\theta| \ll -\log(\mathrm{Im}(Z_{12}))$ such that χ_{12} is still a constant. This region we will call the plateau region, see fig. 4.10. In this region all χ-functions are either zero or constant. Therefore, their value has to be given by an algebraic solution to eq. (4.190) with $f^{--} = f$ and $h^{--} = h$. Only three algebraic solutions to eq. (4.190) exist

$$\begin{aligned} f &= 3, & f &= 0, & f &= -1, \\ h &= 2, & h &= -1, & h &= 0, \end{aligned} \tag{4.191}$$

We choose the right solution by considering the limit as $\ell \to \bar{\ell}$. From section 4.6.3 we know that in this limit

$$\begin{aligned} f &\approx \chi_{12}(\theta^*) = -\frac{1}{1-x_2}, \\ h &\approx \left(1+\chi_{12}(\theta^*)\right)^2 \chi_{13}(\theta^*) = \frac{x_2}{1-x_2}. \end{aligned} \tag{4.192}$$

We see that the first solutions does not correspond to realisable cross-ratios. The second corresponds to $x_2 \to \infty$ and the last to $x_2 \to 0$. Therefore, we are clearly interested only in the last solution in eq. (4.191). However, we have to keep in mind that outside the limit as $\ell \to \bar{\ell}$ the plateau values of the χ-functions do not necessarily encode the values of the cross-ratios. This is because the plateau solution is not valid at $\theta = 0, i\pi$.

When writing the χ-functions corresponding to the third solution in eq. (4.191), we notice that χ_{13} diverges; therefore, we must write it in terms of ϵ and take $\epsilon \to 0$

$$\begin{aligned}
\chi_{12} &= -(1-\epsilon^2), \\
\chi_{34} &= -(1-\epsilon^2) e^{-\pi\,\Delta\,(\ell-\bar{\ell})\cosh\theta}, \\
\chi_{13} &= \chi_{24} = \frac{1}{\epsilon}, \\
\chi_{14} &= -\frac{\epsilon}{1-\epsilon^2}\, e^{-\pi\,\Delta\,(1-\ell)\cosh\theta}, \\
\chi_{23} &= -\frac{\epsilon}{1-\epsilon^2}\, e^{-\pi\,\Delta\,(1+\bar{\ell})\cosh\theta}.
\end{aligned} \tag{4.193}$$

Eq. (4.193) is the solution to the χ-system in the OPE plateau region to leading order in the limit as $\epsilon \to 0$. In order to understand our system in the $w_2 \to w_2^+$ limit, we would have to solve the χ-system in the region where $\chi_{34}, \chi_{14}, \chi_{23}$ are not small, subject to the asymptotics given by the plateau solution in eq. (4.193). In this respect the limit when $w_2 \to w_2^\pm$ is similar to the Virasoro limit described in section 4.4.

If we take the plateau solution in eq. (4.193) as the new asymptotics and iterate them with eq. (4.91) we find that after taking the limit $\epsilon \to 0$ the factors of 0 and ∞ do not change with iterations. Therefore, we are tempted to conclude that the new asymptotics are the full χ-functions and to read off the cross-ratio $x_2 = 0$ using eq. (4.8). On the other hand, eq. (4.193) is not a solution to the χ-system when $\chi_{34}, \chi_{14}, \chi_{23}$ cannot be neglected. Similarly as in section 4.4.3 we conclude that in the limit when $w_2 \to w_2^\pm$ the system of integral equation in eq. (4.91) for the *uudd* spike configuration in the tetrahedral triangulation does not converge.

4.6.5 Discussion of OPE

In this section we have considered the limit when $w_2 \to w_2^\pm$. First, we have shown that in this limit the zeros of the stress-energy tensor collide in a way that has a particularly nice physical interpretation. They collide on a WKB line that joins the two operators that at weak

coupling would have no Wick contractions. Therefore, we argue that this limit corresponds to the OPE limit when operators prefer to Wick contract to the closest partners. Moreover, the extended minimal surface degenerates into a closed-up string. After the collision all of the zeros of the stress-energy tensor are along the real axis. Thus, they must be along the string fold-line for the *uudd* spike configuration. If they lie along the fold-line, they cannot source the γ field, hence, $A_{fin} = 0$ outside the $w_2^- < w_2 < w_2^+$ region. This means that the string does not form an extended surface but degenerates into a closed-up string.

Looking at the χ-system we have observed that imposing the $w_2 \to w_2^\pm$ limit results in the χ-functions developing plateaux. The onset of the plateau gives a finite contribution to A_{fin}, whilst the solution in the plateau region gives new asymptotics of the χ-functions.

In the special case when $\ell = -\bar{\ell}$, we were able to solve this limit for the *uudd* spike configuration. We have found that it corresponds to the OPE limit when two operators of the same magnitude but opposite sign of R-charge come close. Calculating the area of this configuration and comparing with section 4.2.5, we found that it corresponds to an exchange of a heavy operator. In fact, it corresponds to an exchange of the heaviest possible operators that comes from mixing $\mathrm{Tr}\, Z^{\mathbf{\Delta}}$ with $\mathrm{Tr}\, \overline{Z}^{\mathbf{\Delta}}$. Therefore, it is sub-dominant in the OPE limit[15], compared to the geodesic string discussed in section 4.2 that corresponds to the *udud* spike configuration.

For case when $\ell \neq \pm\bar{\ell}$ the system of integral equations diverges in the limit when $w_2 \to w_2^\pm$. As a result we were not able to find the cross-ratio that corresponds to this limit.

4.7 Numerical results

In the previous section, we have explored specific limits of the χ-system that were available for analytical treatment. In order to understand the system away from those limits, in this section, we introduce the numerical implementation of the χ-system and present a broad range of numerical studies.

4.7.1 Implementation

We have numerically implemented the χ-system in Wolfram Mathematica. For the purpose of numerical tests, we chose to discretise the value of the spectral parameter θ and worked

[15] In fact, it is the maximally dominants configuration consistent with R-charge conservation.

on a grid. It proved sufficient to have $2^8 = 256$ grid points equispaced between the imposed cut-off values, $-\Theta < \theta < \Theta$. We have chosen the cut-off Θ such that the asymptotics of the χ-function with the smallest value of mass Z decays by a factor of 10^{-100} at the cut-off. However, in the case when Θ calculated in this way was below 10, we used $\Theta = 10$.

$$\Theta = \text{Max}\left(10,\ \text{ArcCosh}\left(\frac{100\log(10)}{Z_{min}}\right)\right). \tag{4.194}$$

We solve the χ-system iteratively. First, for a given set of masses Z_E we calculate the values of the asymptotics for all χ-functions for all grid points. We use these as an initial approximation of the full χ-functions. At the n-th step we evaluate the right hand side of eq. (4.91) with the current approximation of values of the χ-functions to find the value of the χ-functions at the $n+1$ step. In particular, we have implemented the convolution integration in eq. (4.91) with the Fourier methods for much shorter runtime. We have iterated the χ-functions until the numerically obtained area converged to a desired precision of 1‰.

In order to check the numerical implementation of the χ-system, we have checked a few points against relaxation method developed in [3]. Table 4.1 summarises the values we compared.

Table 4.1: Numerical results obtained with relaxation method for $j = 1$, $\ell = \bar{\ell} = 0$.

w_2	Z_{12}	A_{fin}
0.005	$-0.283\,i$	0.147
0.050	$-0.902\,i$	0.632
0.125	$-1.445\,i$	0.632
0.250	$-2.094\,i$	1.191
0.550	$-2.941\,i$	1.313

In the following sections, we present concrete examples of numerical studies of the χ-system. We were able to obtain stable numerical values for a considerable part of the parameter space. The biggest obstacle when obtaining numerical results with the χ-system numerics proved to be lack of convergence of the Fourier method when the masses of the χ-functions differed considerable. When two masses differ by a large factor we expect a significant separation of their length scales, which makes the numerics unstable. On the other hand, the same separation of scales enabled us to get an analytical understating of the OPE limit in section 4.6. In this sense the current section on numerical results exactly compliments section 4.6.

4.7.2 Symmetric configuration

In the next two subsections we compare the contributions from two different saddle points to the four-point function at strong coupling. One of the saddle points is the extended

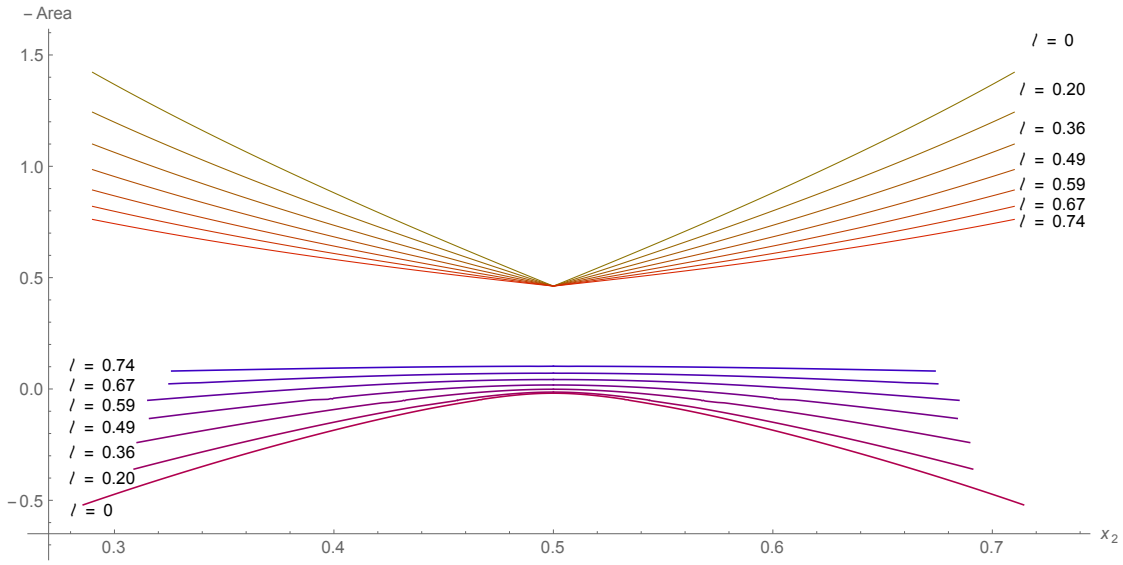

Figure 4.12: The negative of the area of two saddle points for different values of the cross-ratio x_2 for $\bar{\ell} = 0$. The curves in red to brown colour represent the area of the triple two-point function saddle point. The dark blue to purple curves are represent the extended minimal surface *i.e.* the *uudd* spike configuration.

minimal surface that corresponds to the *uudd* spike configuration. The other saddle point is composed of three geodesic strings joining the four operators in sequence. We conjecture it arises from the *udud* spike configuration. In principle one would like to compare the areas of both saddle points for all $\Delta \in \mathbb{R}^+$, $0 < x_2 < 1$, $-1 < \ell < 1$ and $-1 < \bar{\ell} < 1$. In this study we take $\Delta = 1$. We sample the space of possible ℓ, $\bar{\ell}$ along $\bar{\ell} = 0$ in this subsection and along $\ell = -\bar{\ell}$ in the next section.

First, we look at the case when $\bar{\ell} = 0$, and the four-point function is invariant under the crossing symmetry. We have plotted the negative of the area against the cross-ratio in fig. 4.12. The curves in red to brown colour represent the geodesic saddle point composed of three two-point functions and depicted in part c) of fig. 4.4. The area of the geodesic saddle point at strong coupling is the same as at weak coupling, therefore, we plot eq. (4.12). On the other hand, the dark blue to purple curves are data points from the χ-system numerics for the *uudd* spike configuration.

For the values of ℓ presented, the triple two-point function saddle point is dominant.

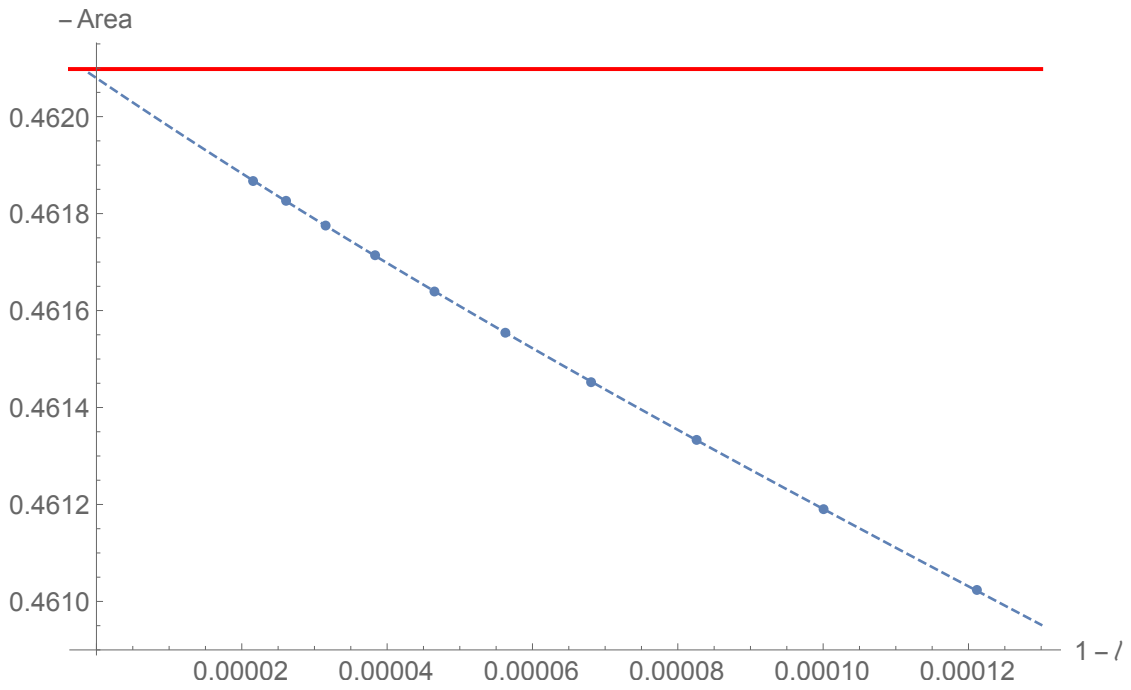

Figure 4.13: The negative of the area of two saddle points for different values of ℓ for the symmetric configuration $x_2 = w_2 = 1/2$ and $\bar{\ell} = 0$. The red curve represents the area of the triple two-point function saddle point. The blue curve represents the extended minimal surface *i.e.* the *uudd* spike configuration.

However, it looks like increasing the values of ℓ we might eventually cross the cusp in the area of the triple two-point function saddle point at $x_2 = 1/2$ with one of the blue-purple lines. If this was the case, we would find a region of parameter space where the minimal surface dominates over the triple two-point function saddle, and there is a phase transition. Unfortunately, this region is not accessible by the χ-system numerics because of large differences between the masses for $\ell \to 1$.

In order to check this hypothesis, we use the results of section 4.6.2. The point $w_2 = x_2 = 1/2$ is self-dual under crossing symmetry, and we have solved its χ-system exactly and presented the area as an integral that can be evaluated numerically. We have implemented these integrals which enabled us to probe much smaller values of $1 - \ell$ than possible with the χ-system numerics. Within the numerical precision we have checked that the area of the minimal surface approaches the area of the triple two-point function saddle point when $\ell \to 1$ from below, see fig. 4.13. Therefore, the triple two-point function saddle point remains dominant for all $-1 < \ell < 1$.

4.7.3 Special case

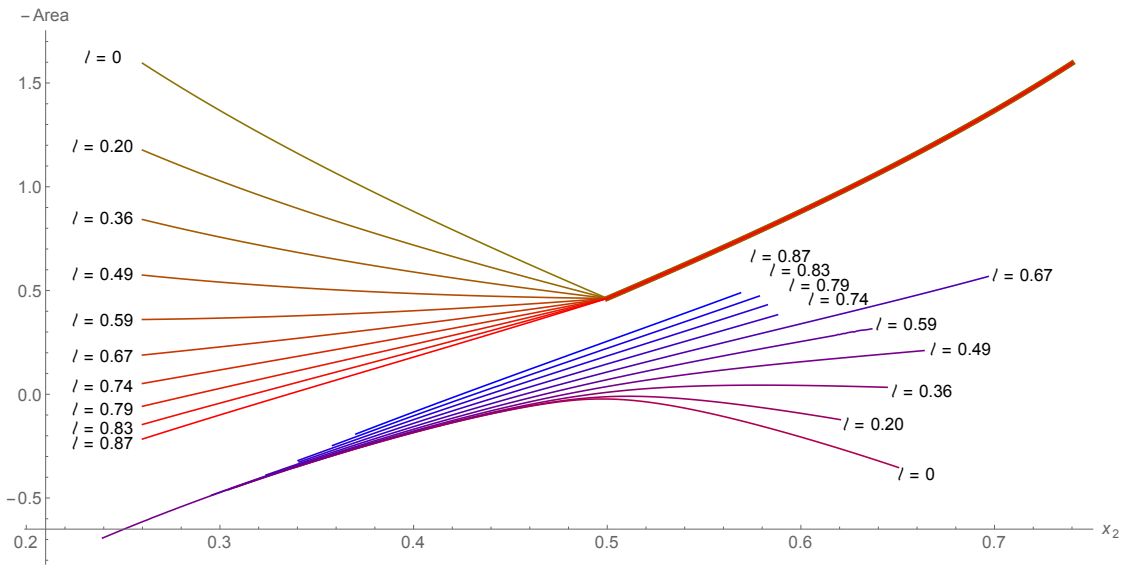

Figure 4.14: The negative of the area of two saddle points for different values of the cross-ratio x_2 for $\ell = -\bar{\ell}$. The curves in red to brown colour represent the area of the triple two-point function saddle point. The dark blue to purple curves are represent the extended minimal surface *i.e.* the *uudd* spike configuration.

In this subsection we take a closer look at the $\ell = -\bar{\ell}$ case. We call it the special case due to the fact that in the limit $x_2 \to 0$ we collide operators with exactly the opposite R-charge. In fact, in section 4.6.3 we were able to solve this OPE limit exactly. Here in fig. 4.14, we present the numerical results.

First, we notice that for $x_2 \to 1$ all the blue to purple curves converge and approach the result of section 4.6.3 which does not depend on ℓ. Once again for all values of ℓ presented the triple two-point function saddle point is dominant over the *uudd* saddle point.

Once again we might hypothesise that for large enough ℓ the minimal surface becomes dominant over the two disconnected two-point functions. In fig. 4.15 we present an extrapolation of the results for $x_2 = 1/2$. From the plot it looks like the two curves approach one another for $\ell \to 1$, and so the minimal surface stays sub-dominant for all ℓ.

4.8 Conclusions

We have considered a classical integrable model arising when we study a minimal surface of a string in AdS_2 space with non-zero energy momentum tensor [3]. This model gave us not just one, but two different minimal surfaces depending on the choice of the spikes. We have

imposed the Virasoro constraint and argued that one of the spike configurations produced a closed up geodesic string configuration. Next, we found that the area of the minimal surface is invariant under the crossing symmetry.

We have argued that the two spike configurations contribute as two saddle points to the four-point function of four heavy operators on a line. The geodesic saddle point is composed of three geodesic strings. The three two-point functions join the four operators in sequence. The numerical implementation of the integrable system showed that the geodesic saddle point dominates for all of the configuration points we could force the numerics to converge. On the other hand, the other spike configuration that forms an extend minimal surface remains sub-dominant.

In the special case when $\ell = \bar{\ell}$, the extend minimal surface competes with a saddle point composed of the two disconnected two-point functions. In this case, we were able to show that the minimal surface is sub-dominant not only for intermediate values of the cross-ratio when the χ-system numerics converge, but also in the OPE limit when the operators with opposite R-charge come close together.

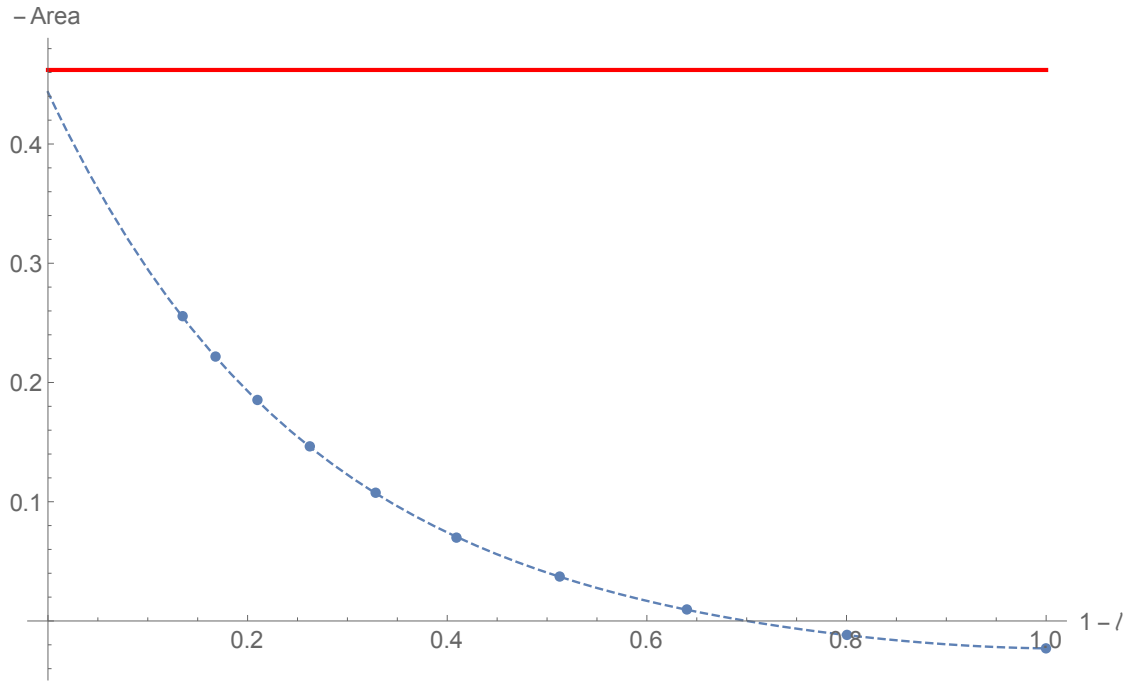

Figure 4.15: The negative of the area of two saddle points for different values of ℓ for the symmetric configuration $x_2 = 1/2$ and $\ell = -\bar{\ell}$. The red curve represents the area of the two disconnected two-point functions saddle point. The blue curve represents the extended minimal surface *i.e.* the *uudd* spike configuration.

Moreover, in the limit when the weight of one of the operators vanishes $l \to 1$, we found that the minimal surface area approaches the area of the geodesic saddle point. This provides as a check for our calculations, as we know that the saddle point for the three-point function of the heavy operators with zero net R-charge does not develop a extended minimal surface and collapses to two geodesic strings [135, 144].

Assuming that there is no other saddle point that dominates over the geodesic saddle point, we find that the four-point function at strong coupling on a line is given by eq. (4.12) at both weak and strong coupling. The cusp at $q = 1$ from weak coupling persist to strong coupling limit. This cusp arises when two different geodesic saddle points switch between being dominant and sub-dominant, as discussed in section 4.2. Moreover, as eq. (4.12) does not receive corrections at one-loop level, one could be even more bold and conjecture that it is protected from receiving quantum corrections at any value of the coupling constant.

Chapter 5

Summary and outlook

In this thesis we have addressed the topic of correlation functions in the planar $\mathcal{N}=4$ SYM theory. We made use of the procedure of Lagrangian insertion in chapter 2, Mellin-Barnes and Twistor techniques in chapter 3, finally, we used the classical integrability of the string equations of motion in AdS space in chapter 4. Here, we would like to summarise our findings and give a pointer to possible future directions.

In chapters 2 and 3 we were able to compute the correlation function of a null Wilson loop with four edges and a local operator up to two loops. Unfortunately, the perturbative calculation even at three loops is prohibitively long to carry out. Moreover, it might be practical to employ recursive methods to find higher loop results. In fact, a BCFW-like recursion relation in the twistor space formalism for such correlators has already been derived in [72]. For now, we leave this as a possible future direction.

In chapter 4 we were able to compute the four point correlation function of the BMN operators on a line at strong coupling. We have found that to the leading order

$$\langle \mathcal{O}^{\mathbf{\Delta}_1}(x_1)\,\overline{\mathcal{O}}^{\mathbf{\Delta}_2}(x_2)\,\mathcal{O}^{\mathbf{\Delta}_3}(x_3)\,\overline{\mathcal{O}}^{\mathbf{\Delta}_4}(x_4)\rangle = \mathcal{F}(u,v)\prod_{A>B}^{4}(x_{AB}^2)^{\mathbf{\Delta}_{AB}}, \tag{5.1}$$

$$\log\mathcal{F}(u,v) = \left(-\frac{2}{3}+\frac{\ell+\bar{\ell}}{2}\right)\mathbf{\Delta}\log u + \left(\frac{1}{3}-\frac{\ell+\bar{\ell}}{2}\right)\mathbf{\Delta}\log v + \ldots \qquad q<1, \tag{5.2}$$

$$\log\mathcal{F}(u,v) = \left(\frac{1}{3}-\frac{\ell-\bar{\ell}}{2}\right)\mathbf{\Delta}\log u + \left(-\frac{2}{3}+\frac{\ell-\bar{\ell}}{2}\right)\mathbf{\Delta}\log v + \ldots \qquad q>1,$$

$$\text{where} \quad \mathbf{\Delta}_{AB} = \left(\sum_{C=1}^{4}\frac{\mathbf{\Delta}_C}{3}\right) - \mathbf{\Delta}_A - \mathbf{\Delta}_B, \quad u = \frac{x_{14}^2x_{23}^2}{x_{13}^2x_{24}^2}, \quad v = \frac{x_{12}^2x_{34}^2}{x_{13}^2x_{24}^2}, \quad q = \frac{u}{v},$$

$$\mathbf{\Delta}_1 = \mathbf{\Delta}\,(1+\ell), \quad \mathbf{\Delta}_2 = \mathbf{\Delta}\,(1+\bar{\ell}) \quad \mathbf{\Delta}_3 = \mathbf{\Delta}\,(1-\ell), \quad \mathbf{\Delta}_4 = \mathbf{\Delta}\,(1-\bar{\ell}), \tag{5.3}$$

at both weak and strong coupling. Consequently, we have conjectured that this is the case for all values of the coupling constant.

A natural generalisation would be to consider the operators not being located on a line. In this more general case, in order for the duality between correlation functions and Wilson loops to be satisfied, the minimal surface saddle point cannot be sub-dominant for all values of the cross-ratios. In fact, one of the main reasons for chapter 4 was to test the χ-system analytically and numerically before publishing results the author obtained in collaboration with Jonathan Toledo for the more general case. The plan was to numerically consider the correlation function close to the null limit and check if it reproduces the divergences of the four point Wilson loop, which are characterised by strong coupling value of the cups anomalous dimension. The difficult step is to make the numerics stable enough in the considered limit to confirm this expectation. Lack of convincing results discourages the author from including those results in the thesis.

Another interesting extension of this work would be to consider a higher number of operators in the correlation function. What are the saddle points in these cases? How many independent choices do we have for the spikes at the zeros of the stress-energy tensor[1]? Are there any phase transitions? Which saddle point is dominant? These are some of the more interesting questions.

[1]It turn out that these points also arise as the conical defect at weak coupling and carry an important role, see for example recent [154]

Appendix A

Correlation functions in N=4, permutation symmetry and procedure of Lagrangian insertions

In this appendix we would like to give a brief review of the procedure of Lagrangian insertions in the context of $\mathcal{N}=4$ SYM theory. This review is mainly based on [65–67]. The main purpose is to provide the reader with the necessarily background for chapter 2.

A.1 N=4 SYM stress-tensor supermultiplet

We are going to concentrate on the correlation functions of half-BPS operators that belong to the $20'$ representation of the R-symmetry group $SO(6)$. The lowest-weight state of this multiplet, a superconformal primary, can be constructed from the real scalar fields Φ^I of $\mathcal{N}=4$ SYM, where $I=1,...,6$,

$$\mathcal{O}^{IJ}_{20'} = \mathrm{Tr}(\Phi^I\Phi^J) - \frac{1}{6}\,\delta^{IJ}\,\mathrm{Tr}(\Phi^K\Phi^K), \tag{A.1}$$

where we have subtracted the trace corresponding to the Konishi operator. One way of dealing with the free indices is to project them on an auxiliary six dimensional null vector called Y, so that

$$\mathcal{O}(x,y) = Y_I\,Y_J\,\mathcal{O}^{IJ}_{20'}(x) = Y_I\,Y_J\,\mathrm{Tr}(\Phi^I(x)\Phi^J(x)), \qquad \text{where} \qquad Y_I\,Y_I = 0. \tag{A.2}$$

The rest of the $20'$ multiplet can be recovered by repeated application of supersymmetry generator[1] Q^α_a :

$$\mathcal{T}(x,\rho,y) = e^{\rho^a_\alpha\,Q^\alpha_a}\,\mathcal{O}(x,y) = \mathcal{O}(x,y) + \,...\, + \,\rho^4\,\mathcal{L}_{\mathcal{N}=4}(x). \tag{A.3}$$

[1] We are going to described the superspace in which the generators Q^α_a live in the following section.

The top component is equal to the chiral Lagrangian of $\mathcal{N}=4$ SYM up to terms that vanish due to equations of motion. As a result we call it the $\mathcal{N}=4$ SYM stress-tensor supermultiplet. Moreover, it is a half-BPS multiplet, half of the $\mathcal{N}=4$ supercharges Q annihilate it, and its scaling dimension is protected, $\Delta_{20'}=2$ for all values of the coupling constant.

We can pick a particular component of $\mathcal{T}$ by performing appropriate Grassmann integrals, for example, the on-shell action of $\mathcal{N}=4$ SYM

$$S_{\mathcal{N}=4}=\int d^4x \int d^4\rho\, \mathcal{T}(x,\rho,y). \tag{A.4}$$

This property will turn out to be particularly useful soon, as well as the fact that the action is independent of y variables.

A.2 Harmonic superspace

Typically, we parametrise the translations in superspace as

$$G(x,\theta,\bar{\theta})=exp(-ix^\mu p_\mu+i\theta Q+i\bar{\theta}\bar{Q}) \tag{A.5}$$

with fermionic Grassmann coordinates θ^A_α, where α is the spinor index, and A labels copies of the supersymmetry generators and is sometimes referred to as the R-symmetry index (the R-symmetry is $SO(6)$ for the case of $\mathcal{N}=4$ SYM). However, there is no off-shell formulation of $\mathcal{N}=4$ superspace, therefore, we are going to use $\mathcal{N}=2$ harmonic superspace [155]. We decompose θ^A_α into two halves by splitting the index as $A=(a,a')$, where $a,a'=1,2$. Introducing

$$\rho^a_\alpha=\theta^a_\alpha+\theta^{a'}_\alpha\, y^a_{a'} \tag{A.6}$$

we can change the coordinates from $(\theta^A_\alpha,\,\bar{\theta}^{\dot{\alpha}}_A)$ to $(\rho^a_\alpha,\,\theta^{a'}_\alpha,\,\bar{\rho}^{\dot{\alpha}}_a,\,\bar{\theta}^{\dot{\alpha}}_{a'})$ which are the coordinates of the harmonic superspace. $y^a_{a'}$ are the harmonic variables with $SU(4)$ indices related to the previously introduced Y_I [65] such that

$$Y_1\cdot Y_2=\sum_{I=1}^{6}(Y_1)_I\,(Y_2)_I=\frac{1}{2}\epsilon_{ab}\epsilon^{a'b'}(y_1-y_2)^a_{a'}(y_1-y_2)^b_{b'}=(y_1-y_2)^2\equiv y^2_{12}. \tag{A.7}$$

The aforementioned stress-tensor supermultiplet of $\mathcal{N}=4$ SYM is independent of $\theta^{a'}_\alpha$, $\bar{\theta}^{\dot{\alpha}}_{a'}$

$$\mathcal{T}=\mathcal{T}(x,\rho^a_\alpha,\,\bar{\rho}^{\dot{\alpha}}_a,\,y^a_{a'}), \tag{A.8}$$

and, as a result, it is half-BPS and the multiplet in eq. (A.3) is short. When we introduced the harmonic variables $y^a_{a'}$, we have broken the R-symmetry group $SO(6) \sim SU(4)$ to

$$SU(4) \to SU(2) \times SU(2)' \times U(1). \tag{A.9}$$

Under this $U(1)$ symmetry ρ and y have weight $+1$, whilst Y has weight $+2$, such that the stress-tensor supermultiplet has uniform weight $+4$.

A.3 Lagrangian insertion technique

Let us consider the four point function of the operators we have just described

$$G_4(1,2,3,4) = \langle \mathcal{O}(x_1,y_1)\mathcal{O}(x_2,y_2)\mathcal{O}(x_3,y_3)\mathcal{O}(x_4,y_4)\rangle = \sum_{\ell=0}^{\infty} a^l \, G_4^{(\ell)}, \tag{A.10}$$

where $a = g_{YM}N/(8\pi^2)$ is a rescaled coupling constant. If we take a derivative of the correlator with respect to the coupling constant[2] we get

$$a\frac{\partial}{\partial a}G_4 = a\frac{\partial}{\partial a}\int D\Phi \;\; \mathcal{O}(x_1,y_1)\mathcal{O}(x_2,y_2)\mathcal{O}(x_3,y_3)\mathcal{O}(x_4,y_4)\; e^{-\frac{1}{a}S_{\mathcal{N}=4}[\Phi]} \tag{A.11}$$

$$= \int d^4x_5 \; \langle \mathcal{O}(x_1,y_1)\mathcal{O}(x_2,y_2)\mathcal{O}(x_3,y_3)\mathcal{O}(x_4,y_4)\mathcal{L}_{\mathcal{N}=4}(x_5)\rangle. \tag{A.12}$$

We can see that the 1-loop contribution to G_4 is just the integrated tree-level correlator with a Lagrangian insertion. One can readily generalise it to ℓ-loops:

$$G_4^{(\ell)} = \int d^4x_5 \ldots d^4x_{4+\ell} \langle \mathcal{O}(x_1,y_1)\ldots\mathcal{O}(x_4,y_4)\mathcal{L}_{\mathcal{N}=4}(x_5)\ldots\mathcal{L}_{\mathcal{N}=4}(x_{4+\ell})\rangle^{(0)}. \tag{A.13}$$

The magic of $\mathcal{N}=4$ SYM emerges when we consider a supercorrelator of the $20'$ multiplet

$$\mathcal{G}_n = \langle \mathcal{T}(x_1,\rho_1,y_1)\ldots\mathcal{T}(x_n,\rho_n,y_n)\rangle = \sum_{k=0}^{n-4}\sum_{\ell=0}^{\infty} a^{\ell+k} \, G^{(\ell)}_{n;k}(1,\ldots,n), \tag{A.14}$$

where $G_{n;k}$ is a homogeneous polynomial in the Grassmann variables ρ of degree $4k$. We find that G_4 as well as its cousins with the Lagrangian insertion are all components of $\mathcal{G}_n$, for example:

$$G_4^{(\ell)}(1,2,3,4) = \frac{1}{\ell!}\int d^4x_5 \ldots d^4x_{4+\ell} \int d^4\rho_5 \ldots d^4\rho_{4+\ell} \;\; G^{(0)}_{4+\ell;\ell}(1,\ldots,4+\ell). \tag{A.15}$$

[2]Here, we have rescaled all the fields such that the coupling constant appears only as an overall multiplicative constant in the action.

The result is that the integrand $G^{(0)}_{4+\ell,\ell}$ for the four point correlation function before performing the Grassmann integrals is invariant under $S_{4+\ell}$, the permutation symmetry of all $4+\ell$ insertion points. In the following section we are going to find the form of the integrand for G_4 taking advantage of this permutation symmetry.

A.4 Integrand

Considering the supercorrelators $\mathcal{G}_n$ at tree-level the authors of [65] find for the first few orders in ℓ

$$\mathcal{G}^{(0)}_{4+\ell;\ell}(1,...,4+\ell) = \frac{2(N^2-1)}{(-4\pi^2)^{4+\ell}} \times \mathcal{I}_{4+\ell} \times f^{(\ell)}(x_1,...,x_{4+\ell}). \tag{A.16}$$

The assumption is that the higher orders follow the same pattern, and $\mathcal{I}_n$ has the following properties:

- It carries all dependence on the Grassmann variables ρ.
- It is a homogeneous polynomial in ρ variables of degree $4(n-4)$.
- It is symmetric under S_n permutation of all insertion points.
- It is invariant under the chiral part of the $\mathcal{N}=4$ superconformal symmetry.
- It has conformal weight -2 for each point.
- It has $U(1)$ charge $+4$ for each point.

These requirements fix the form of $\mathcal{I}_{4+\ell}$ up to a conformally invariant factor dependent only on the positions x_i [65]. Actually, we are only interested in the $(\rho_5)^4...(\rho_n)^4$ component which gives the integrand for the correlator in eq. (A.10):

$$G^{(\ell)}_4 = \frac{2(N^2-1)}{(4\pi^2)^4} \times R(1,2,3,4) \times F^{(\ell)} \qquad \text{for } l \geq 1, \tag{A.17}$$

where

$$F^{(\ell)}(x_1,x_2,x_3,x_4) = \frac{x_{12}^2 x_{13}^2 x_{14}^2 x_{23}^2 x_{24}^2 x_{34}^2}{\ell!(-4\pi^2)^\ell} \int d^4x_5...d^4x_{4+\ell}\, f^{(\ell)}(x_1,...,x_{4+\ell}), \tag{A.18}$$

$$\begin{aligned} R(1,2,3,4) =& \frac{y_{12}^2 y_{23}^2 y_{34}^2 y_{14}^2}{x_{12}^2 x_{23}^2 x_{34}^2 x_{14}^2}(x_{13}^2 x_{24}^2 - x_{12}^2 x_{34}^2 - x_{14}^2 x_{23}^2) \\ &+ \frac{y_{12}^2 y_{13}^2 y_{24}^2 y_{34}^2}{x_{12}^2 x_{13}^2 x_{24}^2 x_{34}^2}(x_{14}^2 x_{23}^2 - x_{12}^2 x_{34}^2 - x_{13}^2 x_{24}^2) \\ &+ \frac{y_{13}^2 y_{14}^2 y_{23}^2 y_{24}^2}{x_{13}^2 x_{14}^2 x_{23}^2 x_{24}^2}(x_{12}^2 x_{34}^2 - x_{13}^2 x_{24}^2 - x_{14}^2 x_{23}^2) \\ &+ \frac{y_{12}^4 y_{34}^4}{x_{12}^2 x_{34}^2} + \frac{y_{13}^4 y_{24}^4}{x_{13}^2 x_{24}^2} + \frac{y_{14}^4 y_{23}^4}{x_{14}^2 x_{23}^2}. \end{aligned}$$

It is particularly nice to write $f^{(\ell)}$ as

$$f^{(\ell)}(x_1, ..., x_{4+\ell}) = \frac{P^{(\ell)}(x_1, ..., x_{4+\ell})}{\prod_{1\leq i<j\leq 4+\ell} x_{ij}^2}. \tag{A.19}$$

Then $P^{(\ell)}$ must have the following properties:

- It is a function of x_i only.
- It is $S_{4+\ell}$ symmetric.
- It has a conformal weight $-l+1$ for each point.

The problem of finding all possible polynomials that satisfy these conditions can be mapped into a graph theory problem of finding multi-graphs with $4+\ell$ vertices of degree $\ell-1$. At one loop, we find

$$P^{(1)} \propto 1. \tag{A.20}$$

At two loops, the corresponding graph is

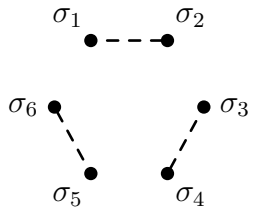

$$P^{(2)} \propto \sum_{\sigma\in S_6} x^2_{\sigma_1\sigma_2} x^2_{\sigma_3\sigma_4} x^2_{\sigma_5\sigma_6}. \tag{A.21}$$

At three loops, we find four different multi-graphs.

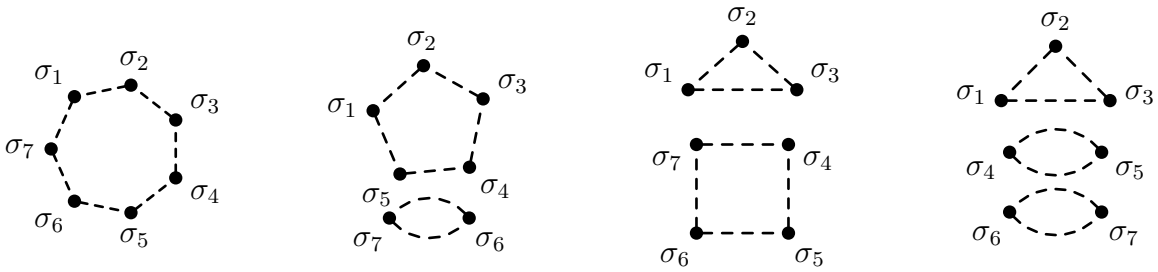

Therefore, $P^{(3)}$ is a linear combination of four terms corresponding to these four graphs with arbitrary coefficients

$$\begin{aligned} P^{(3)} = \sum_{\sigma\in S_7} (&c_1\, x^2_{\sigma_1\sigma_2} x^2_{\sigma_2\sigma_3} x^2_{\sigma_3\sigma_4} x^2_{\sigma_4\sigma_5} x^2_{\sigma_5\sigma_6} x^2_{\sigma_6\sigma_7} x^2_{\sigma_7\sigma_1} + c_2\, x^2_{\sigma_1\sigma_2} x^2_{\sigma_2\sigma_3} x^2_{\sigma_3\sigma_4} x^2_{\sigma_4\sigma_5} x^2_{\sigma_5\sigma_1} x^4_{\sigma_6\sigma_7} \\ &+c_3\, x^2_{\sigma_1\sigma_2} x^2_{\sigma_2\sigma_3} x^2_{\sigma_3\sigma_1} x^2_{\sigma_4\sigma_5} x^2_{\sigma_5\sigma_6} x^2_{\sigma_6\sigma_7} x^2_{\sigma_7\sigma_4} + c_4\, x^2_{\sigma_1\sigma_2} x^2_{\sigma_2\sigma_3} x^2_{\sigma_3\sigma_1} x^4_{\sigma_4\sigma_5} x^4_{\sigma_6\sigma_7}). \end{aligned} \tag{A.22}$$

In order to find these arbitrary coefficients we can use the duality between correlation function and scattering amplitudes [49, 60] which states that

$$\lim_{x_{i,i+1}^2 \to 0} \frac{G_4(x)}{G_4^{(0)}(x)} = \left(\frac{A_4(p)}{A_4^{(0)}(p)} \right)^2, \tag{A.23}$$

where $A_4(p)$ is the four point scattering amplitude in $\mathcal{N} = 4$ SYM, and we identify the momenta of the particles through

$$p_i = x_i - x_{i+1}. \tag{A.24}$$

It is most convenient to compare correlation functions and scattering amplitudes at the level of the integrand. Comparing the integrands in eq. (A.17-A.22) using eq. (A.23-A.24) with [52] one can find the numerical coefficients

$$f^{(1)}(x_1, ..., x_5) = \frac{1}{\prod_{1 \le i < j \le 5} x_{ij}^2}, \tag{A.25}$$

$$f^{(2)}(x_1, ..., x_6) = \frac{1}{48} \frac{\sum_{\sigma \in S_6} x_{\sigma_1\sigma_2}^2 x_{\sigma_3\sigma_4}^2 x_{\sigma_5\sigma_6}^2}{\prod_{1 \le i < j \le 6} x_{ij}^2}, \tag{A.26}$$

$$f^{(3)}(x_1, ..., x_7) = \frac{1}{20} \frac{\sum_{\sigma \in S_7} x_{\sigma_1\sigma_2}^4 x_{\sigma_3\sigma_4}^2 x_{\sigma_4\sigma_5}^2 x_{\sigma_5\sigma_6}^2 x_{\sigma_6\sigma_7}^2 x_{\sigma_7\sigma_3}^2}{\prod_{1 \le i < j \le 6} x_{ij}^2}. \tag{A.27}$$

We use these expressions in chapter 2 to derive the integrand of the correlation function of a null Wilson loop with four edges and a local operator up to two loops.

Bibliography

[1] L. F. Alday, P. Heslop, and J. Sikorowski, *Perturbative correlation functions of null Wilson loops and local operators*, *JHEP* **03** (2013) 074, [arXiv:1207.4316].

[2] L. F. Alday, J. M. Henn, and J. Sikorowski, *Higher loop mixed correlators in N=4 SYM*, *JHEP* **1303** (2013) 058, [arXiv:1301.0149].

[3] J. Caetano and J. Toledo, *χ-Systems for Correlation Functions*, arXiv:1208.4548.

[4] P. Bechtle, T. Plehn, and C. Sander, *Supersymmetry*, in *The Large Hadron Collider: Harvest of Run 1* (T. Schörner-Sadenius, ed.), pp. 421–462. 2015. arXiv:1506.0309.

[5] C.-N. Yang and R. L. Mills, *Conservation of Isotopic Spin and Isotopic Gauge Invariance*, *Phys. Rev.* **96** (1954) 191–195.

[6] G. 't Hooft, *Renormalization of Massless Yang-Mills Fields*, *Nucl. Phys.* **B33** (1971) 173–199.

[7] G. 't Hooft, *Renormalizable Lagrangians for Massive Yang-Mills Fields*, *Nucl. Phys.* **B35** (1971) 167–188.

[8] J. Rojo, *Recent progress in QCD at the LHC*, *Nuovo Cim.* **C037** (2014), no. 6 101–109, [arXiv:1404.7071].

[9] N. Brambilla et al., *QCD and Strongly Coupled Gauge Theories: Challenges and Perspectives*, *Eur. Phys. J.* **C74** (2014), no. 10 2981, [arXiv:1404.3723].

[10] J. M. Drummond, J. Henn, G. P. Korchemsky, and E. Sokatchev, *Dual superconformal symmetry of scattering amplitudes in N=4 super-Yang-Mills theory*, *Nucl. Phys.* **B828** (2010) 317–374, [arXiv:0807.1095].

[11] J. M. Drummond, J. M. Henn, and J. Plefka, *Yangian symmetry of scattering amplitudes in N=4 super Yang-Mills theory*, *JHEP* **05** (2009) 046, [arXiv:0902.2987].

[12] N. Beisert et al., *Review of AdS/CFT Integrability: An Overview*, *Lett. Math. Phys.* **99** (2012) 3–32, [arXiv:1012.3982].

[13] J. M. Maldacena, *The Large N limit of superconformal field theories and supergravity*, *Int. J. Theor. Phys.* **38** (1999) 1113–1133, [hep-th/9711200]. [Adv. Theor. Math. Phys.2,231(1998)].

[14] S. S. Gubser, I. R. Klebanov, and A. M. Polyakov, *Gauge theory correlators from noncritical string theory*, *Phys. Lett.* **B428** (1998) 105–114, [hep-th/9802109].

[15] E. Witten, *Anti-de Sitter space and holography*, *Adv. Theor. Math. Phys.* **2** (1998) 253–291, [hep-th/9802150].

[16] G. 't Hooft, *A Planar Diagram Theory for Strong Interactions*, *Nucl. Phys.* **B72** (1974) 461.

[17] G. 't Hooft, *Dimensional reduction in quantum gravity*, in *Salamfest 1993:0284-296*, pp. 0284–296, 1993. gr-qc/9310026.

[18] L. Susskind, *The World as a hologram*, *J. Math. Phys.* **36** (1995) 6377–6396, [hep-th/9409089].

[19] O. Aharony, S. S. Gubser, J. M. Maldacena, H. Ooguri, and Y. Oz, *Large N field theories, string theory and gravity*, *Phys. Rept.* **323** (2000) 183–386, [hep-th/9905111].

[20] D. E. Berenstein, J. M. Maldacena, and H. S. Nastase, *Strings in flat space and pp waves from N=4 superYang-Mills*, *JHEP* **04** (2002) 013, [hep-th/0202021].

[21] M. Blau, J. M. Figueroa-O'Farrill, C. Hull, and G. Papadopoulos, *A New maximally supersymmetric background of IIB superstring theory*, *JHEP* **01** (2002) 047, [hep-th/0110242].

[22] R. R. Metsaev, *Type IIB Green-Schwarz superstring in plane wave Ramond-Ramond background*, *Nucl. Phys.* **B625** (2002) 70–96, [hep-th/0112044].

[23] I. Bena, J. Polchinski, and R. Roiban, *Hidden symmetries of the AdS(5) x S**5 superstring*, *Phys. Rev.* **D69** (2004) 046002, [hep-th/0305116].

[24] S. Frolov and A. A. Tseytlin, *Multispin string solutions in AdS(5) x S**5*, *Nucl. Phys.* **B668** (2003) 77–110, [hep-th/0304255].

[25] S. Frolov and A. A. Tseytlin, *Rotating string solutions: AdS / CFT duality in nonsupersymmetric sectors*, *Phys. Lett.* **B570** (2003) 96–104, [hep-th/0306143].

[26] G. Arutyunov, S. Frolov, J. Russo, and A. A. Tseytlin, *Spinning strings in AdS(5) x S**5 and integrable systems*, *Nucl. Phys.* **B671** (2003) 3–50, [hep-th/0307191].

[27] N. Beisert, C. Kristjansen, and M. Staudacher, *The Dilatation operator of conformal N=4 superYang-Mills theory*, *Nucl. Phys.* **B664** (2003) 131–184, [hep-th/0303060].

[28] J. A. Minahan and K. Zarembo, *The Bethe ansatz for N=4 superYang-Mills*, *JHEP* **03** (2003) 013, [hep-th/0212208].

[29] G. Arutyunov, S. Frolov, and M. Staudacher, *Bethe ansatz for quantum strings*, *JHEP* **10** (2004) 016, [hep-th/0406256].

[30] R. Hernandez and E. Lopez, *Quantum corrections to the string Bethe ansatz*, *JHEP* **07** (2006) 004, [hep-th/0603204].

[31] R. A. Janik, *The AdS(5) x S**5 superstring worldsheet S-matrix and crossing symmetry*, *Phys. Rev.* **D73** (2006) 086006, [hep-th/0603038].

[32] N. Beisert, R. Hernandez, and E. Lopez, *A Crossing-symmetric phase for AdS(5) x S**5 strings*, *JHEP* **11** (2006) 070, [hep-th/0609044].

[33] N. Gromov, V. Kazakov, and P. Vieira, *Exact Spectrum of Anomalous Dimensions of Planar N=4 Supersymmetric Yang-Mills Theory*, *Phys. Rev. Lett.* **103** (2009) 131601, [arXiv:0901.3753].

[34] D. Bombardelli, D. Fioravanti, and R. Tateo, *Thermodynamic Bethe Ansatz for planar AdS/CFT: A Proposal*, *J. Phys.* **A42** (2009) 375401, [arXiv:0902.3930].

[35] N. Gromov, V. Kazakov, A. Kozak, and P. Vieira, *Exact Spectrum of Anomalous Dimensions of Planar $N = 4$ Supersymmetric Yang-Mills Theory: TBA and excited states*, *Lett. Math. Phys.* **91** (2010) 265–287, [arXiv:0902.4458].

[36] G. Arutyunov and S. Frolov, *Thermodynamic Bethe Ansatz for the AdS(5) x S(5) Mirror Model*, *JHEP* **05** (2009) 068, [arXiv:0903.0141].

[37] N. Gromov, V. Kazakov, S. Leurent, and D. Volin, *Quantum Spectral Curve for Planar $\mathcal{N} =$ Super-Yang-Mills Theory*, *Phys. Rev. Lett.* **112** (2014), no. 1 011602, [arXiv:1305.1939].

[38] N. Gromov, V. Kazakov, S. Leurent, and D. Volin, *Quantum spectral curve for arbitrary state/operator in AdS_5/CFT_4*, arXiv:1405.4857.

[39] N. Gromov, F. Levkovich-Maslyuk, and G. Sizov, *Analytic Solution of Bremsstrahlung TBA II: Turning on the Sphere Angle*, *JHEP* **10** (2013) 036, [arXiv:1305.1944].

[40] N. Gromov, F. Levkovich-Maslyuk, G. Sizov, and S. Valatka, *Quantum spectral curve at work: from small spin to strong coupling in $\mathcal{N} = 4$ SYM*, *JHEP* **07** (2014) 156, [arXiv:1402.0871].

[41] M. Alfimov, N. Gromov, and V. Kazakov, *QCD Pomeron from AdS/CFT Quantum Spectral Curve*, *JHEP* **07** (2015) 164, [arXiv:1408.2530].

[42] S. J. Parke and T. R. Taylor, *An Amplitude for n Gluon Scattering*, *Phys. Rev. Lett.* **56** (1986) 2459.

[43] E. Witten, *Perturbative gauge theory as a string theory in twistor space*, *Commun. Math. Phys.* **252** (2004) 189–258, [hep-th/0312171].

[44] F. Cachazo, P. Svrcek, and E. Witten, *MHV vertices and tree amplitudes in gauge theory*, *JHEP* **09** (2004) 006, [hep-th/0403047].

[45] A. Brandhuber and G. Travaglini, *Quantum MHV diagrams*, in *Continuous advances in QCD. Proceedings, 7th Workshop, QCD 2006, Minneapolis, USA, May 11-14, 2006*, pp. 443–456, 2006. hep-th/0609011.

[46] R. Britto, F. Cachazo, B. Feng, and E. Witten, *Direct proof of tree-level recursion relation in Yang-Mills theory*, *Phys. Rev. Lett.* **94** (2005) 181602, [hep-th/0501052].

[47] N. Arkani-Hamed, J. L. Bourjaily, F. Cachazo, A. B. Goncharov, A. Postnikov, and J. Trnka, *Scattering Amplitudes and the Positive Grassmannian*, arXiv:1212.5605.

[48] N. Arkani-Hamed and J. Trnka, *The Amplituhedron*, *JHEP* **10** (2014) 30, [arXiv:1312.2007].

[49] L. F. Alday and J. M. Maldacena, *Gluon scattering amplitudes at strong coupling*, *JHEP* **06** (2007) 064, [arXiv:0705.0303].

[50] L. F. Alday, *Review of AdS/CFT Integrability, Chapter V.3: Scattering Amplitudes at Strong Coupling*, *Lett. Math. Phys.* **99** (2012) 507–528, [arXiv:1012.4003].

[51] J. M. Drummond, J. Henn, G. P. Korchemsky, and E. Sokatchev, *Conformal Ward identities for Wilson loops and a test of the duality with gluon amplitudes*, *Nucl. Phys.* **B826** (2010) 337–364, [arXiv:0712.1223].

[52] Z. Bern, L. J. Dixon, and V. A. Smirnov, *Iteration of planar amplitudes in maximally supersymmetric Yang-Mills theory at three loops and beyond*, *Phys. Rev.* **D72** (2005) 085001, [hep-th/0505205].

[53] L. J. Dixon, J. M. Drummond, C. Duhr, and J. Pennington, *The four-loop remainder function and multi-Regge behavior at NNLLA in planar $N = 4$ super-Yang-Mills theory*, *JHEP* **06** (2014) 116, [arXiv:1402.3300].

[54] J. M. Drummond, G. P. Korchemsky, and E. Sokatchev, *Conformal properties of four-gluon planar amplitudes and Wilson loops*, *Nucl. Phys.* **B795** (2008) 385–408, [arXiv:0707.0243].

[55] A. Brandhuber, P. Heslop, and G. Travaglini, *MHV amplitudes in N=4 super Yang-Mills and Wilson loops*, *Nucl. Phys.* **B794** (2008) 231–243, [arXiv:0707.1153].

[56] J. M. Drummond, J. Henn, G. P. Korchemsky, and E. Sokatchev, *On planar gluon amplitudes/Wilson loops duality*, *Nucl. Phys.* **B795** (2008) 52–68, [arXiv:0709.2368].

[57] J. M. Drummond, J. Henn, G. P. Korchemsky, and E. Sokatchev, *The hexagon Wilson loop and the BDS ansatz for the six-gluon amplitude*, *Phys. Lett.* **B662** (2008) 456–460, [arXiv:0712.4138].

[58] J. M. Drummond, J. Henn, G. P. Korchemsky, and E. Sokatchev, *Hexagon Wilson loop = six-gluon MHV amplitude*, *Nucl. Phys.* **B815** (2009) 142–173, [arXiv:0803.1466].

[59] A. V. Belitsky, G. P. Korchemsky, and E. Sokatchev, *Are scattering amplitudes dual to super Wilson loops?*, *Nucl. Phys.* **B855** (2012) 333–360, [arXiv:1103.3008].

[60] L. F. Alday, B. Eden, G. P. Korchemsky, J. Maldacena, and E. Sokatchev, *From correlation functions to Wilson loops*, *JHEP* **1109** (2011) 123, [arXiv:1007.3243].

[61] B. Basso, A. Sever, and P. Vieira, *Spacetime and Flux Tube S-Matrices at Finite Coupling for N=4 Supersymmetric Yang-Mills Theory*, *Phys. Rev. Lett.* **111** (2013), no. 9 091602, [arXiv:1303.1396].

[62] L. F. Alday, D. Gaiotto, J. Maldacena, A. Sever, and P. Vieira, *An Operator Product Expansion for Polygonal null Wilson Loops*, *JHEP* **04** (2011) 088, [arXiv:1006.2788].

[63] B. Basso, A. Sever, and P. Vieira, *Hexagonal Wilson Loops in Planar $\mathcal{N} = 4$ SYM Theory at Finite Coupling*, arXiv:1508.0304.

[64] N. Beisert, C. Kristjansen, J. Plefka, G. Semenoff, and M. Staudacher, *BMN correlators and operator mixing in N=4 superYang-Mills theory*, *Nucl.Phys.* **B650** (2003) 125–161, [hep-th/0208178].

[65] B. Eden, P. Heslop, G. P. Korchemsky, and E. Sokatchev, *Hidden symmetry of four-point correlation functions and amplitudes in N=4 SYM*, *Nucl.Phys.* **B862** (2012) 193–231, [arXiv:1108.3557].

[66] B. Eden, P. Heslop, G. P. Korchemsky, and E. Sokatchev, *The super-correlator/super-amplitude duality: Part I*, *Nucl.Phys.* **B869** (2013) 329–377, [arXiv:1103.3714].

[67] B. Eden, P. Heslop, G. P. Korchemsky, and E. Sokatchev, *The super-correlator/super-amplitude duality: Part II*, *Nucl.Phys.* **B869** (2013) 378–416, [arXiv:1103.4353].

[68] B. Eden, P. Heslop, G. P. Korchemsky, and E. Sokatchev, *Constructing the correlation function of four stress-tensor multiplets and the four-particle amplitude in N=4 SYM*, *Nucl.Phys.* **B862** (2012) 450–503, [arXiv:1201.5329].

[69] B. Eden, P. Heslop, G. P. Korchemsky, V. A. Smirnov, and E. Sokatchev, *Five-loop Konishi in N=4 SYM*, *Nucl.Phys.* **B862** (2012) 123–166, [arXiv:1202.5733].

[70] L. Alday, E. Buchbinder, and A. Tseytlin, *Correlation function of null polygonal Wilson loops with local operators*, *JHEP* **1109** (2011) 034, [arXiv:1107.5702].

[71] O. T. Engelund and R. Roiban, *On correlation functions of Wilson loops, local and non-local operators*, *JHEP* **1205** (2012) 158, [arXiv:1110.0758].

[72] T. Adamo, *Correlation functions, null polygonal Wilson loops, and local operators*, *JHEP* **1112** (2011) 006, [arXiv:1110.3925].

[73] B. Eden, P. S. Howe, C. Schubert, E. Sokatchev, and P. C. West, *Four point functions in N=4 supersymmetric Yang-Mills theory at two loops*, *Nucl.Phys.* **B557** (1999) 355–379, [hep-th/9811172].

[74] B. Eden, P. S. Howe, C. Schubert, E. Sokatchev, and P. C. West, *Simplifications of four point functions in N=4 supersymmetric Yang-Mills theory at two loops*, *Phys.Lett.* **B466** (1999) 20–26, [hep-th/9906051].

[75] F. Gonzalez-Rey, I. Park, and K. Schalm, *A Note on four point functions of conformal operators in N=4 superYang-Mills*, *Phys.Lett.* **B448** (1999) 37–40, [hep-th/9811155].

[76] B. Eden, C. Schubert, and E. Sokatchev, *Three loop four point correlator in N=4 SYM*, *Phys.Lett.* **B482** (2000) 309–314, [hep-th/0003096].

[77] Z. Bern, L. J. Dixon, D. C. Dunbar, and D. A. Kosower, *One loop n point gauge theory amplitudes, unitarity and collinear limits*, *Nucl.Phys.* **B425** (1994) 217–260, [hep-ph/9403226].

[78] G. Duplancic and B. Nizic, *Dimensionally regulated one loop box scalar integrals with massless internal lines*, *Eur.Phys.J.* **C20** (2001) 357–370, [hep-ph/0006249].

[79] A. Brandhuber, P. Heslop, and G. Travaglini, *One-Loop Amplitudes in N=4 Super Yang-Mills and Anomalous Dual Conformal Symmetry*, *JHEP* **0908** (2009) 095, [arXiv:0905.4377].

[80] D. E. Berenstein, R. Corrado, W. Fischler, and J. M. Maldacena, *The Operator product expansion for Wilson loops and surfaces in the large N limit*, *Phys. Rev.* **D59** (1999) 105023, [hep-th/9809188].

[81] I. A. Korchemskaya and G. P. Korchemsky, *On lightlike Wilson loops*, *Phys. Lett.* **B287** (1992) 169–175.

[82] B. Eden, G. P. Korchemsky, and E. Sokatchev, *From correlation functions to scattering amplitudes*, *JHEP* **12** (2011) 002, [arXiv:1007.3246].

[83] L. F. Alday, J. M. Henn, J. Plefka, and T. Schuster, *Scattering into the fifth dimension of N=4 super Yang-Mills*, *JHEP* **01** (2010) 077, [arXiv:0908.0684].

[84] J. M. Henn, S. Moch, and S. G. Naculich, *Form factors and scattering amplitudes in N=4 SYM in dimensional and massive regularizations*, *JHEP* **12** (2011) 024, [arXiv:1109.5057].

[85] J. M. Drummond and J. M. Henn, *Simple loop integrals and amplitudes in N=4 SYM*, *JHEP* **05** (2011) 105, [arXiv:1008.2965].

[86] L. J. Dixon, J. M. Drummond, and J. M. Henn, *Analytic result for the two-loop six-point NMHV amplitude in N=4 super Yang-Mills theory*, *JHEP* **01** (2012) 024, [arXiv:1111.1704].

[87] A. Hodges, *Eliminating spurious poles from gauge-theoretic amplitudes*, *JHEP* **05** (2013) 135, [arXiv:0905.1473].

[88] L. J. Mason and D. Skinner, *Dual Superconformal Invariance, Momentum Twistors and Grassmannians*, *JHEP* **11** (2009) 045, [arXiv:0909.0250].

[89] N. Arkani-Hamed, J. L. Bourjaily, F. Cachazo, S. Caron-Huot, and J. Trnka, *The All-Loop Integrand For Scattering Amplitudes in Planar N=4 SYM*, *JHEP* **01** (2011) 041, [arXiv:1008.2958].

[90] N. Arkani-Hamed, J. L. Bourjaily, F. Cachazo, and J. Trnka, *Local Integrals for Planar Scattering Amplitudes*, *JHEP* **06** (2012) 125, [arXiv:1012.6032].

[91] J. M. Drummond, J. M. Henn, and J. Trnka, *New differential equations for on-shell loop integrals*, *JHEP* **04** (2011) 083, [arXiv:1010.3679].

[92] L. F. Alday, *Some analytic results for two-loop scattering amplitudes*, *JHEP* **07** (2011) 080, [arXiv:1009.1110].

[93] V. Smirnov, *Feynman integral calculus*. Springer-Verlag, Berlin Heidelberg, 2006.

[94] J. A. M. Vermaseren, *Harmonic sums, Mellin transforms and integrals*, *Int. J. Mod. Phys.* **A14** (1999) 2037–2076, [hep-ph/9806280].

[95] J. L. Bourjaily, A. DiRe, A. Shaikh, M. Spradlin, and A. Volovich, *The Soft-Collinear Bootstrap: N=4 Yang-Mills Amplitudes at Six and Seven Loops*, *JHEP* **1203** (2012) 032, [arXiv:1112.6432].

[96] T. Gehrmann and E. Remiddi, *Using differential equations to compute two loop box integrals*, *Nucl. Phys. Proc. Suppl.* **89** (2000) 251–255, [hep-ph/0005232].

[97] S. Caron-Huot and K. J. Larsen, *Uniqueness of two-loop master contours*, *JHEP* **10** (2012) 026, [arXiv:1205.0801].

[98] J. M. Henn, S. G. Naculich, H. J. Schnitzer, and M. Spradlin, *Higgs-regularized three-loop four-gluon amplitude in N=4 SYM: exponentiation and Regge limits*, *JHEP* **04** (2010) 038, [arXiv:1001.1358].

[99] E. Remiddi and J. A. M. Vermaseren, *Harmonic polylogarithms*, *Int. J. Mod. Phys.* **A15** (2000) 725–754, [hep-ph/9905237].

[100] D. Maitre, *HPL, a mathematica implementation of the harmonic polylogarithms*, *Comput. Phys. Commun.* **174** (2006) 222–240, [hep-ph/0507152].

[101] S. Gubser, I. Klebanov, and A. M. Polyakov, *A Semiclassical limit of the gauge / string correspondence*, *Nucl.Phys.* **B636** (2002) 99–114, [hep-th/0204051].

[102] S. Frolov and A. A. Tseytlin, *Semiclassical quantization of rotating superstring in AdS(5) x S**5*, *JHEP* **06** (2002) 007, [hep-th/0204226].

[103] N. Gromov, F. Levkovich-Maslyuk, and G. Sizov, *Quantum Spectral Curve and the Numerical Solution of the Spectral Problem in AdS5/CFT4*, arXiv:1504.0664.

[104] M. Bianchi, S. Kovacs, G. Rossi, and Y. S. Stanev, *Properties of the Konishi multiplet in N=4 SYM theory*, *JHEP* **0105** (2001) 042, [hep-th/0104016].

[105] K. Okuyama and L.-S. Tseng, *Three-point functions in $N = 4$ SYM theory at one-loop*, *JHEP* **0408** (2004) 055, [hep-th/0404190].

[106] R. Roiban and A. Volovich, *Yang-Mills correlation functions from integrable spin chains*, *JHEP* **0409** (2004) 032, [hep-th/0407140].

[107] L. F. Alday, J. R. David, E. Gava, and K. Narain, *Structure constants of planar $N = 4$ Yang Mills at one loop*, *JHEP* **0509** (2005) 070, [hep-th/0502186].

[108] J. Escobedo, N. Gromov, A. Sever, and P. Vieira, *Tailoring Three-Point Functions and Integrability*, *JHEP* **1109** (2011) 028, [arXiv:1012.2475].

[109] J. Escobedo, N. Gromov, A. Sever, and P. Vieira, *Tailoring Three-Point Functions and Integrability II. Weak/strong coupling match*, *JHEP* **1109** (2011) 029, [arXiv:1104.5501].

[110] N. Gromov, A. Sever, and P. Vieira, *Tailoring Three-Point Functions and Integrability III. Classical Tunneling*, *JHEP* **1207** (2012) 044, [arXiv:1111.2349].

[111] N. Gromov and P. Vieira, *Quantum Integrability for Three-Point Functions of Maximally Supersymmetric Yang-Mills Theory*, *Phys.Rev.Lett.* **111** (2013), no. 21 211601, [arXiv:1202.4103].

[112] N. Gromov and P. Vieira, *Tailoring Three-Point Functions and Integrability IV. Theta-morphism*, *JHEP* **1404** (2014) 068, [arXiv:1205.5288].

[113] O. Foda, *N=4 SYM structure constants as determinants*, *JHEP* **1203** (2012) 096, [arXiv:1111.4663].

[114] I. Kostov, *Classical Limit of the Three-Point Function of N=4 Supersymmetric Yang-Mills Theory from Integrability*, *Phys.Rev.Lett.* **108** (2012) 261604, [arXiv:1203.6180].

[115] I. Kostov, *Three-point function of semiclassical states at weak coupling*, *J.Phys.* **A45** (2012) 494018, [arXiv:1205.4412].

[116] Y. Jiang, I. Kostov, F. Loebbert, and D. Serban, *Fixing the Quantum Three-Point Function*, *JHEP* **1404** (2014) 019, [arXiv:1401.0384].

[117] A. Tsuji, *Holography of Wilson loop correlator and spinning strings*, *Prog.Theor.Phys.* **117** (2007) 557–568, [hep-th/0606030].

[118] R. A. Janik, P. Surowka, and A. Wereszczynski, *On correlation functions of operators dual to classical spinning string states*, *JHEP* **1005** (2010) 030, [arXiv:1002.4613].

[119] E. Buchbinder and A. Tseytlin, *On semiclassical approximation for correlators of closed string vertex operators in AdS/CFT*, *JHEP* **1008** (2010) 057, [arXiv:1005.4516].

[120] K. Zarembo, *Holographic three-point functions of semiclassical states*, *JHEP* **1009** (2010) 030, [arXiv:1008.1059].

[121] M. S. Costa, R. Monteiro, J. E. Santos, and D. Zoakos, *On three-point correlation functions in the gauge/gravity duality*, *JHEP* **1011** (2010) 141, [arXiv:1008.1070].

[122] R. Roiban and A. Tseytlin, *On semiclassical computation of 3-point functions of closed string vertex operators in AdS_5xS^5*, *Phys.Rev.* **D82** (2010) 106011, [arXiv:1008.4921].

[123] R. Hernandez, *Three-point correlation functions from semiclassical circular strings*, *J.Phys.* **A44** (2011) 085403, [arXiv:1011.0408].

[124] S. Ryang, *Correlators of Vertex Operators for Circular Strings with Winding Numbers in AdS5xS5*, *JHEP* **1101** (2011) 092, [arXiv:1011.3573].

[125] G. Georgiou, *Two and three-point correlators of operators dual to folded string solutions at strong coupling*, *JHEP* **1102** (2011) 046, [arXiv:1011.5181].

[126] J. Russo and A. Tseytlin, *Large spin expansion of semiclassical 3-point correlators in AdS_5xS^5*, *JHEP* **1102** (2011) 029, [arXiv:1012.2760].

[127] C. Park and B.-H. Lee, *Correlation functions of magnon and spike*, *Phys.Rev.* **D83** (2011) 126004, [arXiv:1012.3293].

[128] E. Buchbinder and A. Tseytlin, *Semiclassical four-point functions in AdS_5xS^5*, *JHEP* **1102** (2011) 072, [arXiv:1012.3740].

[129] D. Bak, B. Chen, and J.-B. Wu, *Holographic Correlation Functions for Open Strings and Branes*, *JHEP* **1106** (2011) 014, [arXiv:1103.2024].

[130] A. Bissi, C. Kristjansen, D. Young, and K. Zoubos, *Holographic three-point functions of giant gravitons*, *JHEP* **1106** (2011) 085, [arXiv:1103.4079].

[131] D. Arnaudov, R. Rashkov, and T. Vetsov, *Three and four-point correlators of operators dual to folded string solutions in AdS_5xS^5*, *Int.J.Mod.Phys.* **A26** (2011) 3403–3420, [arXiv:1103.6145].

[132] R. Hernandez, *Three-point correlators for giant magnons*, *JHEP* **1105** (2011) 123, [arXiv:1104.1160].

[133] C. Ahn and P. Bozhilov, *Three-point Correlation functions of Giant magnons with finite size*, *Phys.Lett.* **B702** (2011) 286–290, [arXiv:1105.3084].

[134] T. Klose and T. McLoughlin, *A light-cone approach to three-point functions in AdS_5xS^5*, *JHEP* **1204** (2012) 080, [arXiv:1106.0495].

[135] E. Buchbinder and A. Tseytlin, *Semiclassical correlators of three states with large S^5 charges in string theory in AdS_5xS^5*, *Phys.Rev.* **D85** (2012) 026001, [arXiv:1110.5621].

[136] S. Ryang, *Three-Point Correlator of Heavy Vertex Operators for Circular Winding Strings in AdS5xS5*, *Phys.Lett.* **B713** (2012) 122–128, [arXiv:1204.3688].

[137] G. Georgiou, *SL(2) sector: weak/strong coupling agreement of three-point correlators*, *JHEP* **1109** (2011) 132, [arXiv:1107.1850].

[138] A. Bissi, T. Harmark, and M. Orselli, *Holographic 3-Point Function at One Loop*, *JHEP* **1202** (2012) 133, [arXiv:1112.5075].

[139] G. Georgiou, V. Gili, A. Grossardt, and J. Plefka, *Three-point functions in planar N=4 super Yang-Mills Theory for scalar operators up to length five at the one-loop order*, *JHEP* **1204** (2012) 038, [arXiv:1201.0992].

[140] P. Bozhilov, P. Furlan, V. Petkova, and M. Stanishkov, *On the semiclassical 3-point function in AdS_3*, *Phys.Rev.* **D86** (2012) 066005, [arXiv:1204.1322].

[141] G. Grignani and A. Zayakin, *Matching Three-point Functions of BMN Operators at Weak and Strong coupling*, *JHEP* **1206** (2012) 142, [arXiv:1204.3096].

[142] P. Caputa, R. d. M. Koch, and K. Zoubos, *Extremal versus Non-Extremal Correlators with Giant Gravitons*, *JHEP* **1208** (2012) 143, [arXiv:1204.4172].

[143] G. Grignani and A. Zayakin, *Three-point functions of BMN operators at weak and strong coupling II. One loop matching*, *JHEP* **1209** (2012) 087, [arXiv:1205.5279].

[144] R. A. Janik and A. Wereszczynski, *Correlation functions of three heavy operators: The AdS contribution*, *JHEP* **1112** (2011) 095, [arXiv:1109.6262].

[145] Y. Kazama and S. Komatsu, *On holographic three point functions for GKP strings from integrability*, *JHEP* **1201** (2012) 110, [arXiv:1110.3949].

[146] Y. Kazama and S. Komatsu, *Wave functions and correlation functions for GKP strings from integrability*, *JHEP* **1209** (2012) 022, [arXiv:1205.6060].

[147] Y. Kazama and S. Komatsu, *Three-point functions in the SU(2) sector at strong coupling*, *JHEP* **1403** (2014) 052, [arXiv:1312.3727].

[148] L. F. Alday and J. Maldacena, *Minimal surfaces in AdS and the eight-gluon scattering amplitude at strong coupling*, arXiv:0903.4707.

[149] L. F. Alday and J. Maldacena, *Null polygonal Wilson loops and minimal surfaces in Anti-de-Sitter space*, *JHEP* **0911** (2009) 082, [arXiv:0904.0663].

[150] L. F. Alday, D. Gaiotto, and J. Maldacena, *Thermodynamic Bubble Ansatz*, *JHEP* **1109** (2011) 032, [arXiv:0911.4708].

[151] L. F. Alday, J. Maldacena, A. Sever, and P. Vieira, *Y-system for Scattering Amplitudes*, *J.Phys.* **A43** (2010) 485401, [arXiv:1002.2459].

[152] J. Caetano and J. Escobedo, *On four-point functions and integrability in N=4 SYM: from weak to strong coupling*, *JHEP* **1109** (2011) 080, [arXiv:1107.5580].

[153] D. Gaiotto, G. W. Moore, and A. Neitzke, *Wall-crossing, Hitchin Systems, and the WKB Approximation*, arXiv:0907.3987.

[154] Y. Jiang, S. Komatsu, I. Kostov, and D. Serban, *The hexagon in the mirror: the three-point function in the SoV representation*, arXiv:1506.0908.

[155] L. Andrianopoli, S. Ferrara, E. Sokatchev, and B. Zupnik, *Shortening of primary operators in N extended SCFT(4) and harmonic superspace analyticity*, *Adv. Theor. Math. Phys.* **4** (2000) 1149–1197, [hep-th/9912007].